RÉPUBLIQUE ALGÉRIENNE DÉMOCRATIQUE ET POPULAIRE
MINISTÈRE DE L'ENSEIGNEMENT SUPÉRIEUR ET DE LA RECHERCHE SCIENTIFIQUE
ÉCOLE NATIONALE POLYTECHNIQUE

École Nationale Polytechnique

Université du Roi Abdullah de Science et Technologie

Département Electronique

Final Year Project Report

For the obtaining of State Engineer degree in Electronics.

Hydration Level Estimation and Classification Using a Capacitive Sensor

---

Student: SI YOUCEF Soumia

Under the Supervision of :

Pr.	ADNANE Mourad	ENP
Pr.	AL-NAFFOURI Tareq	KAUST
Dr.	MAHBOOB Ur Rahman	KAUST

Defended on June 12, 2024, in front of the jury composed of:

President:	Pr.	HAMMAMI Latifa	ENP
Examiner:	Dr.	BOUADJENEK Nesrine	ENP

ENP 2024

Department of Electronics / ENP, 10 Rue des Frères OUDEK, El Harrach 16200 Algiers Algeria.

RÉPUBLIQUE ALGÉRIENNE DÉMOCRATIQUE ET POPULAIRE
MINISTÈRE DE L'ENSEIGNEMENT SUPÉRIEUR ET DE LA RECHERCHE SCIENTIFIQUE
ÉCOLE NATIONALE POLYTECHNIQUE

École Nationale Polytechnique

Université du Roi Abdullah de Science et Technologie

Département Electronique

Final Year Project Report

For the obtaining of State Engineer degree in Electronics.

Hydration Level Estimation and Classification Using a Capacitive Sensor

---

Student: SI YOUCEF Soumia

Under the Supervision of :

Pr.	ADNANE Mourad	ENP
Pr.	AL-NAFFOURI Tareq	KAUST
Dr.	MAHBOOB Ur Rahman	KAUST

Defended on June 12, 2024, in front of the jury composed of:

President:	Pr.	HAMMAMI Latifa	ENP
Examiner:	Dr.	BOUADJENEK Nesrine	ENP

ENP 2024

Department of Electronics / ENP, 10 Rue des Frères OUDEK, El Harrach 16200 Algiers Algeria.

RÉPUBLIQUE ALGÉRIENNE DÉMOCRATIQUE ET POPULAIRE
MINISTÈRE DE L'ENSEIGNEMENT SUPÉRIEUR ET DE LA RECHERCHE SCIENTIFIQUE
ÉCOLE NATIONALE POLYTECHNIQUE

École Nationale Polytechnique

Université du Roi Abdullah de Science et Technologie

Département Electronique

Mémoire de projet de fin d'études

Pour l'Obtention du Diplôme d'Ingénieur d'état en Electronique .

Estimation et Classification du Niveau d'Hydratation à l'Aide d'un Capteur Capacitif

---

Étudiante: SI YOUCEF Soumia

Sous la direction de :

Pr.	ADNANE Mourad	ENP
Pr.	AL-NAFFOURI Tareq	KAUST
Dr.	MAHBOOB Ur Rahman	KAUST

Présenté et soutenu publiquement le (12/06/2024), devant le jury composé de:

Président:	Pr.	HAMMAMI Latifa	ENP
Examinatrice:	Dr.	BOUADJENEK Nesrine	ENP

ENP 2024

Département Electronique / ENP, 10 Rue des Frères OUDEK, El Harrach 16200 Algiers Algeria.

ملخص

هذا العمل يقدم حلاً لتقييم الترطيب عند الإنسان، معالجاً الحاجة الحرجة لأساليب سهلة الاستخدام لاستبدال التقنيات السريرية التي تتطلب التدخل الطبي و هذا لضمان الترطيب السليم عبر شرائح سكانية متنوعة. نقترح استخدام الاستشعار السعوي، بشكل خاص وحدة FDC2114 المزودة باثنين من أجهزة الاستشعار السعوي، لتقدير مستويات الترطيب. مستوحاة من التغيرات في السعة عندما يوضع الإصبع على شاشة الهاتف، تهدف رؤيتنا المستقبلية إلى دمج هذه التقنية في الهواتف الذكية لمراقبة الترطيب بسهولة. تتضمن منهجية العمل جمع البيانات، التحضير المسبق، خوارزميات التصنيف، وزيادة البيانات.

الكلمات مفتاحية: تقييم الترطيب - أساليب سهلة الاستخدام - أجهزة الاستشعار السعوي - مستويات الترطيب - مراقبة الترطيب.

Résumé

Ce travail présente une solution pour l'évaluation non invasive de l'hydratation, répondant au besoin critique de méthodes conviviales pour remplacer les techniques cliniques invasives et assurer une hydratation adéquate à travers des populations diverses. Nous proposons d'utiliser la détection capacitive, en particulier le module FDC2114 équipé de deux capteurs capacitifs, pour estimer les niveaux d'hydratation. Inspirés par les changements de capacité lorsque le doigt est placé sur un écran de téléphone, notre vision est d'intégrer cette technologie dans les smartphones pour un suivi facile de l'hydratation. La méthodologie implique la collecte de données, le prétraitement, les algorithmes de classification et l'augmentation des données, suivis de l'analyse et réseau neuronal.

Mots-clés : Évaluation non invasive de l'hydratation - Méthodes conviviales - Capteurs capacitifs - Niveaux d'hydratation - Surveillance de l'hydratation.

Abstract

This work presents a solution for non-invasive hydration assessment, addressing the critical need for user-friendly methods to replace invasive clinical techniques and ensure proper hydration across diverse populations. We propose using capacitive sensing, specifically the FDC2114 module equipped with two capacitive sensors, to estimate hydration levels. Inspired by the capacitance changes when a finger is placed on a phone screen, our future vision aims to integrate this technology into smartphones for easy hydration monitoring. The methodology involves data collection, preprocessing, classification algorithms, and data augmentation, followed by neural network analysis.

Keywords: Non-invasive hydration assessment - User-friendly methods - Capacitive sensors - Hydration levels - Hydration monitoring.

Dedication

I would like to dedicate this work to myparents, whose unwavering support and encouragement have been the foundation of my academic and research pursuits from the very beginning. To my sisters—Amina, Yasmine, Selma, Sirine, and Lamis—their love and patience have provided me with immense strength and inspiration.

My heartfelt gratitude goes also to my classmates, with special recognition to Abdelbaki Guir, Taibaoui Abdellah, Achraf Djaber, and Zahra Rabet for their camaraderie and shared journey. Lastly, my heartfelt thanks to my dear friends Hind Yahyaoui and Houda Lekmine, for their steadfast friendship and support.

Acknowledgments

I am deeply grateful to my supervisors, Prof. Mourad Adnane from National Polytechnic School and Prof. Tareq Al-Naffouri, Prof. Meriem Taous Laleg and Dr. Mahboob Ur Rahman from King Abdullah University, for their invaluable guidance, support, and expertise throughout my research journey. Their mentorship has been instrumental in shaping my academic and professional growth.

I sincerely appreciate my university staff members, particularly the Head of Department, Prof. Taghi Mohamed, and all the professors from the Electronics Department of the National Polytechnic School, for their encouragement, advice, and contributions to my academic development.

I thank King Abdullah University for the Visiting Student Scholarship, which provided the financial support necessary for my research. My time at the university in Saudi Arabia was a memorable and enriching experience, allowing me to realize my research goals and explore the country's culture and academic environment.

I want to thank my classmates from the National Polytechnic School for their camaraderie and support throughout my academic journey. Special thanks to Rose Al Alaslani, Levina Perzhilla, and Meha Medjati from King Abdullah University for their help during the data collection process.

I extend my heartfelt gratitude to the participants involved in the data collection process at King Abdullah University. Their invaluable contributions, dedication, and cooperation were instrumental in enhancing the quality and scope of my research. I truly appreciate their willingness to dedicate their time and efforts to support and advance the research goals.

I also acknowledge the contribution of graphical designer Ana Bigio from King Abdullah University, a scientific illustrator, for her skillful production of Figure 2.1, which enhanced the presentation of my research findings.

Contents

List of Tables

List of Figures

List of Acronyms

- **EDA** Electrodermal Activity
- **ECG** Electrocardiograph
- **BIA** Bio-impedance Analysis
- **PPG** Photoplethysmography
- **SVM**$_{(1)}$ Support Vector Machine
- **DT**$_{(2)}$ Decision tree
- **RF**$_{(3)}$ Random Forest
- **KNN**$_{(4)}$ k-nearest neighbors
- **LR**$_{(5)}$ Logistic Regression
- **BMI** Body Mass Index
- **RBF** Radial Basis Function
- **HR** Heart Rate
- **TBSR** Total Body Sweat Rate
- **IVC** Inferior Vena Cava
- **AO** Aorta
- **TBW** Total Body Water

General Introduction

Non-invasive hydration assessment means evaluating hydration status in the body without requiring invasive procedures or techniques that penetrate the skin or body tissues.

This work presents a solution for non-invasive hydration assessment, addressing the current need for such methods. Non-invasive hydration monitoring is a trending issue, with researchers striving to integrate hydration monitoring into daily life. Some studies suggest new portable sensors, while others focus on mobile applications, aiming for ease of use and user-friendliness compared to invasive clinical techniques. This need is also driven by the importance of maintaining proper hydration across various populations.

-Problem
There is a critical need for non-invasive, user-friendly methods for hydration assessment to replace invasive clinical techniques and ensure proper hydration across diverse populations.

-Solution proposed
We propose using capacitive sensing to estimate hydration levels within the body using the FDC2114 module equipped with two capacitive sensors.

-Motivation of the proposed solution
The phone screen consists of an array of small capacitance, which induces shifts in values when a finger is placed on the screen. However, accessing this kind of data in off-the-shelf smartphones is difficult. We propose using a capacitive sensor to mimic the phone screen based on this principle. Specifically, we use the FDC2114 module equipped with two capacitive sensors.

-Future Vision of the proposed solution
Our vision is to enable the assessment of hydration states via smartphones, where users place their fingers on the screen to assess their hydration levels.

-Methodology
The methodology follows a classical approach to machine learning solutions, beginning with data collection, followed by data preprocessing and classification algorithms. Subsequently, data augmentation techniques are applied, and the augmented data is fed into neural networks for further analysis.

-Outline
This document is structured into six chapters.

Chapter 1: We offer an overview of hydration states, emphasizing the importance of accurate hydration monitoring.

Chapter 2: Subsequently, we delve into the emerging non-invasive hydration techniques, exploring various sensing technologies from multiple references.

Chapter 3: Next, we outline the operational principles of the module and describe the experimental setup utilized in our study. We establish a hypothesis regarding how capacitive sensing can provide valuable insights into hydration states

Chapter 4: Following this, we offer a detailed account of the data collection process, including the characteristics of the subjects involved.

Chapter 5: We then preprocess the data and investigate different feature combinations to optimize results.

Chapter 6: Finally, we apply data augmentation to assess the robustness of our data against factors such as noise. Moreover, we apply neural network models to our augmented data.

Chapter 1

Background: A short primer on dehydration

1.1 Introduction

Dehydration arises from an insufficient intake of fluids relative to fluid loss, posing a significant health risk with various physiological implications. Adequate hydration enables the body to perform vital functions, including temperature regulation and nutrient transport. Precise evaluation of hydration status is a pivotal factor in the early detection and prevention of dehydration-related health issues. While numerous techniques exist for assessing hydration, the advent of non-invasive and non-contact methodologies offers distinct advantages over invasive approaches [1].
In this chapter, we explore the significance of hydration levels as a biomarker for health, the physiology of dehydration, and current gold-standard methods for monitoring dehydration. We also examine the different hydration levels, associated symptoms, and health risks and identify vulnerable groups. Furthermore, we highlight the need for innovative, non-invasive hydration monitoring methods due to the limitations of current techniques and the demand for accessible healthcare solutions.

1.2 Significance of hydration level as a biomarker

Water, essential for life, influences numerous physiological processes within the human body, and understanding its significance as a biomarker can provide valuable insights into overall health and well-being.
About 60% of the human body consists of water [2], Figure 1.1 illustrates the proportions of water in the human body and its distribution across different organs. It is required to drink approximately 1.5 liters of it daily [3] since it is essential for maintaining proper bodily functions. Beyond hydration, water contributes to weight regulation by boosting metabolic rates [4], supporting brain function [5], aiding in cell membrane formation [6], and facilitating the transportation of nutrients from food [7, 8]. Furthermore, water is integral to processes such as sweating and urination, essential for toxin removal [9, 10].

Dehydration, characterized by a negative water balance resulting from inadequate replenishment of lost fluids, adversely affects physiological parameters and poses numerous health risks [11]. Symptoms range from minor discomforts like headaches and dizziness [12] to severe complications such as seizures, renal failure, and myocardial infarction [11]. Even a slight decrease in body water, as little as 1%-2%, can significantly impair cognitive and motor function [13]. Dehydration affects 17% to 28% of older adults in the United States and not only causes physical discomfort but also exacerbates conditions like childhood obesity resulting from electrolyte imbalances [14].
Hydration levels are significant biomarkers because of their multifaceted impact on human health and well-being. Hydration status is a valuable indicator of overall physiological functioning, reflecting the balance between fluid intake and output in the body. Good monitoring can provide insights into various aspects of health, including kidney function, cardiovascular health, cognitive function, and

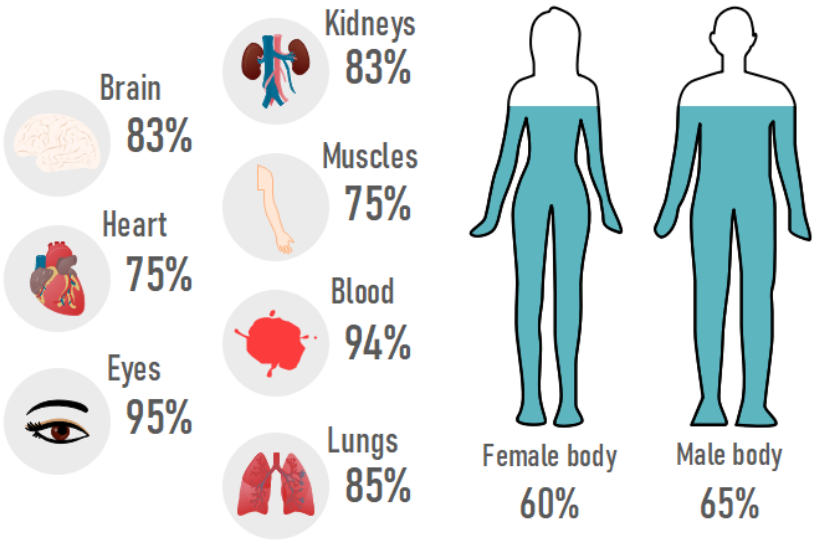

Figure 1.1: Proportions of water in the human body.

metabolic processes.

1.3 Physiology of dehydration

Dehydration is a multifaceted process involving physiological responses from both external and internal factors.
When water loss exceeds intake, specialized brain sensors called osmoreceptors detect declining water levels and trigger thirst signals. Concurrently, increased secretion of antidiuretic hormone from the kidneys facilitates water absorption to maintain fluid equilibrium. Additionally, dehydration-induced low blood pressure prompts the release of renin from the kidneys, initiating a cascade resulting in Aldosterone release. Aldosterone instructs the kidneys to reabsorb more sodium and water, enhancing water retention. As dehydration progresses, available water resources shift from external to internal, leading to dry skin, reduced sweating, and diminished mucous membrane moisture [15].

Conversely, peripheral dehydration involves water loss from peripheral tissues and extremities, often due to factors like exercise-induced sweating or exposure to hot weather [1]. Sweat glands, particularly eccrine glands, play a pivotal role in regulating body temperature by facilitating evaporative cooling and maintaining electrolyte balance through sodium chloride and bicarbonate absorption from the blood [16]. It is imperative to replenish water losses to prevent dehydration, addressing external and internal fluid requirements.

Figure 1.2 illustrates the process of dehydration as water travels from the external layers to the internal organs, while Figure 1.3 depicts dehydration at the peripheral level due to sweating.

1.4 Gold-standard methods for dehydration monitoring

The gold standard techniques for assessing hydration status, such as monitoring body mass changes and body fluid osmometry, are widely acknowledged in dehydration assessment [17], Figure 1.4 shows different gold standard techniques used in hospitals to assess hydration.
Blood and urine analyses are commonly employed by clinicians to evaluate hydration status, plasma osmolality, electrolyte balance, and urinary characteristics like specific gravity and color [18, 19, 20]. While blood remains a trusted fluid for hydration assessment, alternative fluids such as tears or saliva can also provide valuable insights into hormone and electrolyte concentrations, minimizing the need

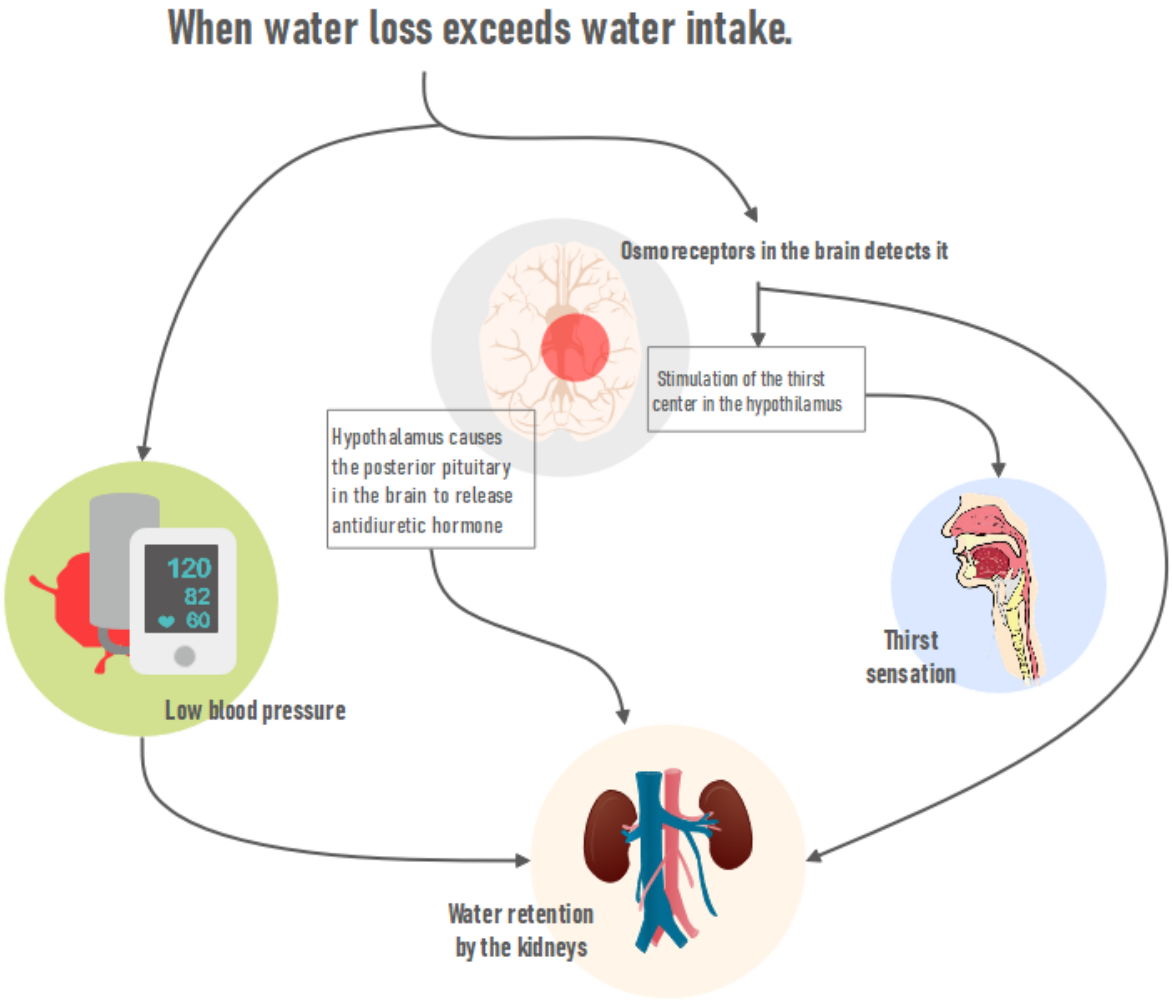

Figure 1.2: Physiology of dehydration.

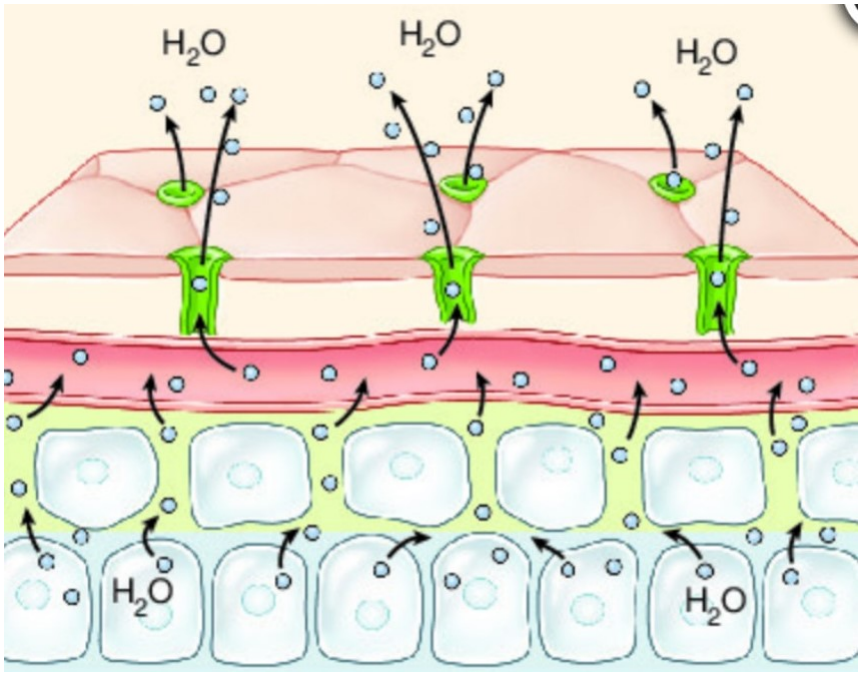

Figure 1.3: Physiology of dehydration at peripheral level [1].

for invasive blood sampling [21, 22].
Urine components, including water and other substances, exhibit concentration changes corresponding to variations in water volume, influenced by factors like fluid intake, diet, medications, and health conditions [23]. Techniques like urine-specific gravity, osmolality, color, and volume contribute to a comprehensive assessment of hydration status, requiring consideration of past ingestion and medical history for accurate interpretation [24].
Similarly, changes in body mass serve as an estimate of water loss, accounting for fluid and food intake and excretion through urine and feces [25]. However, interpreting body mass changes necessitates specific circumstances to accurately reflect variations in water weight, with one gram of body mass typically equating to one milliliter of water loss under controlled conditions [25].

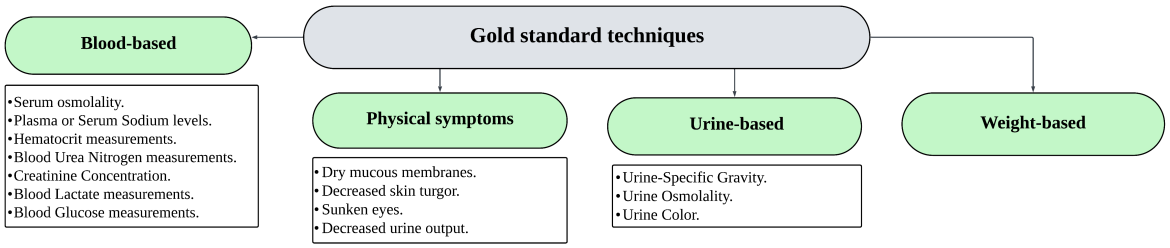

Figure 1.4: Gold-standard techniques to assess dehydration.

In a study focusing on dehydration monitoring methods in soccer players, body mass changes emerged as the most reliable indicator of dehydration, outperforming metrics like hematocrit and urine-specific gravity [26].
Despite the accuracy of these techniques, their implementation demands specialized medical personnel, sophisticated equipment, and thorough laboratory analysis, making them more suitable for intermittent rather than daily monitoring [21]. However, ongoing research and technological advancements continue to refine these gold-standard methods.

1.5 Levels of hydration

Dehydration manifests in varying degrees of severity, with its consequences escalating as it progresses. The more severe the dehydration, the greater the risk to one's life. Furthermore, it is not only dehydration that poses health risks, but overhydration can also lead to significant health complications. Therefore, understanding hydration levels and associated risks is paramount for safeguarding individual health and well-being, Figure 1.5 illustrates different levels of hydration along with their symptoms. At one extreme, over-hydration occurs when the body retains an excessive amount of water [27]. On the other hand, euhydration denotes a state of optimal hydration where the body's fluid balance is maintained. A fluid loss of 1-2% of body weight characterizes mild dehydration. As dehydration progresses to moderate levels, fluid losses reach 3-5% of body weight. Severe dehydration occurs when fluid losses exceed 5% of body weight [28, 29, 30].
The diagram below identifies the symptoms associated with different hydration levels.
Monitoring hydration levels closely and recognizing the associated symptoms are essential for timely intervention to prevent dehydration-related complications.

1.6 Vulnerable groups for dehydration

Dehydration poses a heightened risk to several vulnerable groups, each with unique predisposing factors and susceptibilities.

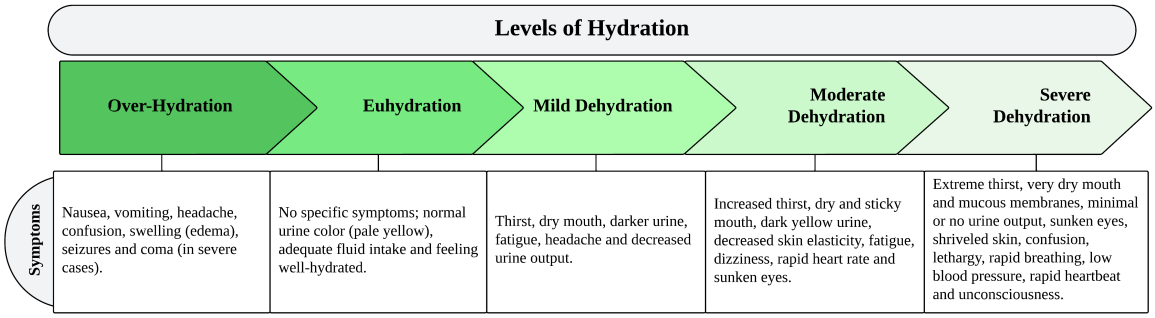

Figure 1.5: Levels of hydration.

- Athletes and individuals engaged in strenuous physical activities and those working outdoors in hot climates are particularly prone to dehydration due to increased fluid loss through sweating.
- Infants, with their limited ability to regulate body temperature and reliance on caregivers for hydration, are also vulnerable to dehydration, especially during illnesses such as diarrhea and vomiting[31].
- Older people face challenges maintaining adequate hydration levels due to age-related declines in thirst sensation and mobility limitations[32, 33].
- Individuals with underlying medical conditions such as cardiovascular diseases, renal disorders, and metabolic disorders like diabetes are at increased risk of dehydration due to factors such as medication side effects, fluid imbalance, and compromised physiological functions[34, 35, 36].
- Heat-related conditions, infectious diseases causing fever, medication-induced diuresis, and neurological/neurodegenerative conditions further exacerbate susceptibility to dehydration in vulnerable populations [37, 38, 39].

Understanding the specific vulnerabilities of these groups is essential for implementing targeted hydration strategies and preventive measures to mitigate the risk of dehydration-related complications.

1.7 Need for novel non-invasive methods for dehydration monitoring

Gold standard methods for hydration assessment have long been considered the benchmark. However, they often pose challenges due to their invasiveness and impracticality. Consequently, there is a growing demand for portable, non-invasive, and contactless solutions. Smartphones have emerged as promising tools for real-time medical diagnostics, thanks to their widespread accessibility and robust sensing capabilities [40].
Smartphones and smartwatches offer a quick, convenient, and cost-effective alternative for routine hydration monitoring compared to traditional laboratory techniques. This necessity for accessible and user-friendly solutions has driven researchers to explore innovative techniques such as Bio-Impedance Analysis (BIA) and Electrodermal Activity (EDA), facilitating seamless integration into everyday devices, and to develop new sensing technologies, enhancing reliability, flexibility, and portability.
Ultimately, integrating hydration monitoring into everyday life is essential for maintaining internal bodily balance and optimal functionality across various demographics, from infants to older people, athletes, and individuals with medical conditions.

1.8 Conclusion

This chapter delves into the details of dehydration, highlighting its significance as a health concern and the multifaceted factors influencing hydration status. From understanding the physiological mech-

anisms involved in dehydration to exploring the importance of hydration levels as biomarkers, this chapter provides insights into the critical role of hydration in overall health and well-being. Furthermore, it examines gold standard methods while acknowledging their limitations regarding invasiveness and practicality for routine use. As we move forward, the need for novel, non-invasive, and non-contact methods for dehydration monitoring becomes apparent, driven by the limitations of conventional techniques.

Chapter 2

Emerging Non-invasive Techniques to assess hydration levels

2.1 Introduction

The emergence of non-invasive techniques for assessing hydration levels marks a significant advancement in healthcare and personal well-being. Unlike invasive methods, these innovative approaches offer a hassle-free and user-friendly monitoring of hydration status. Their convenience and ease of use make them suitable for daily application, seamlessly integrating into everyday routines. By providing quick and non-disruptive assessments, these techniques save valuable time and empower individuals to take proactive steps toward maintaining optimal hydration levels.
In this chapter, we delve into various state-of-the-art techniques for non-invasive hydration monitoring, organized by the types of sensing modalities utilized in each approach. From EDA and Electrocardiograph (ECG) to BIA analysis and Optical methods, Thermal, Radio-frequency, Acoustic, and Fluid-Based sensing modalities. By categorizing these techniques based on their sensing principles, we aim to provide a comprehensive overview of the latest advancements in non-invasive hydration monitoring. Additionally, we examine some applications in targeted populations and specific organs. Finally, we outline future perspectives in this field, highlighting potential avenues for further research and development.
Figure 2.1 allows you to visualize the different techniques discussed in this chapter, each of which is detailed in a separate section.

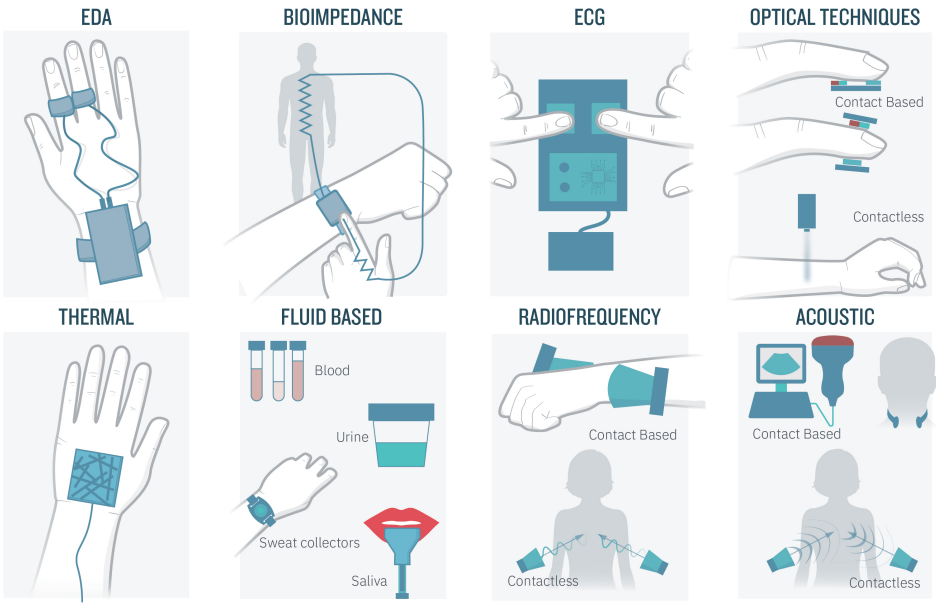

Figure 2.1: Visualization of the emerging non-invasive techniques to assess hydration levels.

2.2 Electrodermal Activity

EDA is a significant marker for assessing hydration levels, reflecting variations in the skin's electrical conductance due to sweat gland activity and nervous system responses. Utilizing EDA sensors, researchers have explored diverse methodologies to monitor hydration status effectively.
The BITalino toolkit [41], a versatile platform for bio-signal acquisition and processing, has been instrumental in several studies for EDA data collection [42, 43, 44, 45, 46]. Figure 2.2 shows an EDA sensor placed on the fingers to take measurements.

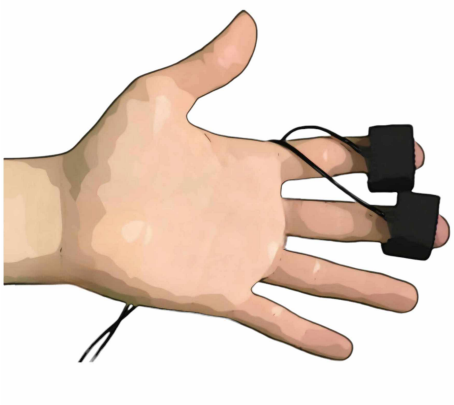

Figure 2.2: EDA sensing [47].

Several advancements highlight the potential of EDA-based approaches in non-invasive hydration monitoring:

- In a study by Liaqat et al., EDA data gathered from participants in different postures were analyzed using Random Forest (RF) algorithm, achieving 91.3% accuracy in predicting hydration status [42].
- Rizwan et al. utilized statistical features extracted from EDA data and the k-Nearest Neighbors (KNN) algorithm to classify hydration status with an accuracy of 87.78% [43].
- In a study by Kulkarni et al., Convolutional Neural Networks (CNNs) processed EDA data from a wristband, leading to the development of the "monitoring my dehydration" mobile application with an accuracy of 84.5% [48].
- Novel approaches such as utilizing the Short-Time Fourier Transform to convert EDA data into time-frequency spectrograms for CNN analysis have shown promising results [46].
- Researchers have explored innovative applications of EDA-based hydration monitoring, including smartphone-based systems utilizing the dynamic time warping algorithm for real-time tracking [49].
- A study leveraged galvanic skin response data alongside Support Vector Machine (SVM) and KNN to classify hydration status accurately, SVM exhibited superior accuracy, achieving 82%, compared to KNN's 64% [50].

Discussion:

EDA has demonstrated effectiveness in assessing hydration status due to its capability for real-time monitoring and potential integration into everyday devices such as smartwatches. Researchers have utilized machine learning techniques and tools like the BITalino toolkit to achieve high accuracy in identifying hydration levels. However, this sensing modality can be influenced by factors such as sweat and the subject's posture, stress levels, and sudden movements, posing challenges in accurately interpreting the data. Therefore, it is essential to adhere to specific protocols when collecting EDA data, including adopting particular postures and gestures and ensuring proper placement of sensors. Future studies should focus on mitigating these stimulus effects, aiming to reduce noise and improve data quality.

2.3 Electrocardiograph

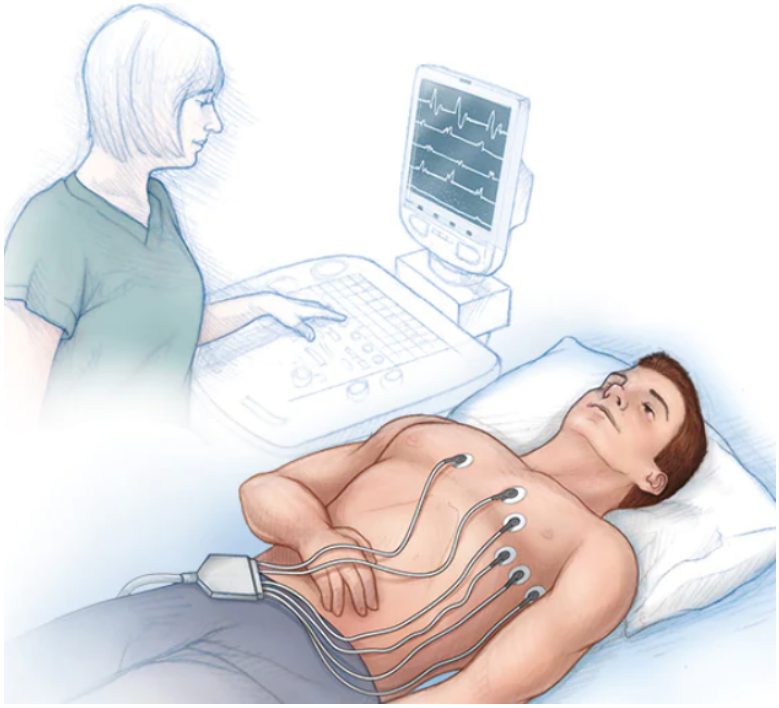

Figure 2.3: ECG sensing [51].

ECG stands as a valuable non-invasive technique for cardiology, used to diagnose heart rhythm and detect cardiac conditions. Various research findings underscore the effectiveness of this technique in offering insights into hydration status within the body. Figure 2.3 illustrates a patient taking ECG measurements in a medical setting.

- In an innovative study by [52], Electric Potential Sensing (EPS) technology was introduced to gauge hydration by measuring the body's electric field. By correlating variations in ECG signal amplitude with hydration status, EPS demonstrated effectiveness in detecting hydration-related changes in ECG amplitude, as validated with five healthy subjects.
- Researchers in [53] sought to classify hydration stages during exercise using SVM classifiers based on 12-lead ECG signals. With measurements taken before and after exercise sessions and subsequent hydration, their SVM classifier achieved a 60% classification accuracy, identifying the RR interval as a pivotal feature indicative of hydration status.
- An SVM classifier leveraging temporal and spectral information from single-lead ECG signals was proposed in [54], yielding a specificity of 57.9% and sensitivity of 96.3% upon testing with the MIT-BIH PhysioNet database [55, 56].
- Researchers analyzed ECG data from 17 male athletes at varying hydration levels, demonstrating the capability of time-domain, frequency-domain, and non-linear parameters to differentiate between phases of hydration and dehydration [57].
- Roshan et al. investigated the impact of dehydration and re-hydration on various ECG and echocardiographic parameters. The study involved fourteen fit high school wrestlers subjected to sauna sessions for controlled body weight loss, with results revealing correlations between measured physiological markers and hydration levels [58].
- Kamran et al. utilized heart rate responses to postural movements as hydration indicators, employing ECG data captured via the Polar H10 chest strap heart monitor (Polar Electro Oy, Kempele, Finland).

Their classification models achieved an overall accuracy of 79%, with specific postural movements yielding higher accuracies, emphasizing the utility of ECG-based hydration monitoring [59].

Discussion:

The potential of ECG technology for monitoring hydration levels is significant, given its widespread availability, accessibility, and non-invasive nature, allowing for potentially real-time assessment. Research has highlighted a correlation between various markers derived from ECG signals and hydration status. However, using ECG signals to extract hydration information poses challenges, as the primary function of ECG is to monitor heart rate rather than hydration. Hence, despite its advantages, employing ECG for hydration monitoring may lack sensitivity and specificity.

In [60], an evaluation of basic cardiac electrophysiology was conducted across a spectrum of dehydration levels (1-7% total body water (TBW) loss), revealing no evidence of impaired cardiac electrophysiology. Thus, relying solely on ECG may not offer a comprehensive hydration assessment, potentially necessitating complementary techniques for more reliable results.

2.4 Bio-impedance Analysis

BIA is the measurement of the characteristic impedance of biological materials. It involves passing a small electrical current through the body and measuring its conductance, offering insights into various physiological features.
Figure 2.4 illustrates the principle of bio-impedance analysis, where a small electrical current is passed through the body to characterize its impedance.

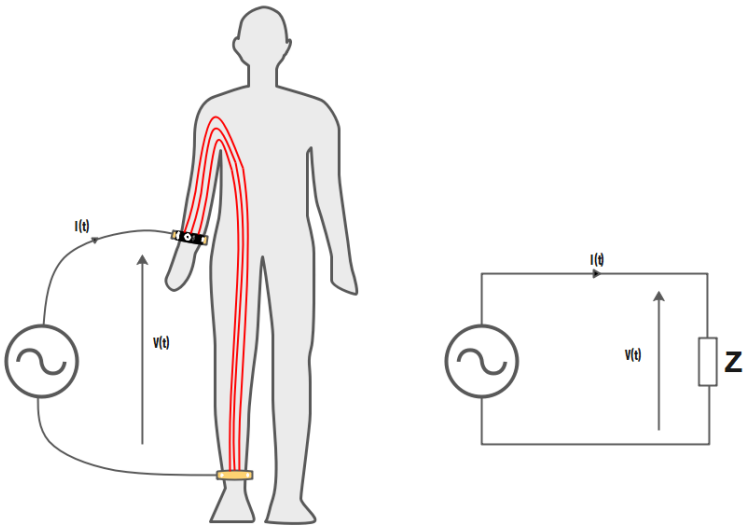

Figure 2.4: Bio-impedance sensing.

Multiple studies showcase the promise of this approach for non-invasive hydration assessment:

- A study by [61] introduced a 3D-printed electrode design to measure Bio-impedance, suggesting rectangular and circular shapes. Results indicated the rectangular shape's superiority due to its larger effective area, although further clinical validation is warranted.
- Researchers in [62] introduced a novel sensor design using textile-based materials to monitor skin hydration levels, demonstrating a strong correlation between hydration levels and skin impedance.

- Another innovative design of a wearable skin hydration sensor was presented in [63], comprising silver nanowires and a polydimethylsiloxane matrix, offering accurate measurements while remaining insensitive to external humidity.

- Huang et al. in [64] proposed an ultra-thin, stretchable sensor system containing miniaturized impedance measurement electrodes to mitigate common-mode interferences, exhibiting excellent precision and accuracy compared to existing devices.

- Nanomesh electrodes were suggested for bio-impedance assessment in [65], showing a negative correlation between skin impedance measurements and hydration levels.

- De Guzman et al. in [66] introduced a wearable tattoo sensor, and AlDisi et al. in [67] investigated the use of interdigitated electrodes to measure bio-impedance, both revealing promising results in correlating bio-impedance with moisture levels.

- In [68], researchers presented an ultra-thin, stretchable device laminated onto the skin's surface, exhibiting stability and high accuracy in detecting changes in surface strain.

- In [69], researchers evaluated three impedance measurement techniques, revealing a strong correlation between methods and tests, particularly in observing distinct hydration stages.

- A wearable device for monitoring hydration status in infants was proposed in [31], demonstrating impedance decrease with increased hydration levels.

- Ring et al. in [70] proposed a technique to address bio-impedance measurement variabilities caused by temperature effects, employing three distinct models: a linear kernel, a probabilistic model, and a Gaussian radial basis function kernel. This method effectively mitigated the influence of temperature on bio-impedance measurements, achieving a correction level of 71%. Finally,

- Researchers in [71] effectively evaluated fat accumulation and hydration levels in the body through BIA, utilizing ZigBee-based mobile wireless sensor networks integrated into intelligent clothing.

Discussion:

Evaluating characteristic impedance in humans presents a promising avenue for assessing hydration levels. Its advantages encompass real-time feedback, non-invasiveness, and user-friendly operation, potentially allowing integration into everyday devices. Numerous innovative studies have explored advanced sensor designs to improve the efficacy and comfort of this technique.
However, it is crucial to consider the impact of external factors on the readings. Given that this sensing method relies on electrode-skin contact, the development of stretchable, flexible, and appropriately designed sensors is paramount. Furthermore, subjects must maintain specific postures and remain motionless during measurements, posing potential challenges. Additionally, careful sensor placement in areas with minimal sweat accumulation is essential to avoid erroneous hydration level indications from sweat interference.

2.5 Optical sensing

Optical sensing utilizes light wave analysis, which can undergo various phenomena like reflection, scattering, absorption, or refraction, providing crucial insights into the surrounding environment or targeted objects through changes in wavelength, light intensity, and other parameters. Optical sensors find extensive applications in diverse fields, such as environmental monitoring, industrial processes, and medical settings.
Researchers have delved into leveraging optical techniques to evaluate hydration levels:

- In [72], the near-infrared region's optical response of human skin was explored as an indicator of hydration status through in vivo tests involving 20 volunteers with varying skin types and moisturizer usage. The results revealed distinct patterns among individuals with differing moisturizing habits.

However, inter-subject variability due to diverse skin types necessitates larger subject pools and statistical regression methods for comprehensive analysis in future studies.

- In another endeavor, researchers in [73] proposed spatially resolved diffuse reflectance spectroscopy (DRS) to evaluate skin hydration, subjecting it to thermal loads, physical activities, and diuretic therapy. The study observed a consistent hydration decrease during thermal loads, indicating dehydration, with recovery only observed post-heat cessation. Physical activity induced rapid water content changes and prompt rehydration, highlighting efficient hydration replenishment. Diuretic therapy for edema syndrome led to decreased hydration levels due to dermal thickness reduction. This underscores DRS's efficacy in detecting dehydration, rehydration, and estimating hydration levels.
- An established technique involving skin illumination with a laser, coupled with periodic vibrations and speckle pattern tracking, was adapted in [74] for skin hydration measurement. Comparative tests against the Corneometer CM 825 validated this non-contact technique's capability in assessing hydration.
- Researchers in [75] evaluated four dehydration markers-capillary refill time, skin recoil time, skin temperature profile, and skin tissue hydration- via infrared spectrometry. Offline data analysis using image processing and optimization techniques demonstrated the technique's effectiveness.

2.5.1 Phone cameras

A phone camera is considered an optical sensor because it functions by capturing and processing optical information, specifically light, to generate images or videos. This optical sensor, integrated into smartphones, utilizes light to detect objects, patterns, or environmental changes. Figure 2.5 shows different techniques to use the phone camera to assess hydration: either by capturing the face or recording the fingers to detect slight changes in skin characteristics due to dehydration.

Figure 2.5: Phone cameras based sensing.

- In [76], the authors utilized a dataset of 2340 face photos and a Siamese neural network model to develop a smartphone application for non-invasive dehydration diagnosis. They achieved a 76.1% accuracy rate in distinguishing between different hydration states.
- Researchers in [77] employed texture analysis and skin marking techniques to conduct skin turgor tests via cellphones. Using image processing algorithms to analyze video frames, they mimicked conventional medical practices for monitoring skin elasticity and recovery during dehydration assessments, thereby determining skin mechanical features and hydration status.
- Rose et al. introduced an innovative strategy utilizing an off-the-shelf smartphone camera for non-invasive dehydration monitoring, categorizing hydration levels on a scale ranging from 1 to 4 [78].

2.5.2 Photoplethysmography

Photoplethysmography (PPG) is an optical technique for non-invasively monitoring variations in blood volume within micro-vascular tissue beds.
PPG sensors function by illuminating a section of the skin and detecting the reflected, absorbed, or scattered light by the network of blood vessels. Alterations in blood flow induce changes in light absorption.
Figure 2.6 shows two different PPG techniques: on the left, the finger is placed between an emitter and a receiver where the receiver collects light passing through the finger; on the right, both emitter and receiver are on the same side where the receiver collects reflected light.

Figure 2.6: PPG sensing.

Multiple research papers highlight the capability of this method in offering insights into physiological characteristics like heart rate, blood pressure, and stroke volume, thereby indirectly assessing hydration status.

- An automated, non-invasive approach for detecting dehydration through PPG signals was developed by Reljin et al. [79]. They collected data from the forehead, ear, and finger of 42 dehydrated patients and employed SVM with a Radial Basis Function (RBF) kernel to classify dehydration, achieving an accuracy of 67.91%.

- In another study [80], researchers utilized a multi-modal approach to assess skin hydration by integrating a novel multi-wavelength optical PPG sensor into a Samsung Galaxy Watch Active 2. Hardware prototypes with specific LED and photo-diode configurations were fabricated and assessed using Monte Carlo simulations to ensure precision. Spectral measurements of skin reflectance and ultrasonic measurements of skin thickness were also conducted. Feature analysis and a binary classification model (LightGBM) were employed to extract insights from PPG signals, achieving accuracy scores exceeding 70%.

- Researchers in [81] investigated a CMOS miniaturized spectrometer's capabilities for dermal H2O measurement and reflective, medically accurate SpO2. This spectrometer, based on PPG and spectroscopy, was utilized in the 750-1050 nm range to study 29 volunteers, including four patients with congestive heart failure and fluid retention in their legs. The spectroscopic model was compared against the gold standard lymph scanner for localized percentage water content, achieving a 3.3% Root Mean Square Error prediction accuracy and accurately identifying congestive heart failure patients.

- In [82], children's dehydration levels were evaluated using two diagnostic variables: capillary refill time measured via green-light PPG and skin turgor assessed through a Cutometer. Regression analysis was performed to determine correlations, suggesting that combining local skin temperature with skin elasticity could aid in evaluating dehydration levels. However, the results were varied, indicating limitations in the dehydration range, participant age group, and experimental setup, with no transparent relationships between variables and dehydration degree.

Discussion:

The optical attributes of human skin offer a non-contact means of monitoring biomarkers, presenting potential integration into everyday devices. Various techniques have been proposed and evaluated, including near-infrared spectroscopy, diffuse reflectance spectroscopy, smartphone-based imaging, skin temperature profiling, and PPG.
Optical sensing has shown rapid responsiveness, providing accurate insights into skin properties. However, despite these advantages, several challenges need to be addressed. Environmental factors like dust and ambient lighting can influence results, necessitating meticulous setup and calibration procedures that may be complex. Furthermore, validation against gold-standard methods is essential. Inter-subject variability poses another significant challenge, as patterns are influenced by factors such as age, skin tone, thickness, and temperature.
Consequently, multiple studies have demonstrated that integrating optical sensing with other modalities like ultrasound, electrical, or thermal properties significantly improves estimation quality.

2.6 Thermal sensing

Thermal sensing involves the detection and measurement of temperature fluctuations using temperature-sensitive devices or sensors. Applied in skin-related contexts, thermal sensing techniques monitor physiological responses and track changes in skin temperature, which can indicate various biomarkers. In dermatology, thermography detects localized temperature alterations on the skin surface, signaling inflammation or infection. Similarly, in sports medicine, monitoring skin temperature aids in evaluating muscle recovery and hydration levels and detecting signs of overexertion or injury.
Figure 2.7 shows the representation of a thermal map of a human body, created using thermal sensors.

Figure 2.7: Thermal sensing.

The transport properties governing substance transfer into a medium are crucial in thermal sensing. These properties, including thermal conductivity, specific heat capacity, and thermal diffusivity, describe heat energy transfer through tissues. small

- In [83], a soft array of epidermal thermal sensors and actuators was developed and tested on 25 subjects across six body regions to study skin thermal transport properties. Positive correlations between thermal properties and skin hydration levels were observed, although factors like local blood flow dynamics and skin structural features may influence these markers. Thus, understanding the complexities of skin thermal properties requires careful consideration of these variables.

- A novel technique proposed in [84] involves small skin patches equipped with flexible thermal sensor modules and wireless Bluetooth platforms, along with Wheatstone bridge circuits, to measure skin hydration levels. Using bilayer skin models with clinical-grade accuracy, the system demonstrated high accuracy levels surpassing some clinical methods for evaluating skin hydration conditions.

- In [85], a skin hydration sensor based on the transient plane source method was introduced to determine skin thermal properties. This method, employing two resistive heaters and temperature sensors, calculates skin thermal conductivity by comparing temperature differences, providing insights into skin hydration state while eliminating the effects of fluctuating ambient temperatures. Tested on 200

patients in dermatology clinics, the device exhibited increased sensitivity and repeatability compared to previous models.

Discussion:

Thermal sensing encounters various challenges, particularly the influence of interfering heat, which complicates data interpretation. Overcoming external heat sources or ambient temperature effects presents significant hurdles. Moreover, solely relying on thermal transport properties may not offer comprehensive insights into physiological markers, given the complexity of understanding skin properties. Therefore, integrating thermal sensing with other modalities could enhance skin hydration level estimation and deepen tissue content understanding. Future endeavors should incorporate more clinical tests to validate technique efficiency and assess the impact of external heat sources on measurement reliability.

2.7 Radio frequency based methods

Radio frequency techniques, operating within a range of electromagnetic frequencies from 3 kilohertz (kHz) to 300 gigahertz (GHz), have emerged as valuable tools for assessing hydration levels. These waves, including microwaves within the R-freq spectrum, offer unique capabilities such as penetrating obstacles and focusing signals for high-speed communication. In hydration monitoring, microwave-based methods exploit changes in dielectric properties in human tissues or skin to gauge moisture levels.Figure 2.8 illustrates some techniques for radiofrequency hydration assessment.

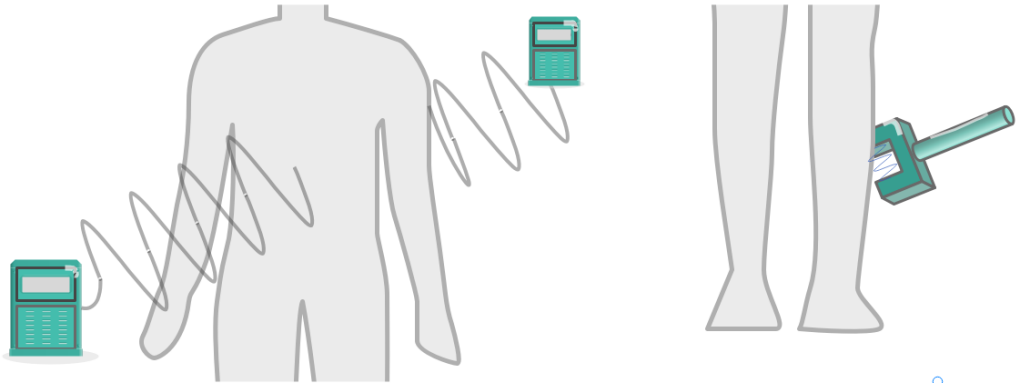

Figure 2.8: Radio frequency based sensing.

- In [86], researchers constructed a broadband antenna using a RO4350 laminate substrate connected to a network analyzer. This setup emitted microwaves and recorded the signals reflected after interacting with the skin. By measuring the amplitude of the returning signals and the frequency at which they occurred, the researchers evaluated the recorded data to assess hydration levels.
- A pioneering wearable device was introduced in [87], leveraging microwave reflectometry and planar sensing to continuously monitor skin hydration levels in real time. Despite successfully establishing a relationship between hydration and microwave reflectometry measurements, [87] acknowledges the need for further improvements, such as enhancing miniaturization and portability.
- Expanding the work done in [87], researchers in [88] investigated the integration of microwave reflectometry with a portable vector network analyzer, aiming for enhanced wearability and accuracy.
- M. Baghelani et al. proposed a novel chipless tag-based approach in [89], utilizing split ring resonator transmission responses to estimate hydration levels, particularly monitoring permittivity and conductivity variations on the earlobe.

- In an attempt to correlate skin permittivity with weight changes due to dehydration, [90] developed a custom measurement system to collect data from young adults before and after exercise.
- in [91], researchers delved into assessing hydration levels by transmitting electromagnetic signals through simulated realistic forearms. The study revealed a promising relationship between water loss and dielectric permittivity in simulated models. This finding was further proved in [92], where in vivo tests on athletes before and after exercise confirmed the earlier results.
- The study in [93] aimed to evaluate hydration in fasting individuals during Ramadan using the same equipment as in [91] and [92]. Researchers recorded changes in permittivity, weight, and urine-specific gravity, observing weight loss in all volunteers and modest changes in urine-specific gravity, indicating the dehydration threshold. Linear regression analysis between weight changes and permittivity revealed a strong correlation, although no clear relationship was found between urine gravity and permittivity, suggesting limitations in detecting subtle hydration changes.
- L. Peng et al. in [94] employed ultrawideband technology and Elman neural network learning models to quantitatively estimate hydration levels.
- J. Kilpijärvi et al. in[95] proposed a microwave sensor coupled with a complementary split ring resonator, demonstrating accurate estimation results on phantoms.
- Innovative approaches such as time-domain reflectometry, as demonstrated in [96], and ultra-high-frequency sensors integrated into clothing, as introduced by [97], offer promising avenues for dehydration monitoring. The results achieved a 100% accuracy rate when sweat textile saturation exceeded 58% [97].
- In [98], researchers presented a flexible R-freq sensor detecting moisture changes through electromagnetic resonance, showcasing distinct trends in hydrated and dehydrated states.
- Utilizing software-defined radios, [99] proposed a non-contact method relying on R-freq signal capture for hydration assessment, achieving high accuracy (93.8% was achieved for the chest technique and 96.15% for the hand-based technique).
- Wang et al. in [100] validated the BioMindR device for hydration assessment (BioMindR, a non-invasive R-freq sensor development company), establishing a linear correlation between received signal strength indicator variations and body water loss percentage.

Discussion:

Researchers have explored numerous innovative approaches to evaluate hydration levels using Radio frequency based technologies. Methods such as time-domain reflectometry, ultrawideband techniques, and advanced antenna designs have demonstrated efficacy in assessing hydration, offering rapid and continuous monitoring suitable for real-time applications. These Radio frequency based techniques have shown the capability to detect subtle moisture level changes by analyzing tissue dielectric permittivity.
However, employing this sensing modality necessitates specialized and costly equipment, which must be carefully maintained and calibrated over time, along with expert interpretation of measurements and analysis of readings. Moreover, integrating Radio frequency based hydration assessment into everyday devices like smartphones poses challenges, highlighting the need for future efforts to focus on device miniaturization, enhanced portability, and cost reduction. Addressing environmental interference is another crucial consideration to improve estimation accuracy.

2.8 Acoustic based methods

Acoustic signals, characterized by pressure oscillations in mediums like air or water, encode data through changes in frequency and amplitude, enabling message transmission. These signals are utilized across various domains, including telecommunications and medical applications.

Leveraging acoustic signals, researchers have explored non-invasive methods for assessing hydration status by analyzing signals traveling through body tissues or fluids. Ultrasound velocity of muscles offers direct insights into muscle composition, including moisture content, as it correlates with density, elasticity, and moisture.
Figure 2.9 illustrates some acoustic-based techniques for hydration monitoring.

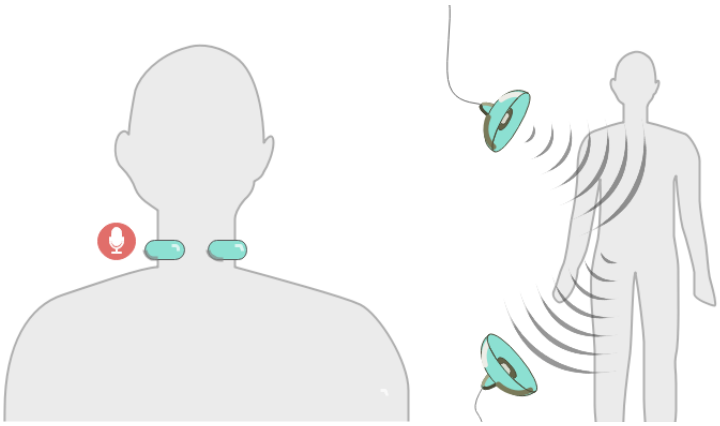

Figure 2.9: Acoustic based sensing.

- In a study by researchers in [101], a handheld device applied to the calf radiated ultrasound waves, measuring their speed through the calf muscles. Preliminary testing on tissue-mimicking phantoms yielded a measurement error range of ± 1 m/s, with subsequent tests on subjects demonstrating the technique's potential, albeit with noted inter-subject variability.
- In [102] utilized a handheld ultrasonic probe on NCAA wrestlers' calves (National Collegiate Athletic Association wrestlers), observing changes in ultrasound wave velocity under different hydration conditions.
- In another innovative approach by Mengistu et al. in [103], the Auto-Hydrate system was proposed, integrating a throat microphone, smartwatch, and smartphone for monitoring drinking activities with 91.5% accuracy using SVM classifiers.
- Researchers in [104] aimed to identify severe dehydration in children with diarrhea and/or vomiting, highlighting ultrasound assessment of the inferior vena cava (IVC) to the aorta (AO) ratio as superior to other techniques, with a sensitivity of 93% and a specificity of 59%.
- El Amrousy et al. in [105] evaluated the IVC/Ao diameter ratio as a predictor of hydration status in infants with acute clinical signs of significant dehydration, demonstrating a sensitivity of 82%, a specificity of 91%, and an accuracy of 87% in predicting considerable dehydration.
- measurements of the largest diameters of IVC and AO before and after fluid therapy in pediatric patients, revealing a higher IVC/AO ratio after fluid administration in [106].
- Researchers in [107] conducted ultrasound examinations of IVC diameter in older patients, revealing disparities in clinical and ultrasound parameters between dehydrated and hydrated subjects, with ultrasound markers having lower values in dehydrated patients. Specific cutoff thresholds were determined to achieve reasonable specificity in diagnosis, highlighting ultrasound technology's potential in assessing hydration status.

Discussion:

Acoustic technologies are emerging as pivotal tools in hydration assessment, offering insights into muscle moisture levels by tracking signal propagation through tissues, enabling non-invasive dehydration

detection.
Additionally, studies employing ultrasound sonography to gauge IVC and AO diameters have shown superior accuracy in assessing hydration status compared to traditional clinical methods. The IVC/AO ratio emerges as a particularly effective hydration indicator, as evidenced by multiple studies. However, challenges persist, including signal variability and interfering factors, necessitating the consideration of signal variability over direct readings and establishing tailored cutoffs, such as age and weight, for precise estimations. Furthermore, ultrasound sonography application requires specialized equipment and trained personnel for result interpretation, limiting its feasibility for routine hydration monitoring. Therefore, efforts are underway to miniaturize and cost-effectively scale these devices for everyday use while exploring strategies to mitigate interference from other parameters.

2.9 Bodily fluids analysis

Non-invasive fluid-based techniques involve assessing markers in bodily fluids obtained without tissue penetration. Parameters like osmolality, ion concentrations, serum creatinine, and specific gravity can be evaluated from fluids such as urine, saliva, and sweat, offering valuable insights into hydration levels.
Urine, a product of kidney function for waste removal, comprises water and dissolved solutes. Saliva, produced by salivary glands to moisturize the mouth, contains water and enzymes. Similarly, sweat, secreted by sweat glands, comprises water and electrolytes and regulates body temperature.
Due to their high water content, dehydration can directly impact these bodily fluids, making their analysis crucial for hydration assessment. In this section, we delve into the existing research and explore methods based on salivary, sweat, and urine analysis. Figure 2.10 illustrates different fluid-based techniques using blood, urine, and salivary samples.

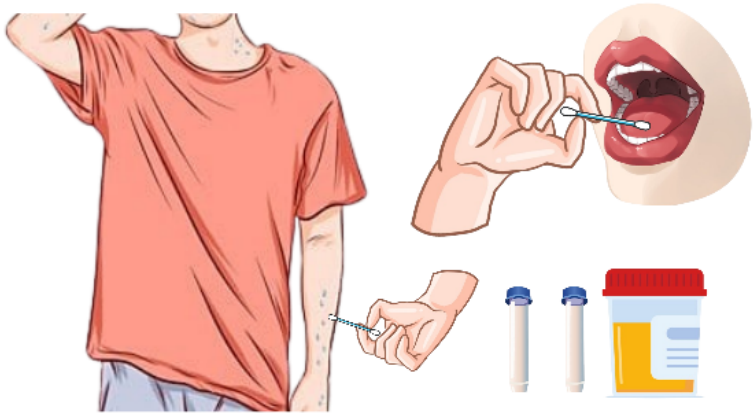

Figure 2.10: Bodily fluids sampling.

2.9.1 Salivary markers

Different approaches for non-invasive dehydration assessment through saliva analysis have been examined:

- In their research, Ring et al. delved further into the investigation outlined in [108], exploring salivary markers as potential indicators of water loss. Their objective was to analyze compounds present in saliva, including electrolytes and hormones, and utilize machine learning algorithms to estimate the extent of dehydration following physical exertion. Their findings revealed an estimation error of around 0.34 liters in TBW loss.
- a non-invasive, portable device developed in [109] aimed to swiftly detect dehydration through saliva analysis, to improve timely hydration assessments and reduce the risks associated with chronic kidney

disease. This device, featuring gold electrodes, efficiently processes small saliva volumes (ranging from 50 to 500 uL). Validation with clinical samples and comparison to serum osmolality standards confirmed its robust ability to accurately detect varying hydration levels.

- the introduction of embedded piezoresistive microcantilever (EMP) sensors in [110] presents a novel approach to monitoring hydration levels by measuring changes in osmolality in body fluids such as urine and saliva. These sensors, comprising a sensing material with a microcantilever embedded within it, detect volumetric shifts upon contact with analyte molecules, which are then measured as changes in resistance. Tests using both simulated and real saliva demonstrated the potential effectiveness of this technique.

- In a related study detailed in [111], 15 male participants engaged in physical activities under different fluid intake conditions to achieve specific body mass loss targets. Saliva osmolality, total protein concentration in saliva, blood osmolality, and urine osmolality were measured for statistical analysis. The results underscored the sensitivity of salivary osmolality and total protein concentration as markers for hydration status.

2.9.2 Sweat analysis

Various methods for non-invasive dehydration assessment using sweat analysis have been explored:

- Ring et al. in [112] investigated the potential of sweat electrolyte concentrations, particularly chloride, and osmolality, as estimators of TBW loss. Their findings suggested significant correlations between sweat chloride concentration, osmolality, and TBW.

- a study by [113] observed elevated sodium, chloride, and potassium concentrations in sweat samples collected from dehydrated subjects during exercise, reinforcing the utility of sweat electrolyte measurements in assessing hydration status.

- Manimegala et al.in[114] proposed targeting changes in sodium and potassium concentrations in sweat for hydration assessment, employing sweat sensor patches based on electrochemistry and ion-selective sensing components. These patches, incorporating reference electrodes and a temperature sensor, transmit data to mobile phones for analysis.

- Further advancements include wearable devices capable of measuring skin temperature and pH levels in sweat [115], real-time colorimetric sensors for tracking sodium concentration variations [116], and specific sensors sensitive to sodium ions utilizing crown ethers [117].

- Researchers in [118] introduced a wearable ionic selective electrode sensor for tracking sodium ion concentrations in sweat. In contrast, Liu et al. [119] proposed a real-time dehydration detection system utilizing artificial sweat and a novel sweat collection device.

- The development of sweat analysis methods based on conductometric sensors integrated with voltage divider circuits [120], and the investigation of hydration monitoring through the permittivity of artificial sweat using R-freq signals [121], further contribute to the field.

- Sahina et al. in [122] explored sweat sensing with nanostructured copper oxide films, revealing significant influences of doping on the films' resistivity, suggesting their potential for hydration monitoring.

- Ria et al. in [123] introduced a novel sweat sensor featuring a capacitive mechanism with an array of interleaved electrodes optimized for wearables, demonstrating robust performance in hydration tracking.

2.9.3 Urine anaysis

In their respective studies, researchers have explored various methods for non-invasive dehydration assessment using urine analysis:

- In [124], the hydration status of 26 young male soccer players was examined through urine analysis, focusing on the validation of urine strips for practical field use. Over three days before the competition, urine color, specific gravity, and osmolality were analyzed, affirming the reliability and convenience of urine strips for athletes in monitoring hydration levels. These strips exhibited a robust correlation with laboratory-specific gravity and osmolality measures.
- In [125], a novel approach was undertaken to assess dehydration via urine color analysis, employing an Arduino Uno integrated with a TCS230 color sensor. This system interprets urine samples, aligning observed colors with a hydration scale to indicate the hydration level accurately.
- In [126], researchers developed a portable, non-invasive device equipped with a thermal sensor to evaluate dehydration and glucose levels by examining variations in urine temperature. This innovative device offers convenience and ease of use for hydration assessment.
- The system proposed in [127] utilizes a wireless standalone chemical sensor platform incorporating humidity sensors based on a nanostructured TiO2 surface for assessing sweat rate and a sensor for measuring potassium concentration in urine to gauge hydration levels. This setup is integrated into a wireless body area network for seamless data transfer among devices and internet connectivity, facilitating sharing with clinical staff or athletes' coaches. Real-life tests and calibrations demonstrated low power consumption and high efficiency in preventing dehydration.

Discussion:

In summary, fluid-based methods offer a means of evaluating hydration status through markers in bodily fluids like sweat, urine, or saliva. Saliva serves as a rapid indicator of dehydration; analysis of urine color and specific gravity has shown convenience in determining hydration levels; and sweat can be utilized for continuous monitoring during physical activities.
These techniques serve as efficient tools for quick dehydration detection, potentially reducing the requirement for costly equipment and facilitating widespread adoption.
However, collecting sweat, saliva, or urine samples may not always be convenient. It can demand time and effort and necessitate adherence to hygienic practices to prevent contamination. The presence of other substances in the fluid may lead to erroneous diagnoses. Moreover, some individuals may feel uncomfortable providing fluid samples, particularly in environments with limited privacy, rendering the technique unsuitable for daily use. Additionally, as discussed in [128], the utilization of osmometry for assessing dehydration encounters various limitations.
However, despite these challenges, fluid-based analysis retains its significance in clinical settings, providing prompt, uncomplicated, and dependable evaluations of hydration status. Practical strategies and empirical thresholds introduced in [128] aim to enhance the precision of hydration assessment, thereby augmenting its clinical applicability.

2.10 Multi-modal methods

Table 2.1 summarizes the respective advantages and disadvantages of the sensing technologies discussed. Combining different advantages and mitigating the inconveniences of individual techniques can enhance effectiveness. It is possible to achieve this by integrating multiple modalities, as demonstrated by various studies presented in this section.

2.10.1 PPG & EDA

In [129], researchers investigated dehydration by analyzing EDA and PPG data from 17 participants. EDA was measured using stainless steel electrodes connected to a skin response module, while PPG signals were captured with a wearable device worn on the left wrist. Various machine learning algorithms were applied to the data to assess the body's response to the Stroop test. In this test, participants are presented with color words printed in different colors and are asked to name the ink color while ignoring the word's meaning. Using the SVM technique, they achieved a 91.2% accuracy

Modality	Pros	Cons
EDA	• Non-invasive. • Can be integrated into daily tools. • Achieved a high accuracy.	• Susceptibility to external factors such as temperature, sweat, and emotional stress. • Vulnerability to postural changes and sudden movements.
ECG	• Widespread technology. • Non-invasive and can be integrated into daily tools.	• primarily dedicated to monitoring heart rate. • Limited validation against gold standard methods.
Fluid-Based	• Non-invasive and Affordable. • More suitable for clinical use. • Non-invasive.	• Not suitable for daily use and requires hygienic precautions. • Vulnerable to external factors. • Variability in the composition of body fluids among subjects.
BIA	• Non-invasive. and can be integrated into daily tools. • Advancement in sensor design.	• Susceptibility to external factors such as temperature and sweat. • Vulnerability to postural changes and movements.
Acoustic	• Non-invasive and can be contactless. • Achieved a high precision by measuring IVC/AO ratio.	• Not suitable for daily use nd costly. • Require specialized equipment • Requires specific cut-off thresholds tailored, for example to weight.
Radio frequency	• Ability to detect subtle changes in hydration levels. • Non-invasive and can be contactless.	• Costly and require specialized equipment. • Not suitable for daily use.
Optical	• Can be integrated into daily tools. • Non-invasive and can be contactless.	• Vulnerable to environmental factors. • Initial setup and calibration can be complex. • Limited validation against gold standard methods.
Thermal	• Non-invasive. • Can detect localized and subtle variations. • Can be integrated into daily tools.	• Vulnerable to environmental factors like ambient temperature. • Initial setup and calibration can be complex. • Limited validation against gold standard methods.

Table 2.1: Comparison of different sensing modalities for dehydration monitoring.

rate in identifying dehydration. Similarly, [130] collected EDA, skin temperature, PPG readings, and Body Mass Index (BMI) data from 16 individuals during circuit training sessions, successfully detecting different hydration levels. In [131], a combination of PPG and galvanic biosensors was used to monitor hydration levels in 240 subjects. The method was evaluated both before and after exercise. Results closely estimated TBW loss, with a mean root square error of approximately 2%. Bland-Altman analysis revealed that fewer than 5% of values deviated beyond the 95% confidence interval limits of agreement, with all observed differences distributed around the line of equality.

2.10.2 Optical & electrical tissue properties

Researchers in [132] combined bio-impedance sensing and optical spectroscopy to monitor skin hydration levels. Optical spectroscopy identifies skin water absorption peaks, while tetra-polar bio-impedance minimizes measurement errors. The device underwent in vivo and ex vivo testing, with skin dehydration associated with an increased voltage output from the optical sensor and decreased bio-impedance. Multiple linear regression models demonstrated a robust correlation between the collected data and hydration states, highlighting the effectiveness of a multi-modal approach for skin hydration monitoring.

2.10.3 Thermal & Electrical Properties

Researchers in [133] proposed leveraging the electrical and thermal characteristics of the skin for hydration monitoring. Extensive in vitro experiments were conducted using porcine skin samples, followed by in vivo tests on 20 patients, affirming the technique's ability to estimate hydration levels with solid alignment with established methods. Additionally, [134] presents an in vitro proof-of-concept utilizing ink-jet-printed interdigitated electrodes for hydration monitoring. Measurements of local surface impedance, temperature, and body impedance were obtained, and linear approximations were employed for data processing. While the results show a correlation between the measurements and hydration states, researchers note that linear approximations may be inadequate in practical settings, suggesting adopting suitable machine learning models for future investigations.

2.10.4 +3 Sensing modalities combined

Some studies have integrated three types of sensing techniques into a single solution to estimate hydration levels:

- Sabry et al. in [135] presented a novel wearable device designed for assessing hydration levels by integrating multiple sensors, including an accelerometer, magnetometer, gyroscope, galvanic skin response sensor, PPG sensor, temperature sensor, and barometric pressure sensor. The study evaluates machine learning models, such as Extra Trees, Deep Neural Networks, and RF, based on prediction error, model size, and training time. Remarkably, the Extra Trees model demonstrates superior performance with the lowest prediction error, followed by RF and Deep Neural Networks.

- Rosales et al. in [136] introduced a novel system for non-invasive hydration assessment, incorporating ultrasonic sensors, load cells, and BIA modules to collect crucial data for estimating an individual's TBW percentage. The system gathers data on height, weight, body impedance, and gender. It utilizes an artificial neural network with the scaled conjugate gradient approach to classify hydration status into under-hydrated, hydrated, or over-hydrated categories based on TBW percentage.

- Solovei et al. in [137] proposed a multifaceted approach for non-invasive, continuous monitoring of dehydration, integrating measurements of skin-relative humidity, body weight, and potassium ion concentration in urine. The system utilizes a humidity sensor based on nanostructured titanium dioxide to quantify transdermal water loss and employs a potassium-ion-selective electrode for detailed urine analysis.

- Wang et al. in [138] predicted hydration status by leveraging a combination of physiological and sweat biomarkers. Data collected from a single subject undergoing various exercises under different conditions include parameters such as heart rate (HR), core temperature, sweat sodium concentration, and total body sweat rate (TBSR), with sweat patches positioned across five different body regions. Three machine learning algorithms Logistic Regression (LR), SVM, and RF trained using different data combinations. The study finds that TBSR and HR achieve the highest accuracy in predicting hydration status, with patches placed on the arms yielding more accurate results than other body regions.

Discussion:

Combining various sensing methods enhances our ability to gauge hydration levels accurately. While individual techniques offer valuable insights, they may fall short individually due to inherent limitations and measurement variability. By integrating modalities such as bio-impedance, optical spectroscopy, and thermal monitoring, we can capture a broader spectrum of physiological parameters relevant to hydration.
Incorporating temperature data, for instance, has been shown to significantly improve the predictive accuracy of machine learning models in hydration assessment. Employing a multi-parametric approach helps compensate for the drawbacks of individual methods, thereby enhancing the overall precision and reliability of hydration prediction.

2.11 Assessments of hydration in targeted populations or body organs

In light of the significant impact of water accumulation in certain organs and among specific patient groups, it becomes imperative to devise accurate methodologies and advanced technologies for evaluating hydration status and fluid retention. This section delves into the assessment of water accumulation in particular organs, such as the heart and lungs, as well as the hydration levels across diverse patient groups:

- Hospitalized patients experiencing acute ischemic strokes often face sudden neurological impairments resulting from focal cerebral ischemia. Assessing hydration levels becomes paramount in such cases, given that dehydration can exacerbate neurological damage and influence clinical outcomes.[139] explored the feasibility of utilizing the Non-Invasive Cardiac Output Monitor (NICOM) to assess hydration status. This study compared NICOM with the blood urea nitrogen/creatinine ratio, an indirect indicator of volume reduction, demonstrating a 70% agreement between the two methods.
- Researchers in [140] investigated the potential of Electrical Impedance Tomography (EIT) to assess cerebral fluid content in patients with brain edema. Their custom EIT monitoring system, equipped with 16 electrodes, allowed for the generation of impedance distribution tomography, offering insights into brain water content by analyzing variations in impedance.
- For patients with acute heart failure, careful hydration monitoring is essential to mitigate the risk of fluid overload. Marino et al. in [141] employed bio-impedance vector analysis to evaluate the hydration status of these patients, demonstrating its effectiveness in tracking fluid reduction during the healing process post-hospital discharge.
- In the realm of wound healing, Sattar et al. in [142] developed biosensors based on body temperature and oxygenation levels to monitor wound hydration. These sensors, integrated with a fuzzy inference system, showed promising results in predicting wound hydration states, although further clinical validations are warranted.
- A wearable multi-modal sensing system, as described in [143], was utilized to monitor changes in cardiopulmonary status, mainly focusing on lung fluids and respiratory markers. This system, incorporating various components such as multi-channel lung sounds, bio-impedance spectroscopy, and impedance pneumography, demonstrated its efficacy in detecting variations in lung fluids and respiratory rate among both healthy individuals and heart failure patients.

In conclusion, precise monitoring of fluid levels in specific organs and among diverse patient groups is imperative for timely intervention and improved clinical outcomes. Further research and clinical trials are needed.

2.12 Perspectives

While many approaches have demonstrated accuracy in indicating hydration levels and have shown promising results, there is still room for improvement, and further development is crucial to focus on enhancing instrumentation by exploring new sensing techniques or refining existing ones. Many current modalities suffer from high noise and low precision, while others necessitate extensive precautions to obtain reliable measurements. Overcoming these limitations will not only enable the acquisition of high-quality data but also streamline pre-treatment procedures and facilitate data analysis.
Furthermore, it is essential to categorize the types of dehydration and identify appropriate monitoring techniques for each. For instance, blood indices may better suit chronic fluid deficits, especially in older individuals. In contrast, urine analysis may be more sensitive to sudden changes in fluid status, making it ideal for athletes who frequently experience mild dehydration post-exercise or extreme temperatures. However, techniques like EDA may pose challenges in urgent situations due to their sensitivity to cognitive stress and minor movements, rendering them less suitable for rapid hydration assessment.
Additionally, establishing specific cutoff values and thresholds based on age, height, and weight is

imperative for specific sensing modalities, such as acoustic techniques, to enhance accuracy. This necessitates extensive testing on diverse populations encompassing various body types and age groups. Moreover, integrating multiple sensor types to obtain multi-parametric data proves advantageous in overcoming the limitations of individual sensing modalities. Relying solely on one technique may not provide a comprehensive understanding of hydration states, as various physiological factors can influence hydration. Employing multi-modal methods offers a more holistic and accurate depiction of hydration status.
Furthermore, monitoring hydration states as an independent biological marker has posed challenges. Some studies have reported a lack of correlation between measurements and hydration levels, primarily due to the indirect estimation of moisture levels through other markers, making it challenging to perform statistical analysis and extract relevant features. In this regard, machine learning has shown promise, offering solutions to existing challenges.
Properly trained machine learning models, fueled by data obtained from high-precision devices, can effectively extract pertinent features and accurately estimate hydration stages, thus overcoming current limitations and enhancing overall efficacy.

2.13 Conclusion

This chapter delves into the advancements made in non-invasive hydration assessment, exploring various sensing techniques and combinations. It presents the different work done in each field and the results achieved, along with an overall representation of the advantages and limitations of each technique. By addressing the limitations of different approaches, several paths for research are opened, increasing the accuracy of various methods. Additionally, it highlights applications in targeted populations and specific organs. Finally, it outlines future perspectives in this expansive field, highlighting potential avenues for further research and development.

Chapter 3

The Proposed Technique

3.1 Introduction

In our study, we investigate the use of the FDC2114 module by Texas Instruments to estimate hydration levels. The FDC2114 is a high-resolution capacitance-to-digital converter released by Texas Instruments in 2019. This module is designed to measure capacitance with high precision and accuracy, making it suitable for various applications.
In this chapter, we delve into the principle of operation of the FDC2114 module, detailing its underlying technology and functionality. We also describe the experimental setup used in our study, explaining how the module provides insights into human hydration states.

3.2 Functioning of the FDC2114 module

All the details about the description and functioning of the module, the schematics, and the clocking diagrams were derived from the datasheet of the module [144].

3.2.1 Description

Capacitive sensing is an efficient, cost-effective, and high-resolution sensing technique applicable to various fields, including proximity detection, gesture recognition, and remote liquid-level sensing. One significant challenge with capacitive sensing is its susceptibility to noise. However, the FDC2114 module addresses this issue with its innovative Electro Magnetic Interference (EMI) resistant architecture, ensuring reliable performance even in noisy environments.
The FDC2114 is a versatile, multi-channel family of noise—and EMI-resistant capacitance-to-digital converters. These high-resolution, high-speed devices are designed for implementing advanced capacitive sensing solutions. They utilize a cutting-edge narrow-band architecture that provides excellent noise and interference rejection while maintaining high resolution and speed. Additionally, the FDC2114 supports a broad range of excitation frequencies, offering significant flexibility in system design. Figure 3.1 shows the FDC2114 module equipped with 2 capacitive sensors.

The devices employ an innovative narrow-band based architecture to offer high rejection of noise and interferers while providing high resolution at high speed.
Narrow-band means that the devices are designed to operate within a specific, limited range of frequencies. By focusing on a narrow bandwidth, the architecture can effectively filter out unwanted signals and noise outside of this range.

Features:

- EMI and noise Resistant Architecture.
- Maximum Output Rates for one active channel: 13.3 ksps.
- Maximum Input Capacitance: 250 nF at 10 kHz with 1 mH inductor.
- Sensor Excitation Frequency: 10 kHz to 10 MHz

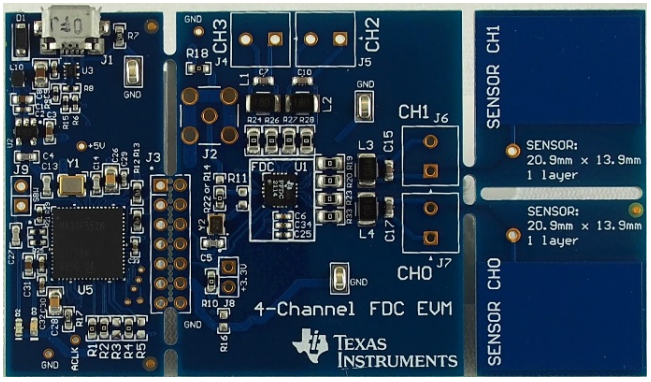

Figure 3.1: FDC2114 Module [144].

- Number of channels: 4.
- Resolution: up to 28 bits.
- System Noise Floor: 0.3 fF at 100 sps.
- Supply Voltage: 2.7 V to 3.6 V.
- Power Consumption: Active: 2.1 mA.
- Low-Power Sleep Mode: 35 uA.
- Shutdown: 200 nA.
- Temperature range: -40°C to +125°C.

3.2.2 Schematics

Figure 3.2 represents the simplified schematic of the module and its 2 sensors.

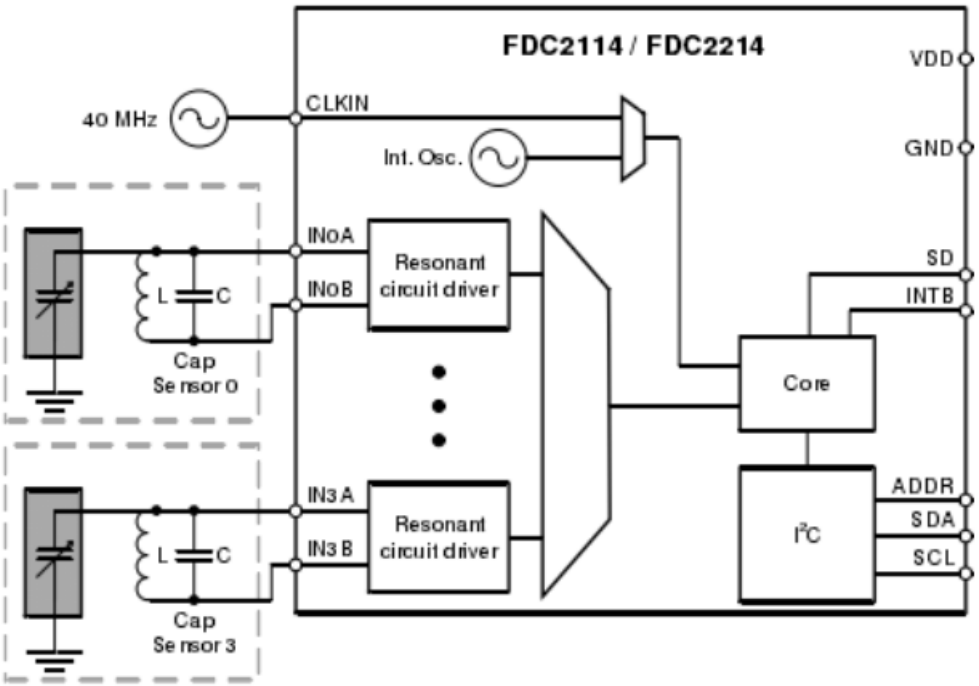

Figure 3.2: FDC2114 Module Simplified Schematic [144].

- The FDC 2114 module operates based on capacitance sensing, with its primary function being the measurement of subtle changes in capacitive sensors. The module features four channels designed to interface with capacitive sensors, with two of these channels already equipped with sensors.
- At its core, the FDC module comprises a resonant circuit consisting of capacitance and inductance, which possesses a fixed resonance frequency. This resonant circuit is linked to the capacitive sensors.
- The capacitive sensor equipped with the module comprises a metallic plate where a target object, such as a human finger, interacts.
- Placing the finger atop the plate forms a capacitance with it. This new capacitance operates in parallel with the capacitance of the LC resonant circuit, leading to shifts in the resonant frequency.
- The module itself consists of front-end resonant circuit drivers for each channel, which are followed by a multiplexer that sequentially switches through the active channels and connects them to the core responsible for measuring and digitizing the sensor frequency.
- The I2C interface is used to support device configuration and to transmit the digitized frequency values to a host processor.
- Based on the frequency value, the additional capacitance introduced is computed to characterize the target object, providing valuable data about its presence and properties.

3.2.3 Possible configuration

The FDC supports two sensor configurations. Both configurations use an LC tank to set the frequency of oscillation. A typical choice by default is an 18 μH shielded SMD inductor in parallel with a 33 pF capacitor, which results in a 6.53 MHz oscillation frequency.
In the single-ended configuration, a conductive plate is connected to IN0B, as shown in Figure 3.3. Together with a target object, the conductive plate forms a variable capacitor with the target object.

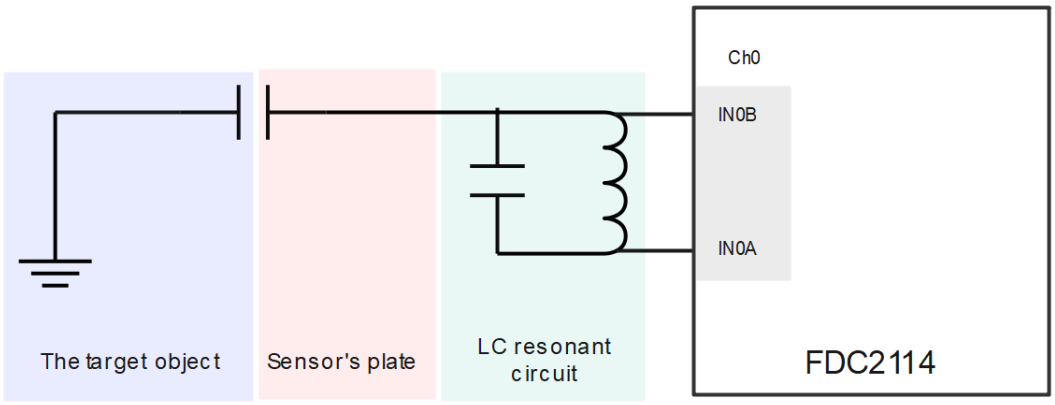

Figure 3.3: Single-ended sensor configuration.

In the differential sensor configuration, one conductive plate is connected to IN0A, and a second is connected to IN0B, as shown in Figure 3.4. Together, they form a variable capacitor.

The single-ended configuration allows a higher sensing range than the differential configuration for a given total sensor plate area. In applications in which high sensitivity at proximity is desired, the differential configuration performs better than the single-ended configuration.

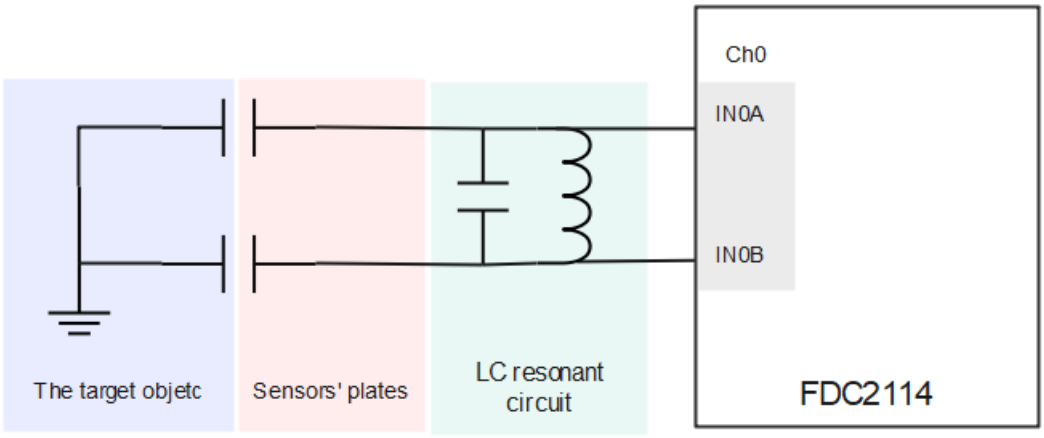

Figure 3.4: Differential sensor configuration.

3.2.4 Clocking Architecture

The primary frequencies are f_{IN}, f_{REF}, and f_{CLK}.:

- The f_{CLK} clock can be selected from either an internal or an external clock source CLK_{IN}.
- The frequency measurement reference clock, f_{REF}, is derived from the f_{CLK} source.
- For precision applications, it is recommended to use an external master clock that meets the stability and accuracy requirements of the application. The internal oscillator is suitable for applications that are cost-sensitive and do not need high precision.
- The $f_{\text{IN}x}$ clock for channel x is derived from the sensor frequency, $f_{\text{SENSOR}x}$. Both $f_{\text{REF}x}$ and $f_{\text{IN}x}$ must comply with the requirements listed in Table 3.1, depending on whether f_{CLK} (the master clock) is internal or external.

Figure 3.5 illustrates the clocking architecture of the module.

Mode	CLK_{IN}	**Valid $f_{\text{REF}x}$ range (MHz)**	**Valid $f_{\text{IN}x}$ range**
Multi-channel	Internal	$f_{\text{REF}x} < 55$	$< f_{\text{REF}x}$ / 4
	External	$f_{\text{REF}x} < 40$	$< f_{\text{REF}x}$ / 4
Single-channel	Either internal or external	$f_{\text{REF}x} < 35$	$< f_{\text{REF}x}$ / 4

Table 3.1: Clock Configuration Requirements.

3.2.5 Mathematical model

- The functioning of the FDC2114 is based on measuring the resonance frequency of a circuit composed of a constant LC resonant circuit (C_0 and L_0) shown in Figure 3.6, along with an additional capacitance C_{sen} that represents the target object.

- If no target object interacts with the sensor plate, the resonance frequency will remain constant at f_0.

$$f_0 = \frac{1}{2\pi\sqrt{L_0 C_0}}$$

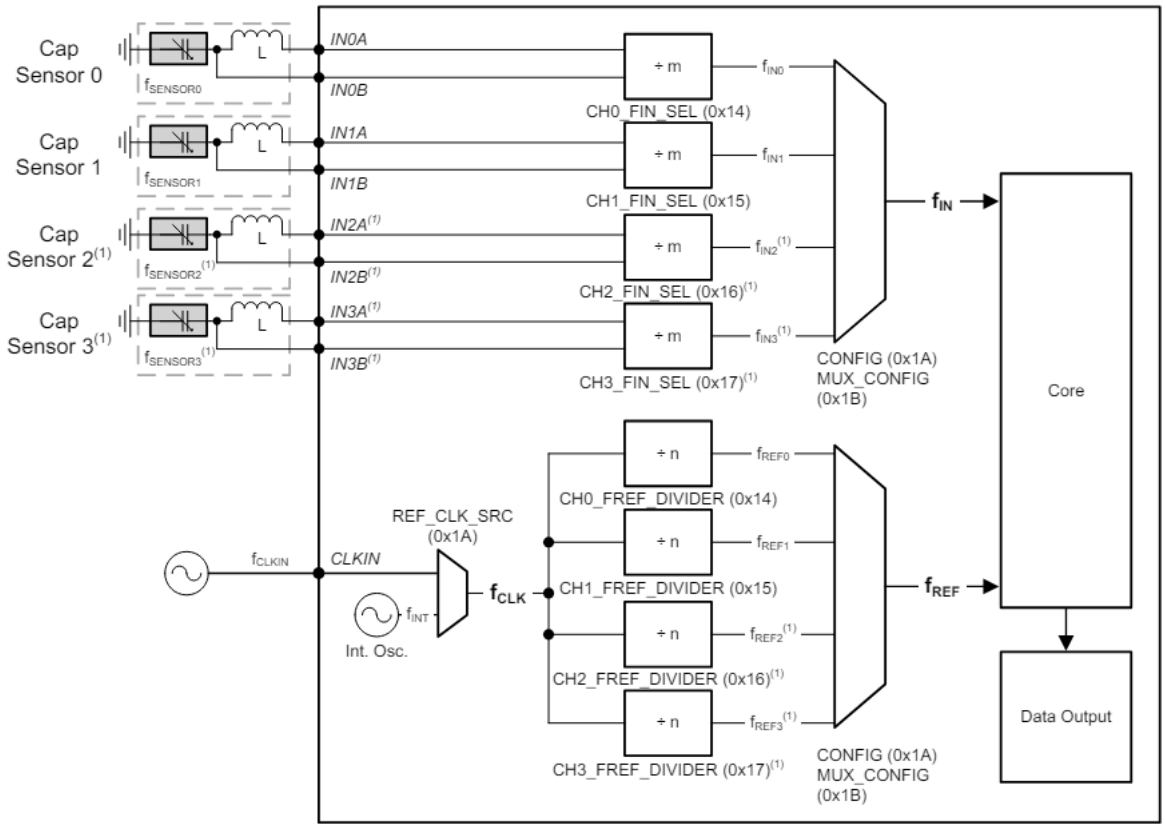

Figure 3.5: Clocking Diagram [144].

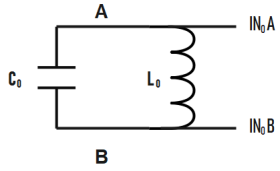

Figure 3.6: LC resonant circuit (C_0 and L_0).

- An important equivalence that we need later is as follows: if we have a capacitance C_{eq} between two points A and B, this capacitance is equivalent to two capacitors (C_1 and C_2), each with a capacitance of 2C, with a ground (GND) between them, as shown in Figure 3.7.

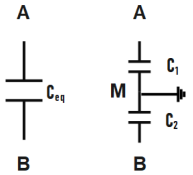

Figure 3.7: Equivalent capacitance configuration with ground.

Demonstration:

1. **Capacitors in Series:**
   When two capacitors are in series, their equivalent capacitance C_{eq} is given by:

$$\frac{1}{C_{\text{eq}}} = \frac{1}{C_1} + \frac{1}{C_2} \tag{3.1}$$

For two capacitors of $2C$ in series:

$$\frac{1}{C_{\text{eq}}} = \frac{1}{2C} + \frac{1}{2C} = \frac{1}{2C} + \frac{1}{2C} = \frac{2}{2C} = \frac{1}{C} \tag{3.2}$$

Therefore, the equivalent capacitance C_{eq} is:

$$C_{\text{eq}} = C \tag{3.3}$$

2. **Potential Differences:**
   The potential difference between point A and ground M is V_{AG}.
   The potential difference between ground M and point B is V_{GB}.
   Since the capacitors are in series:
   $$V_{AB} = V_{AM} + V_{MB} \tag{3.4}$$

   $$V_{AM} = V_{MB} = \frac{V_{AB}}{2} \tag{3.5}$$

3. **Charge stored:**
   For capacitors Q=CV, and in our case:
   For C_1 and C_2:
   $$Q = C_1 \cdot V_{AM} = C_2 \cdot V_{MB} \tag{3.6}$$

   For C_{eq}:
   $$Q_{eq} = C_{eq} \cdot V_{AB} \tag{3.7}$$

   From Equation (3.3), we have $C_1 = C_2 = 2C_{\text{eq}}$ and from Equation (3.5), we have $V_{AM} = V_{MB} = \frac{V_{AB}}{2}$ Substituting these into Equation (3.6), we get:

   $$Q = 2C_{\text{eq}} \cdot V_{AM} = 2C_{\text{eq}} \cdot V_{MB} \tag{3.8}$$

   $$Q = 2C_{\text{eq}} \cdot \frac{V_{AB}}{2} = 2C_{\text{eq}} \cdot \frac{V_{AB}}{2} \tag{3.9}$$

   Simplifying, we obtain:
   $$Q_{eq} = C_{eq} \cdot V_{AB} \tag{3.10}$$

4. **Conclusion:** The configuration with a single capacitance C between points A and B is equivalent to two capacitors, each with a capacitance of $2C$, in series with a ground between them.

- **Single-ended sensor configuration**

As seen in Section 3 of this chapter, the single-ended sensor configuration is presented below:

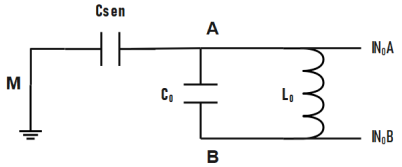

Figure 3.8: Circuit 1.

We replace the capacitance C_0 with two capacitors, each equal to 2 C_0, with a ground in between, as shown in circuit 2.

By joining the two points labeled M in circuit 2 and arranging the components for better clarity, we

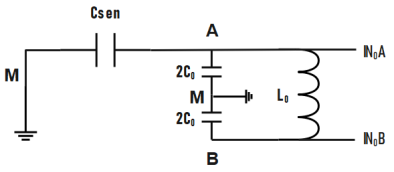

Figure 3.9: Circuit 2.

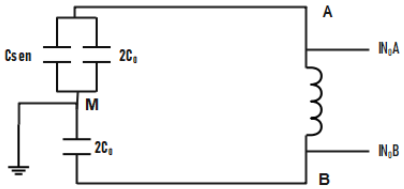

Figure 3.10: Circuit 3.

obtain circuit 3.

We have C_{sen} and $2C_0$ in parallel, both in series with $2C_0$. Those capacitors can be replaced with C_{tot} where:

$$C_{\text{tot}} = \frac{2C_0(2C_0 + C_{\text{sen}})}{4C_0 + C_{\text{sen}}} \tag{3.11}$$

Remark

A ground connection between two capacitors in series does not affect the conventional equivalent capacitance (3.1). If we introduce a ground connection between C_1 and C_2, it does not alter the formula for C_{eq}, as the ground acts as a reference point and does not affect the voltage across the capacitors $V_{AB} = V_{AG} + V_{GB}$

- **Differential sensor configuration**

As seen in Section 3 of this chapter, differential sensor configuration is presented below:

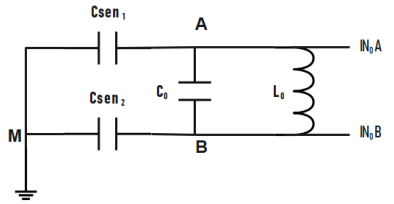

Figure 3.11: Circuit 4.

We replace the capacitance C_0 with two capacitors, each equal to 2 C_0,with a ground in between, as shown in circuit 5.

By joining the two points labeled M in Circuit 5 and arranging the components for better clarity, we obtain Circuit 6.

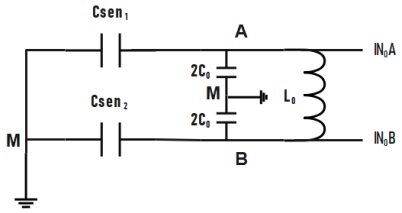

Figure 3.12: Circuit 5.

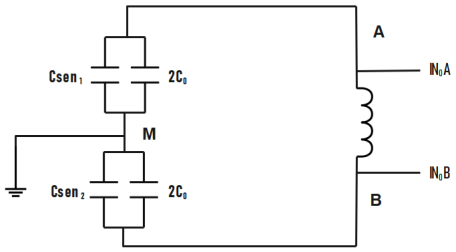

Figure 3.13: Circuit 6.

We have C_{sen1} and $2C_0$ in parallel, both in series with C_{sen2} and $2C_0$ that are in parallel. Those capacitors can be replaced with C_{tot} where:

$$C_{\text{tot}} = \frac{(2C_0 + C_{\text{sen1}})(2C_0 + C_{\text{sen2}})}{4C_0 + C_{\text{sen1}} + C_{\text{sen2}}} \tag{3.12}$$

.

- **Equivalent LC resonant circuit:**
  When the target object interacts with the sensor, the frequency is no longer equal to the resonance frequency f_0, as additional capacitance is introduced.
  For both configurations, the equivalent circuits can be represented as in Circuit 7, where each configuration has its own C_{tot}.

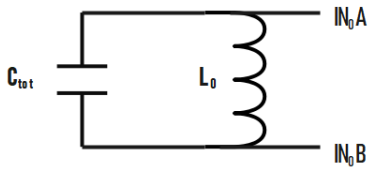

Figure 3.14: Circuit 7.

Consequently, the frequency becomes:

$$f = \frac{1}{2\pi\sqrt{L_0 C_{\text{tot}}}} \tag{3.13}$$

Based on the value of this frequency, the FDC2114 module computes the additional capacitance introduced C_{sen} that characterizes the target object.

3.3 The Setup used in our experiment

In our experiment, we used the default configuration of the module (LC resonant circuit: 18 μH shielded SMD inductor in parallel with a 33 pF capacitor, which resulted in a 6.5 MHz oscillation frequency). We used both capacitive sensors equipped with the module. Each sensor is connected to one channel, and each sensor is in a single-ended configuration, as shown in the Printed circuit board

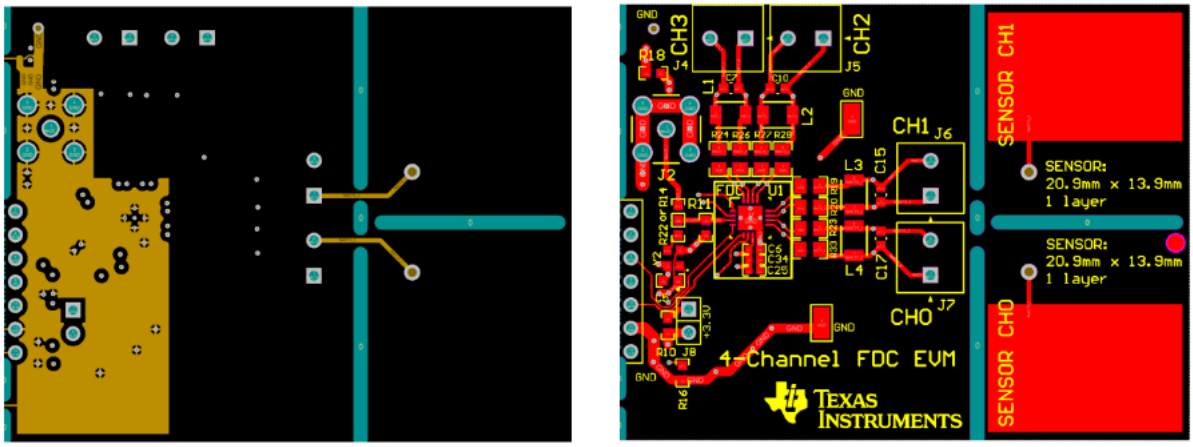

Figure 3.15: Printed circuit board layout [144].

layout in Figure 3.15 .
The clock frequency is 40 MHz. Since we are using 2 channels and multiplexing between them, the frequency of readings in each channel is 20 MHz.
Each sensor plate is connected to one channel pin, forming a single-ended configuration. The subjects' fingers are considered the target objects, and measurements from both channels are considered. Subjects simultaneously place the same type of finger (thumb, index, middle, ring, or pinky) from both hands on the corresponding sensors: the right sensor for the right hand and the left sensor for the left hand, as shown in Figure 3.16.

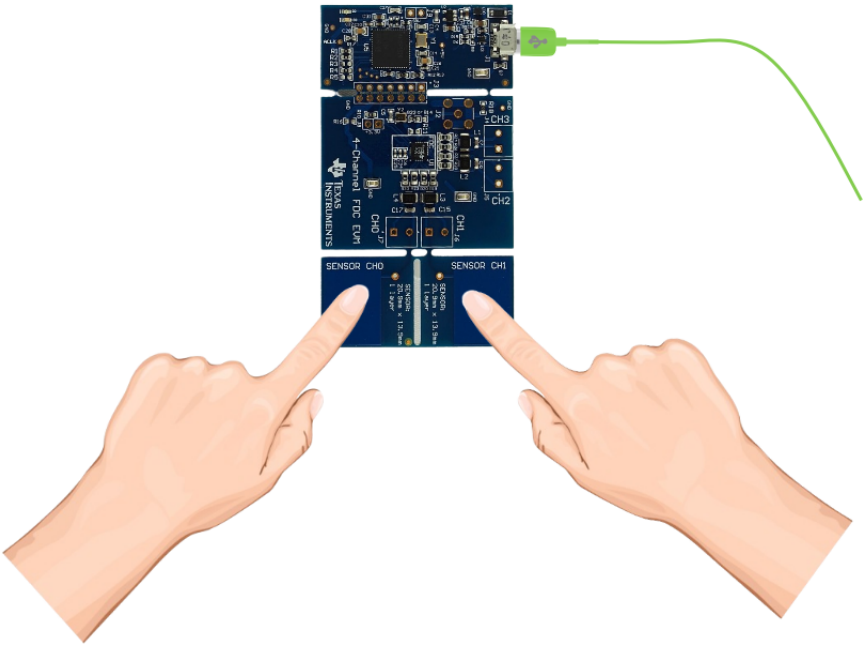

Figure 3.16: Subject placing his index fingers atop the two sensors connected to the FDC2114.

3.4 Hypothesis

The electrical properties of the human body and skin change due to fluctuations in moisture content at different hydration levels. When fingers are placed on the sensors, they induce varying frequency shifts due to the diverse capacitance created. These differences arise from the varied dielectric properties of the target objects at different hydration states.

3.5 Conclusion

It is important to understand the technology behind the module and its electronic model. Our proposed solution for estimating hydration levels relies on variations in the dielectric properties of the skin due to changes in hydration states, we aim to capitalize on this by characterizing these variations through capacitance values.
This chapter describes the module along with its electronic representations and mathematical equations. It also determines the setup used in our experiment to clearly depict the model and aid in understanding the system's functioning.

Chapter 4

Data Collection

4.1 Introduction

The most important aspect of any machine learning system is its data. In our study, we pay close attention to gathering our data and creating different datasets to train and work with. For this task, we used the FDC2114 module from Texas Instruments to collect data from 45 subjects, including people of various ages, heights, and weights.
Our data collection took place at King Abdullah University of Science and Technology during Ramadan 1445 Hijri (2024), focusing on fasting individuals and athletes participating in sports activities within the university.
In this chapter, we explore the characteristics of the subjects involved and detail the procedure we follow for data collection.

4.2 Subjects characteristics

The total number of subjects is 45, comprising 21 females and 24 males. None of the subjects have any specific medical conditions, and their activity during the day of data collection can be considered normal. Table 4.1 represents subjects' characteristics, including age, height, and weight.

	Age (Y)		**Height (m)**		**Weight (Kg)**	
Gender	**Female**	**Male**	**Female**	**Male**	**Female**	**Male**
min	21	21	1.53	1.6	41.72	55.12
max	49	49	1.73	1.88	97.86	117.04
Average	27.18	27.5	1.62	1.75	63.36	75.76
Standard deviation	6.980	6.807	0.066	0.065	9.796	14.409

Table 4.1: Subjects Characteristics

Body Mass Index

BMI is a measure that combines a person's weight and height to assess their body fatness and overall health. The BMI is calculated by dividing a person's weight in kilograms by the square of their height in meters.

$$\text{BMI} = \frac{\text{weight (kg)}}{\text{height (m)}^2}$$

Table 4.2 represents some statistics about the subjects' BMI.
Figure 4.1 illustrates the BMI scale as follows: if the BMI is less than 18.5, the person is considered underweight; if it falls between 18.5 and 25, the person is normal; if it ranges from 25 to 30, the person is overweight; and if it exceeds 30, the person is obese. According to this scale, among all the subjects, two subjects are obese, one is underweight, and five are slightly overweight, while the rest fall within the normal weight range.

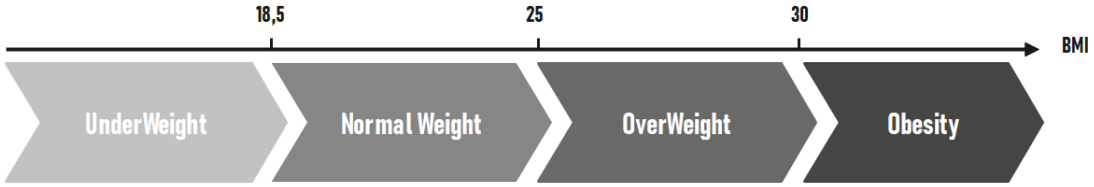

Figure 4.1: BMI scale.

	Min		Max		Average		Standard Deviation	
Gender	**Female**	**Male**	**Female**	**Male**	**Female**	**Male**	**Female**	**Male**
BMI	17.82	18.63	34.11	34.94	24.13	24.56	3.68	3.87

Table 4.2: Subjects BMI.

4.3 Ramadan data collection

Ramadan is the ninth month of the Islamic calendar. It corresponds to one of the five pillars of Islam, which is Fasting. Muslims must refrain from eating and drinking from sunrise to sunset. The fast is typically broken with the iftar meal after sunset, and preceded by the suhoor meal before dawn, ensuring proper hydration with adequate water intake.
Our study involved data collection conducted five times per day from 35 participants. Sessions were scheduled at 10 a.m., 12:30 p.m., 3 p.m., 5:30 p.m., and 8 p.m., with the final session taking place after iftar that was around 6:30 p.m. Participants were expected to experience progressive dehydration from session to session until the fifth session, where they would be adequately hydrated. The timeline for Ramadan data collection is presented in Figure 4.2.

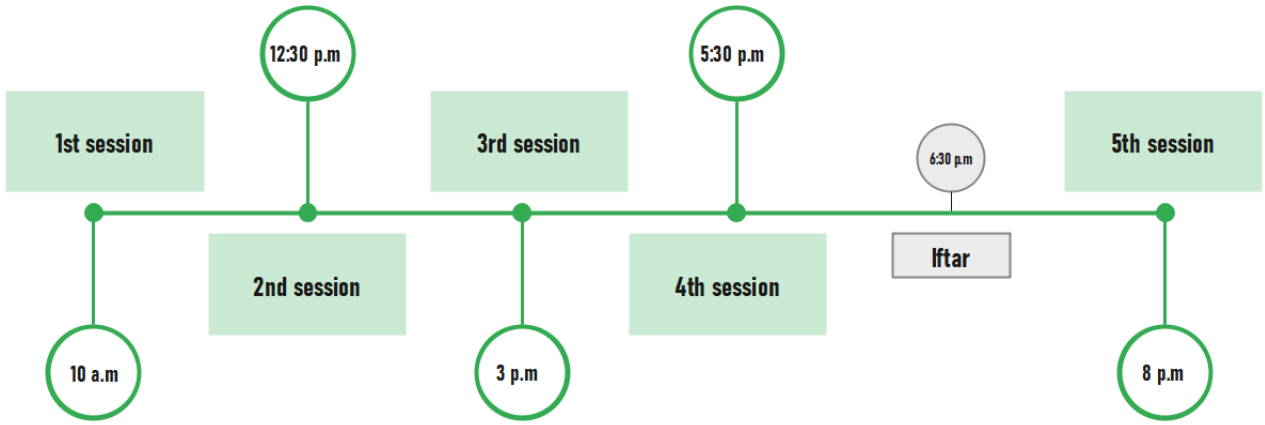

Figure 4.2: Timeline of Ramadan data collection.

The data collection measured induced capacitance between sensor plates and participants' fingers. Participants (17 Females and 18 Males) were instructed to place their fingers on the sensor plate, swiping each finger from both hands twice. Each finger remained in place for approximately 10 seconds to ensure accurate data recording, resulting in 20 samples per subject per session, considering each finger measurement as one sample, totaling 100 samples per subject. With 35 subjects, 3500 samples were collected across the five sessions, averaging 700 samples per session. Each session represents a unique hydration level, constituting different classes for multi-classification models.
Subjects were instructed to maintain stillness during measurements, wipe their hands to remove sweat, and ensure their fingers were centrally positioned on the sensor plates.

4.4 Sportspeople data collection

For the sports data collection, we compiled data from 10 participants (4 Females, 6 Males) , including 8 members of the frisbee team and 2 from the gym. Frisbee, a sport involving throwing a flying disc to teammates to score points, demands vigorous physical exertion such as running, throwing a disc, jumping, and more.
Subjects were directed to participate in a 2-hour training session with restricted water intake. Data were gathered before and after the sports session, resulting in two distinct categories: pre-exercise, adequately hydrated, and post-exercise, dehydrated. The dataset thus comprises two distinct classes suitable for binary classification.
During the data collection, participants were instructed to cleanse their fingers from sweat, maintain stillness during measurements, and position their fingers centrally on the sensor for 5 seconds to ensure precise data capture. Each session involved subjects placing their five fingers from both hands on the sensor plate three times, generating 30 samples per subject per session, considering each finger measurement as one sample. In total, 60 samples were obtained from each subject, 600 samples in total, with 300 samples for each class. The timeline for Sportspeople data collection is presented in Figure 4.3

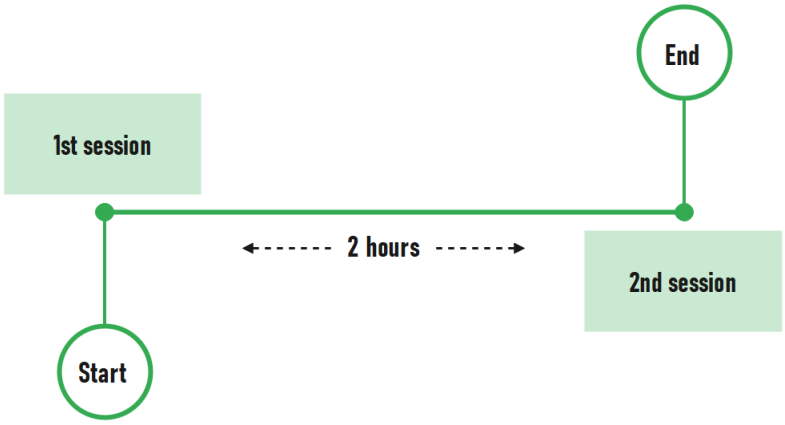

Figure 4.3: Timeline of sportspeople data collection.

4.5 Conclusion

This chapter describes the subjects involved in our study and the data collection procedure. It is essential to consider subjects with typical standard body characteristics, along with a balanced database between males and females, to ensure correct generalization later on. Several measurements were considered for each subject to ensure accurate readings and a large dataset, investigating both scenarios: dehydration acquired by fasting individuals due to water intake restrictions, and dehydration resulting from intense physical activities.

Chapter 5

Data Analysis and Preprocessing

5.1 Introduction

Data quality is crucial for achieving good results in machine learning, and preprocessing the data, even with small actions, can significantly improve results. In this chapter, we delve into the details of our data sets, starting with a visual analysis of the capacitance measurement, addressing the need for centering and normalizing the data. Additionally, we test different representations of the capacitance and various combinations of additional features to identify the best setup. We aim also to explain the trends observed in both datasets.

5.2 Exploratory data analysis

In this section, we are exploring the raw data by analyzing various recordings of fasting subjects and athletes to understand the readings.

5.2.1 Ramadan dataset

As mentioned in Chapter 4, the data was collected using two sensors, each configured in a single-ended configuration. The data from the right hand was collected using the sensor connected to CH1, while the data from the left hand was collected using the sensor connected to CH0. Therefore, readings were considered from both channels, and all subjects were asked to swipe their fingers from both hands twice.

Figure 5.1 displays the recordings from the left hand of a random subject during a random session, illustrating the different rounds of measurements. In Figure 5.2, the recording from Figure 5.1 is segmented into distinct zones, illustrating the different fingers. n represents the index of samples.
The default capacitance represents the value recorded by the module when no finger was placed atop the sensor. However, this value varied among measurements across subjects, resulting in variations not centered around the same value.

Figure 5.3 shows two distinct readings where the default values were not identical.

To address this issue, we centered the values around a standard default value by subtracting the default value from all the readings. This adjustment led to variations centered around zero, facilitating fair comparisons between measurements from different sessions.

To observe the variation in capacitance throughout the day, Figure 5.4 presents the measurements for one random subject across five sessions. For clarity, we display only one round of measurements from the left hand. 1st session is represented in blue, 2nd session in red, 3rd session in green, 4th session in purple, and 5th session in yellow.

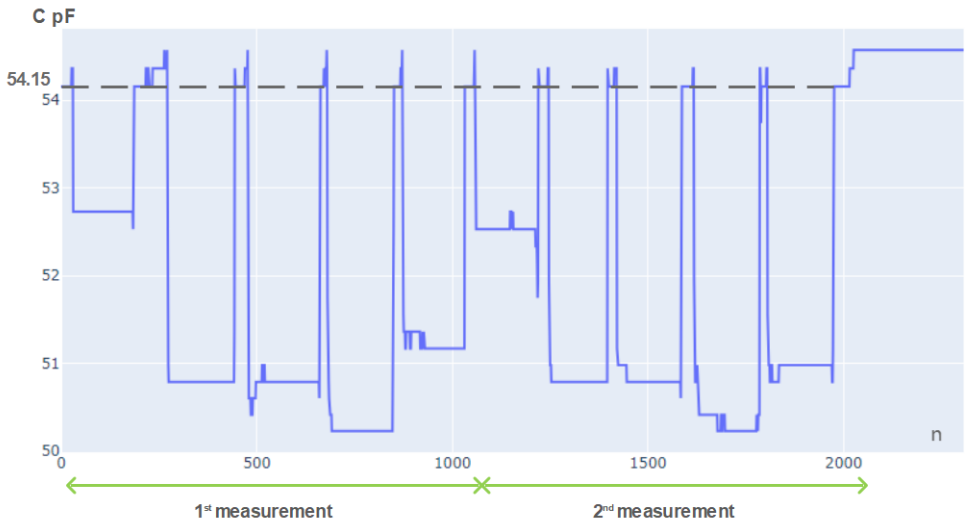

Figure 5.1: Recordings from the left hand of a random subject.

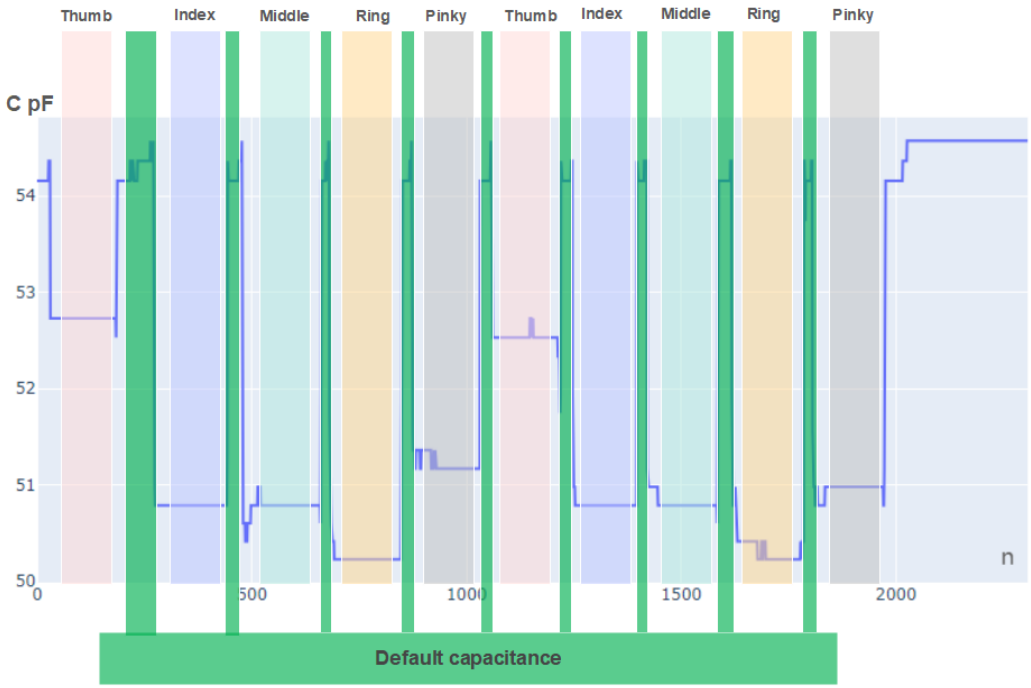

Figure 5.2: Segmentation of left hand recordings into finger zones.

In Figure 5.4, we observe that the variations are centered around zero for all five sessions. Additionally, we observe a decreasing trend in the capacitance values for the four fingers represented from Session 1 to Session 4, with a slight increase noted in Session 5 compared to Session 4.
If we associate these variations with hydration levels, we observe a trend, there is a decrease in capacitance. At the same time, subjects become progressively dehydrated from the first session (blue graph) to the fourth session (purple graph). With reduced moisture in their bodies, fewer charges are stored, leading to decreased capacitance.
However, in the fifth session (yellow graph), we observe a change in this trend. Capacitance either remains the same as in session 4, as we see for the first finger, or increases slightly. This change in the trend is due to fluid intake during iftar. In the fifth session, the body regains some moisture, although it may not be as well hydrated as in the first session, the capacitance does not decrease further.

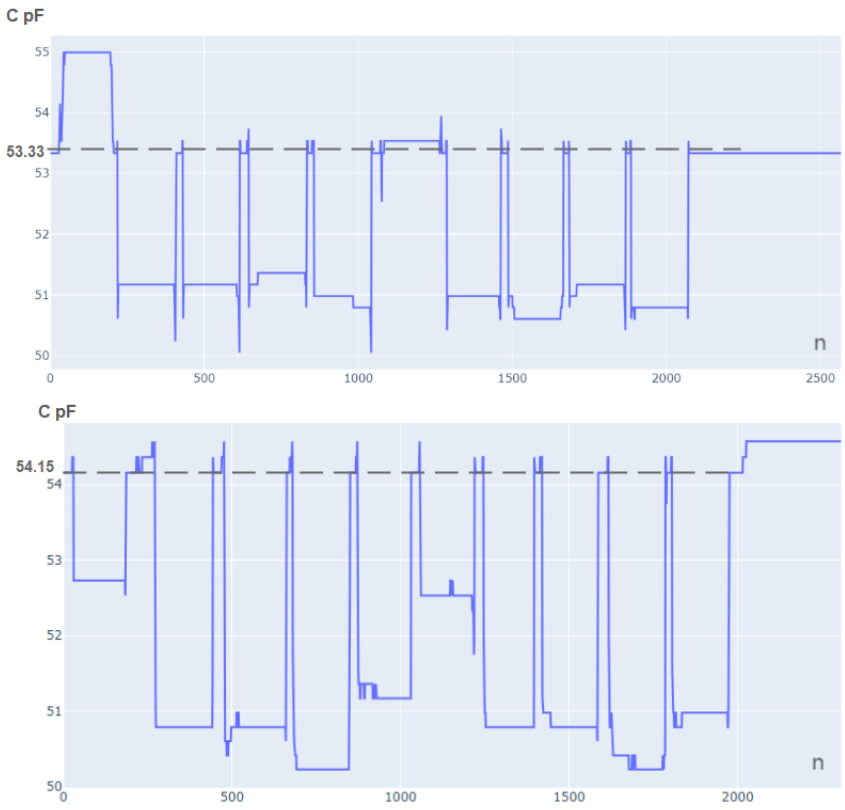

Figure 5.3: Readings with varying default values.

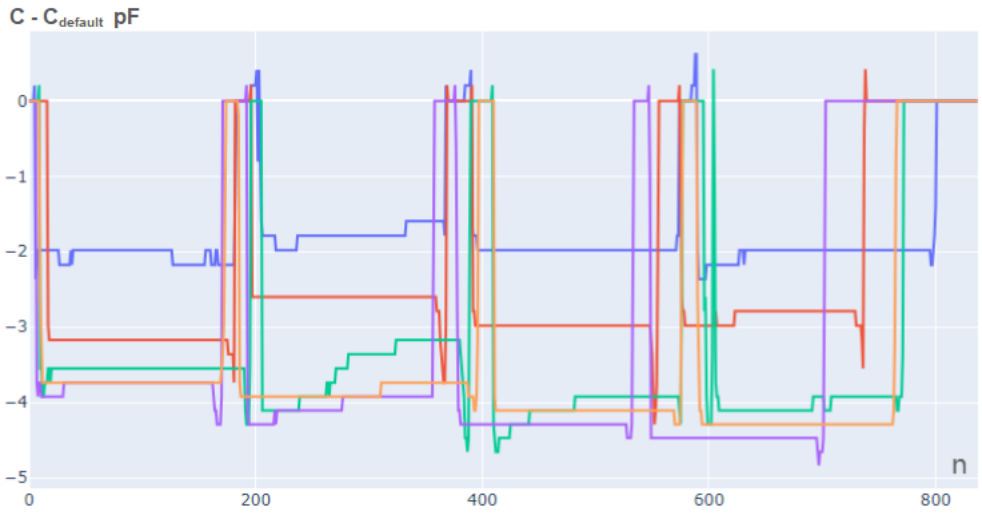

Figure 5.4: Variation in capacitance across five sessions for a single subject.

Remark

This trend was observed among the majority of the subjects; however, in some cases, it was not possible to determine whether capacitance was consistently increasing or decreasing throughout the day. Capacitance values fluctuated, with some sessions showing higher values followed by lower values in subsequent sessions. In this chapter, section 4, we aim to address these abnormalities and explain inconsistencies in our data.

5.2.2 Sportspeople dataset

All subjects were asked to swipe their fingers from both hands three times. Figure 5.5 displays the recordings from the left hand of a random subject during a random session, illustrating the different rounds of measurements. In Figure 5.6, the recording from Figure 5.5 is segmented into distinct zones, illustrating the different fingers.

Figure 5.5: Recordings from the left hand of a random subject.

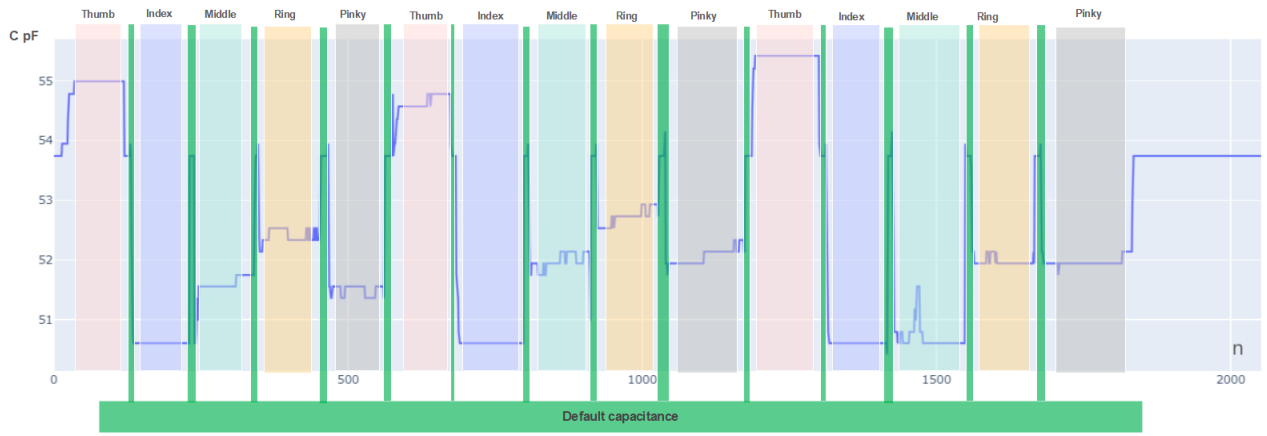

Figure 5.6: Segmentation of left land recordings into finger zones.

The default capacitance varied among measurements across different subjects, resulting in variations not centered around the same value. To address this issue, we centered the values around a common default value by subtracting the default value from all the readings.

To observe the variation in capacitance before and after the exercises, Figure 5.7 presents the measurements for one random subject across the 2 sessions. For clarity, we display only one round of measurements from the left hand. 1st session is represented in blue and 2nd session in red.

In Figure 5.7, we observe that the variations are centered around zero for both sessions. Additionally, we observe an increasing trend in the capacitance values for the five fingers from Session 1 to Session 2.

If we associate these variations with hydration levels, there is an increase in capacitance as subjects become progressively dehydrated from the first session (blue graph) to the second session (red graph). This trend is the same for all the subjects and is opposite to what we observed in fasting subjects. We aim to explain this difference in this chapter, section 4.

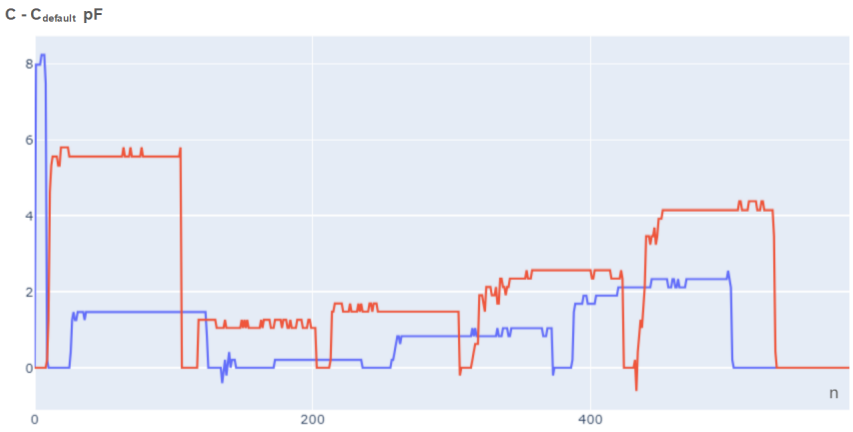

Figure 5.7: Variation in capacitance across the two sessions for a single subject.

5.3 Feature selection

In this section, we explore the optimal combination of features to achieve the highest classification accuracy. To accomplish this, we employ several classifiers with parameters in Table 5.16 while ensuring that all features are centered and normalized. This helps prevent model divergence caused by relatively high values.

First, we test different representations of the capacitance data. We explore four configurations: using one hand's recording as a single sample, removing the thumb finger from the recording due to its considerably higher value compared to the other fingers, taking each finger's data as an individual sample, and finally removing the thumb sample from the previous configuration.

Second, we explore additional features that could improve classification accuracy when combined with capacitance data. We test various combinations of features, including subjects' weight, BMI, gender, and the specific finger used in each sample.

Finally, we aim to determine the optimal data structure for achieving the best results. This involves identifying the best representation of the capacitance data and the most effective combination of additional features.

Remark

When we consider the complete recording as a sample, it was impossible to compute the LR of degree 4 due to the RAM capacity of the computer.
For RF, we tested several number of estimators (n); however, the results were approximately the same. Therefore, we present the results for n=3 and n=100.

5.3.1 Ramadan dataset

Representation of the capacitance:

In this part, we test different representations of the capacitance data for the fasting subjects. We explored four configurations: (1) using one hand's recording as a single sample, (2) removing the thumb finger from the recording, (3) treating each finger's data as an individual sample, and (4) treating each finger's data as an individual sample without the thumb fingers.

Table 5.1 presents the accuracy achieved with different classifiers across various data structures.
For the Ramadan dataset, we test binary and multi-class classification (5 classes). In the binary classification, we consider the recordings from sessions 1, 2, and 5 as hydrated and from sessions 3 and 4

Ramadan												
Data configuration	SVM		D_T		R_F n=100		KNN		L-R 1		max	
Number of classes	5	2	5	2	5	2	5	2	5	2		
(1)	0.32	0.58	0.42	0.65	0.6	0.75	0.36	0.7	0.67	0.82	**0.67**	**0.82**
(2)	0.31	0.59	0.42	0.66	0.56	0.71	0.4	0.61	0.57	0.72	**0.57**	**0.72**
(3)	0.26	0.57	0.27	0.56	0.26	0.55	0.23	0.51	0.18	0.49	**0.27**	**0.57**
(4)	0.25	0.55	0.29	0.56	0.3	0.57	0.27	0.57	0.23	0.52	**0.3**	**0.57**

Table 5.1: Classifiers' accuracy across varied data structures for fasting subjects.

as dehydrated.

The highest accuracy achieved is using linear LR while considering a complete hand recording as one sample: 67% for multi-class and 82% for binary classification.

Combination of additional features:

- In this part, We try to combine additional features with the capacitance data. we consider each finger as a separate sample. Instead of using the complete recording for each finger, we will use the average value of the recording, representing the capacitance for each finger with a single value.

  In Table 5.2, we compare classification accuracy between using the complete recording for each finger and taking an average value for each finger.

	SVM		D_T		R_F n=100		KNN		L-R 1		max	
Number of classes	5	2	5	2	5	2	5	2	5	2		
Complete recording	0.26	0.57	0.27	0.56	0.26	0.55	0.23	0.51	0.18	0.49	**0.27**	**0.57**
Average value	0.22	0.58	0.28	0.56	0.26	0.55	0.24	0.55	0.22	0.52	**0.28**	**0.58**

Table 5.2: Comparison of classification accuracy: complete recording vs. average value per finger.

From Table 5.2, we conclude that taking the average value from the complete recording is approximately the same as considering the complete recording. Indeed, for the majority of the recordings, the value of the capacitance is consistent. Therefore, no additional information exists in the complete recording.
The readings were meticulously treated one by one to remove the noisy parts.

- For the Ramadan data collection, we measured the subjects' weight for each session. Here, We apply classifiers to the weight changes data alone, as well as to the changes in BMI alone.

  Table 5.3 represents the accuracy of classification for the weight changes and the BMI changes.

	SVM		D-T		R-F n=3		R F n=100		KNN		L-R 4		L-R 1		MAX	
Number of classes	5	2	5	2	5	2	5	2	5	2	5	2	5	2		
Weight changes	0.15	0.56	0.67	0.89	0.7	0.88	0.67	0.88	0.73	0.9	0.18	0.52	0.20	0.55	0.7	0.89
BMI changes	0.16	0.49	0.74	0.92	0.75	0.93	0.73	0.92	0.8	0.95	0.19	0.5	0.19	0.54	0.8	0.95

Table 5.3: Classifiers' accuracy across weight and BMI changes.

We can see that relying solely on weight changes throughout the day can achieve high accuracy: 89% for weight changes and 95% for BMI changes, proving that weight loss is a reliable indicator of hydration states.

- In this part, we aim to determine whether adding capacitance values to the weight changes, which already yield good classification results, will improve or deteriorate the accuracy. This help us understanding if capacitance data is useful for classifying hydration levels.

  In Table 5.4, we compare the classification accuracy of weight changes and BMI combined with capacitance.

	SVM		D-T		R-F n=3		R F n=100		KNN		L-R 4		L-R 1		MAX	
Number of classes	5	2	5	2	5	2	5	2	5	2	5	2	5	2		
Capacitance values + Weight changes	0.23	0.55	0.79	0.91	0.54	0.79	0.61	0.8	0.46	0.73	0.27	0.57	0.2	0.54	0.79	0.91
Capacitance values + BMI changes	0.23	0.57	0.82	0.93	0.61	0.8	0.64	0.82	0.46	0.74	0.2	0.51	0.24	0.56	0.82	0.93

Table 5.4: Classifiers' accuracy across weight and BMI changes with capacitance values.

We can see that introducing the capacitance data does not deteriorate the results for weight and BMI changes. We still achieve high classification accuracy, up to 93% for binary classification. We can conclude that capacitance can be a reliable indicator of hydration states for fasting subjects

- In this part, we compare the classification accuracy of different features added to the capacitance data, including finger type, gender, weight, and BMI. In this analysis, weight and BMI are treated as constant values for each subject to ensure that the results are based on capacitance and not weight changes.

  Table 5.5 presents the classification accuracies for different combinations of features.where (C) refers for capacitance value, (F-T) for type of finger, (G) for gender, and (w) for weight.

  From Table 5.5, we can observe that adding the type of finger as a feature deteriorates the results instead of enhancing them. Using weight as a feature yields better results than using BMI. Adding the gender feature slightly enhances the results.

  Among all the different configurations, the one that produces the best results is when we combine capacitance with the weight and gender of each subject, achieving 38% accuracy for multi class classification and 64% for binary classification.

Configuartion					SVM		D-T		R-F n=3		R F n=100		KNN		L-R 4		L-R 1		MAX	
C	F-T	G	W	B																
					0.25	0.55	0.36	0.49	0.37	0.63	0.34	0.6	0.25	0.53	0.23	0.55	0.24	0.56	0.37	0.63
					0.23	0.52	0.36	0.64	0.36	0.62	0.35	0.61	0.29	0.6	0.22	0.52	0.2	0.53	0.36	0.64
					0.2	0.48	0.32	0.59	0.32	0.61	0.32	0.59	0.24	0.56	0.2	0.53	0.22	0.56	0.32	0.61
					0.26	0.54	0.35	0.61	0.33	0.61	0.34	0.61	0.27	0.58	0.21	0.54	0.2	0.52	0.35	0.61
					0.25	0.59	0.27	0.56	0.27	0.57	0.27	0.6	0.26	0.54	0.22	0.52	0.2	0.54	0.27	0.6
					0.24	0.56	0.28	0.56	0.26	0.57	0.26	0.57	0.24	0.56	0.21	0.55	0.22	0.57	0.28	0.57
					0.23	0.56	0.36	0.62	0.33	0.59	0.35	0.61	0.25	0.57	0.21	0.51	0.19	0.55	0.36	0.62
					0.22	0.55	0.32	0.6	0.33	0.59	0.32	0.61	0.25	0.56	0.21	0.54	0.2	0.54	0.33	0.61
					0.25	0.58	0.35	0.62	0.36	0.63	0.38	0.64	0.31	0.61	0.23	0.59	0.19	0.57	0.38	0.64
					0.25	0.58	0.34	0.61	0.35	0.62	0.36	0.64	0.3	0.6	0.22	0.56	0.19	0.54	0.36	0.64

Table 5.5: classification accuracy with different feature combinations added to capacitance data.

5.3.2 Sportspeople dataset

Representation of the capacitance:

Similarly, we test different representations of the capacitance data for the sportspeople. We explored four configurations: (1) using one hand's recording as a single sample, (2) removing the thumb finger from the recording, (3) treating each finger's data as an individual sample, and (4) treating each finger's data as an individual sample without the thumb fingers.

Table 5.6 presents the accuracy achieved with different classifiers across various data structures.

Sportspeople						
Data configuration	SVM	D_T	R_F	KNN	L-R 1	max
(1)	0.7	0.83	0.83	0.87	0.87	**0.87**
(2)	0.7	0.7	0.83	0.83	0.87	**0.87**
(3)	0.61	0.7	0.76	0.68	0.67	**0.76**
(4)	0.68	0.72	0.8	0.65	0.66	**0.8**

Table 5.6: Classifiers' accuracy across varied data structures for Sportspeople.

The highest accuracy achieved is using linear LR and KNN while keeping or removing the thumb finger from the complete hand recording: 87% binary classification

Combination of additional features:

- In this part, we try to combine additional features with the capacitance data. Here, we consider each finger as a separate sample. Instead of using the complete recording for each finger, we use the average value of the recording, representing the capacitance for each finger with a single value.

  In Table 5.7, we compare the classification accuracy by using the complete recording for each finger and taking an average value for each finger.

Data configuration	SVM	D_T	R_F	KNN	L-R 1	max
Complete recording	0.61	0.7	0.76	0.68	0.67	**0.76**
Average value	0.65	0.7	0.68	0.73	0.66	**0.73**

Table 5.7: Comparison of classification accuracy: complete recording vs. average value per finger.

From Table 5.7, we conclude that taking the average value from the complete recording is approximately the same as considering the complete recording. Indeed for the majority of the recordings, the value of the capacitance is consistent, therefore no additional information exists in the complete recording.
The readings were meticulously treated one by one to remove the noisy parts.

- In this part, we compare the classification accuracy of different features added to the capacitance data, including finger type, gender, weight, and BMI. In this analysis, we consider the weight and BMI constant values for each subject to ensure that the results are based on capacitance and not weight changes.

  Table 5.8 presents the classification accuracies for different combinations of features.

Configuartion					SVM	D-T	R-F n=3	R F n=100	KNN	L-R 4	L-R 1	MAX
C	F-T	G	W	B								
					0.67	0.68	0.65	0.63	0.64	0.67	0.7	0.7
					0.6	0.75	0.66	0.7	0.61	0.66	0.64	0.75
					0.62	0.65	0.64	0.65	0.6	0.68	0.6	0.68
					0.61	0.67	0.66	0.62	0.59	0.65	0.71	0.71
					0.6	0.72	0.69	0.71	0.75	0.64	0.68	0.72
					0.63	0.71	0.69	0.64	0.6	0.65	0.62	0.71
					0.63	0.68	0.66	0.66	0.64	0.65	0.62	0.68
					0.6	0.75	0.7	0.64	0.61	0.63	0.66	0.75
					0.63	0.75	0.68	0.69	0.61	0.64	0.65	0.75
					0.67	0.73	0.7	0.66	0.62	0.68	0.69	0.73

Table 5.8: classification accuracy with different feature combinations added to capacitance data.

From the results in Table 5.8, we can observe that adding the finger type does not enhance the results. Using weight as a feature yields better results than using BMI. Adding the gender feature slightly enhances the results.

Among all the different configurations, the highest classification accuracy of 75% is achieved when capacitance is combined with either the weight and gender of each subject, weight only, or the type of finger, gender, and BMI.

5.4 Final configuration

From the exploration of different data structures and additional features in both fasting subjects and sportspeople, we found that considering one hand as a sample and adding the weight and subject's gender yield the best classification accuracy.

Table 5.9 presents the classification results using this final setup.

	SVM		D_T		R_F n=100		KNN		L-R 1		max	
Number of classes	5	2	5	2	5	2	5	2	5	2		
Ramadan dataset	0.42	0.65	0.48	0.74	0.64	0.76	0.36	0.62	0.72	0.87	**0.72**	**0.87**
Sportspeople dataset	/	0.83	/	0.83	/	0.87	/	0.91	/	0.92	**/**	**0.92**

Table 5.9: Classification results using final setup: one hand as a sample with weight and gender features.

Considering the final chosen setup, the classification results can be considered promising. The capacitance value, along with the additional features, proves to be a reliable indicator of hydration levels, achieving 72% accuracy for multi-class and 87% for binary classification in the Ramadan dataset, and 92% for binary classification in sportspeople. In both datasets, the classifier that performs best is linear LR.

Loss value

To compute the loss, we use sparse categorical cross-entropy, suitable for multi-class tasks where labels are provided as integers. Sparse categorical cross-entropy saves memory space by considering only the non-zero elements of the true labels. The formula to compute the loss is as follows:

$$L = -\frac{1}{N}\sum_{i=1}^{N}\log(p_{i,\text{true}})$$

-N is the number of samples in the test set.
-$p_{i,\text{true}}$ is the predicted probability of the true class for sample i.

For the linear LR model (multi-class), the computed loss is :

- L= 1.6 for Ramadan dataset.
- L= 0.44 for sportspeople.

To judge whether the loss values are low or not, it is important to compare it with other values. For our problems, there are no conventional benchmarks to compare this computed loss with. However,

given the high accuracy of classification, it suggests that these loss values may indicate good results. To further assess the significance of this value, we compare it in Table 5.10 with loss values for other configurations trained on the same LR model and exhibits lower accuracy.

Ramadan		
	Accuracy (5 class)	Loss
(1)	**0.67**	1.69
(2)	**0.57**	1.78
(3)	**0.18**	2.24
(4)	**0.23**	2.1
Final setup	**0.72**	1.6

Sportspeople		
	Accuracy	Loss
(1)	0.87	0.65
(2)	0.87	0.58
(3)	0.67	0.95
(4)	0.66	0.87
Final setup	**0.92**	0.44

Table 5.10: Comparison of loss values for different configurations for linear LR model.

(1) using one hand's recording as a single sample,
(2) removing the thumb finger from the recording,
(3) treating each finger's data as an individual sample, and
(4) treating each finger's data as a sample without the thumb fingers.

As we can see in the table, the lowest loss achieved in both the Ramadan and Sportsman datasets is indeed for the final setup, which achieves a high classification accuracy.

Confusion matrix:

Table 5.11 shows the confusion matrix for the 5-class classification among fasting subjects.

		Predicted Labels				
		1	2	3	4	5
True Labels	1	**0.79**	0.04	0	0.01	0.16
	2	0.02	**0.88**	0.09	0.01	0
	3	0.11	0.13	**0.61**	0.06	0.09
	4	0.02	0.07	0.21	**0.67**	0.03
	5	0.13	0.08	0.02	0.05	**0.72**

Table 5.11: Confusion matrix for 5-class classification among fasting subjects.

For reference, the number of samples from each class in the test set is as follows: class 1 (30 samples), class 2 (21 samples), class 3 (31 samples), class 4 (30 samples), and class 5 (28 samples). The test set is unbalanced because the samples were chosen randomly from the dataset.

From the confusion matrix, we can observe that for each class, the majority of samples (more than 60%) are correctly predicted. For the incorrect predictions, class 1 was mostly confused with classes 2

and 5, representing states where subjects were more hydrated than in classes 3 and 4. Classes 2 and 3 were often confused with each other, as they represent successive levels of hydration. Class 4 was mainly confused with class 3, as both are considered dehydrated states. Samples from class 5 were mostly confused with samples from classes 1 and 2 since in session 5, subjects regained some hydration after Iftar.

Table 5.12 represents the confusion matrix for binary classification, where samples labeled 1, 2, and 5 are considered hydrated (class 1), and samples labeled 3 and 4 are considered dehydrated (class 2).

	Hydrated (%)	Dehydrated (%)
Hydrated (%)	94.48	5.51
Dehydrated (%)	22,67	77.32

Table 5.12: Confusion matrix for binary classification among fasting subjects.

The confusion matrix illustrates that the model consistently predicts the hydrated class accurately, whereas it faces challenges in accurately classifying the dehydrated class, often misclassifying it as hydrated. This suggests that class 1 has unique features or characteristics that distinguish it from class 2. However, the model encounters difficulty in predicting some samples from class 2 due to similarities or overlaps in features with samples from class 1.

Table 5.13 shows the confusion matrix for sportspeople, where measurements from session 1 are considered hydrated and from session 2 dehydrated.

	Hydrated (%)	Dehydrated (%)
Hydrated (%)	100	0
Dehydrated (%)	16,66	83,33

Table 5.13: Confusion matrix for hydration state classification among sportspeople.

For reference, the number of samples from each class in the test set is as follows: class 1 (12 samples) and class 2 (12 samples).

Similarly to the findings in fasting subjects, the confusion matrix illustrates that the model consistently predicts the hydrated class accurately. In contrast, it faces challenges in accurately classifying the dehydrated class. This suggests that class 1 has unique features or characteristics that distinguish it from class 2. However, the model encounters difficulty in predicting some samples from class 2 due to similarities or overlaps in features with samples from class 1.

Cross-population tests

In this part, we attempt to reverse the test sets from both datasets (Ramadan and sportspeople) to evaluate how well the LR models generalize to different populations.

Table 5.14 illustrates the classification accuracy of models trained on sportspeople subjects and tested on fasting subjects, and vice versa.

	Ramdan test set	Sportspeople test set
Model trained on Training set of Ramadan data set	**0.87**	**0.41**
Model trained on Training set of Sportspeople data set	**0.52**	**0.92**

Table 5.14: Classification accuracy of generalization across Ramadan and sportspeople datasets.

We can observe that reversing the test set in these two datasets does not yield good results. The model trained on fasting subjects achieves only 41% accuracy when tested on sportspeople, and the model trained on sportspeople achieves 52% accuracy in classifying fasting subjects.
This aligns with the exploratory data analysis, where we noticed a contradiction between the trend in fasting subjects and sportspeople. We observed that capacitance was decreasing with reduced hydration levels in fasting subjects; however, it was increasing in sportspeople.

Computational requirements

For the linear LR model, Table 5.15 presents the memory requirements and the response time needed to estimate one sample.

$$\text{Number of parameters} = \text{weights} + \text{ bias} = nk + k$$

n number of features of a single sample.
k number of classes.
Each parameter is a float 64 (8 bytes).

	n	**k**	**Number of parameters**	**Memory space (MB)**	**Response time (s)**
Fasting subjetcs	3286	5	16435	0.125351	0.100732
Sportspeople	1021	2	2044	0.015579	0.024064

Table 5.15: Memory Requirements and Response Time for LR Models.

- The memory space required for the LR model depends on the number of features and classes within the dataset. The Ramadan dataset has more classes and features, making the model larger than the Sportspeople dataset, which is binary.
- The number of features is larger in the Ramadan dataset because the subjects left their fingers on the sensor for approximately 10 seconds, leading to longer recording, unlike the sportspeople, who left it for about 5 seconds due to time constraints.
- The time to estimate one sample is 5 times shorter with the sportspeople dataset because the model is less complex.

5.5 Trends explanation

After visualizing the recording of the capacitance value in fasting subjects, we notice a decreasing trend from session 1 to session 4, with a slight increase in session 5. This indicates that capacitance is proportional to hydration states; the more moisture the body contains, the higher the capacitance. However, we observe the opposite trend in sportspeople, where capacitance increases as subjects become dehydrated. We confirm this opposition by switching the test set in the linear regression models, which resulted in poor results.

In fact, dehydration due to fasting and exercising differs. While subjects fast with regular body activity, internal organs such as the kidneys retain water after detecting dehydration. The more dehydrated the body becomes, the more water is retained in internal organs, leading to symptoms such as dry skin and increased thirst, Therefore, the body, and especially the skin, store less charges.

In sportspeople, during exercise, the body sweats profusely to regulate temperature. Sweat, produced by eccrine glands, as explained in Chapter 1, contains water and electrolytes. These glands release sweat onto the skin to cool the body and continue to do so even after the exercises until the body temperature is regulated, meaning that even after we clean the subjects' fingers to take measurements right after the training, sweat glands in the skin still retain water, leading to store more charges when the fingers are atop the sensor.

We noted in a remark in this chapter's section 1 that the trend in fasting subjects was not present among all the subjects. Indeed, if we consider the effect of sweat that causes an increase in capacitance, fasting subjects probably also experienced sweating. Some subjects came to take measurements after running or staying outside in hot weather, which means that abnormalities in the trend can be due to sweat, causing rises in capacitance instead of the consistent decrease while getting dehydrated.

5.6 Conclusion

In conclusion, capacitance measurements using the FDC2114 module show promise as a tool to assess hydration states. Achieving high classification accuracies demonstrates the potential of this technique. Moreover, incorporating information about gender and weight contributed to improving the results. This is because, in general, males tend to have larger finger sizes than females, and finger size can also vary depending on a person's weight. These additional features helped the models mitigate inter-finger variability, as capacitance is also related to the contact area of the fingers with the plates.
We have also identified a contradiction between the trends observed in fasting subjects and sportspeople. This disparity is attributed to sweating, which results in the retention of water in sweat glands present on the skin surface. These glands, filled with water and electrolytes, store more charges, leading to higher capacitance values.

Classifier	Characteristics	Classifier	Characteristics
SVM	• Regularization Parameter: 1.0 • Kernel Function: RBF kernel • Degree of the Polynomial Kernel Function: 3 • Independent Term in Kernel Function: 0.0 • shrinking: True • probability: False • Tolerance: 1e-3 • Verbose Output: False • Maximum Number of Iterations: none • Decision Function Shape: One-Vs-Rest • Shuffling Data: random-state	**Decision tree (DT)**	• Criterion: Gini impurity • Splitter: Best split strategy • Max Depth: none • Min Samples Split: 2 • Min Samples Leaf: 1 • Min Weight Fraction Leaf: 0.0 • Max Features: none • Shuffling Data: random-state • Max Leaf Nodes: none • Min Impurity Decrease: none • Min Impurity Split: 0 • Verbose: 0
RF	• Number of Estimators: 100 or 3 • Criterion: Gini impurity • Splitter: Best split strategy • Maximum Depth: none • Minimum Samples Split: 2 • Minimum Samples Leaf: 1 • Minimum Weight Fraction Leaf: 0.0 • Maximum Features: none • Maximum Leaf Nodes: none • Minimum Impurity Decrease: 0.0 • Minimum Impurity Split: none • Bootstrap: True • Out-of-Bag Score: False • Shuffling Data: random-state • Verbose: 0 • Warm Start: False • Cost-Complexity Pruning Alpha: 0.0	**LR**	• Solver: Limited memory Broyden Fletcher Goldfarb Shanno • Maximum Number of Iterations: none • Dual Formulation: False • Tolerance: 1e-3 • Warm Start: False • the degree of polynomial features:1 or 4 • Shuffling Data: random-state • Verbose: 0
KNN	• The number of nearest neighbors: 5 • Distance Metric: Euclidean distance • Weights: Uniform weights		

Table 5.16: Parameter Settings for the Classifiers.

Chapter 6

Data Augmentation and Neural Network Models

6.1 Introduction

Data augmentation serves as a virtual means to expand datasets, allowing for more samples derived from a few originally gathered ones. It not only reduces the effort required to collect more data but also tests the resilience of datasets against external factors such as noise, shifts, and other variations. Data augmentation is particularly crucial when dealing with small datasets, as both deep learning and even simple neural networks demand a considerable amount of data to train effectively.
In this chapter, we aim to apply data augmentation techniques to our datasets and evaluate the performance of classifiers. Additionally, we explore using augmented data in training neural network models.

6.2 Data augmentation

6.2.1 Data augmentation techniques

For the data augmentation process, we investigate three types of augmentation techniques that are suitable for our data:

- Gaussian Noise: noise level = 0.01, mean = 0
  Real-world capacitance measurements are often subjected to random noise due to electronic fluctuations or environmental interferences. By adding Gaussian noise, we simulate these realistic variations, helping the model become more robust to such fluctuations during inference.
  Figure 6.1 represents a random sample (1 hand recording) before and after applying Gaussian noise.

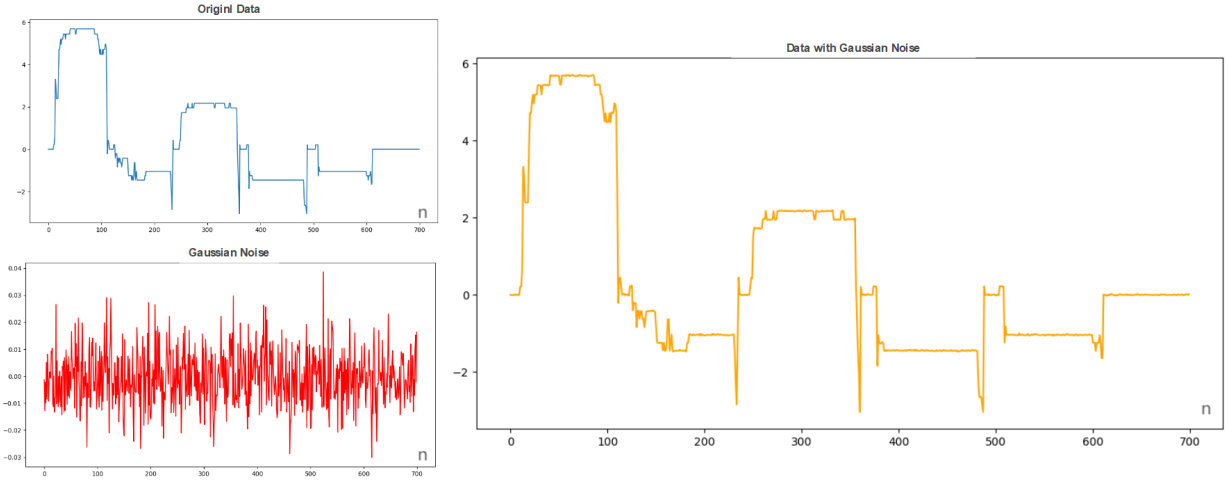

Figure 6.1: A random recording before and after adding Gaussian noise.

- Random Scaling: factor ranging from 0.9 to 1.1.
  Scaling the data simulates changes in the sensitivity of the measurement system or variations in the scale of recording due to different operating conditions. This helps the model to become invariant to different scaling factors.
  Figure 6.2 represents a random sample (1 hand recording) before and after applying random scaling.

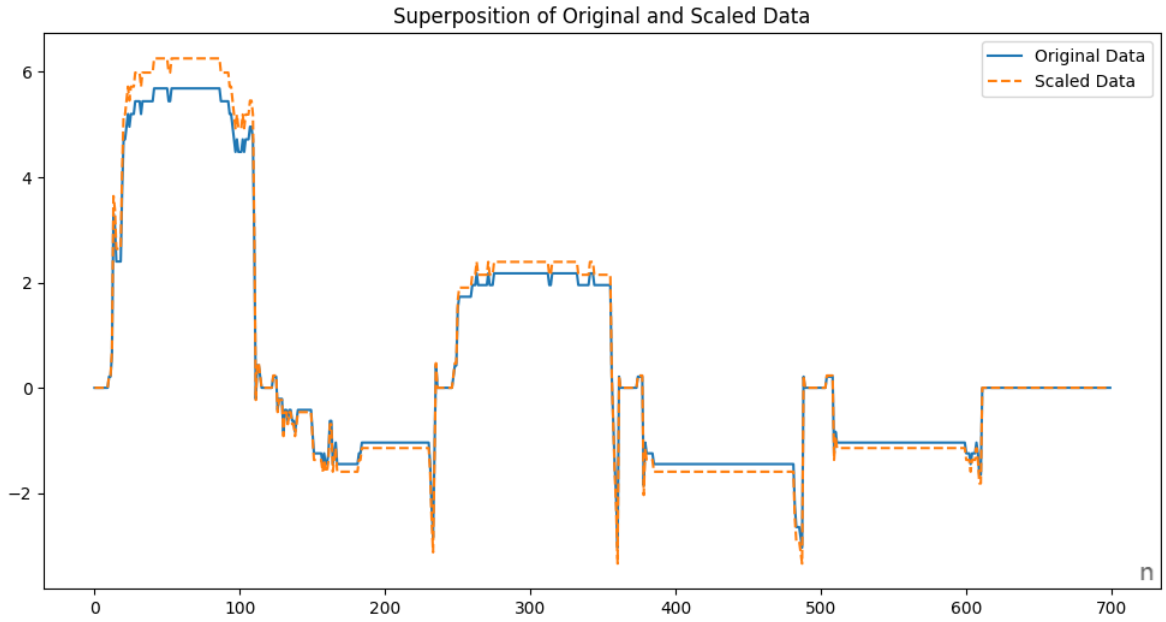

Figure 6.2: A random recording before and after scaling (scaling factor=1.1).

- Random Shifting: shift value ranging from -0.1 to 0.1.
  Shifts in the data can represent baseline drifts or offsets that may occur due to calibration errors or changes in the reference levels. Training the model with shifted data helps it learn to identify and estimate accurately even with shifts' presence.
  Figure 6.3 represents a random sample (1 hand recording) before and after applying random shifting.

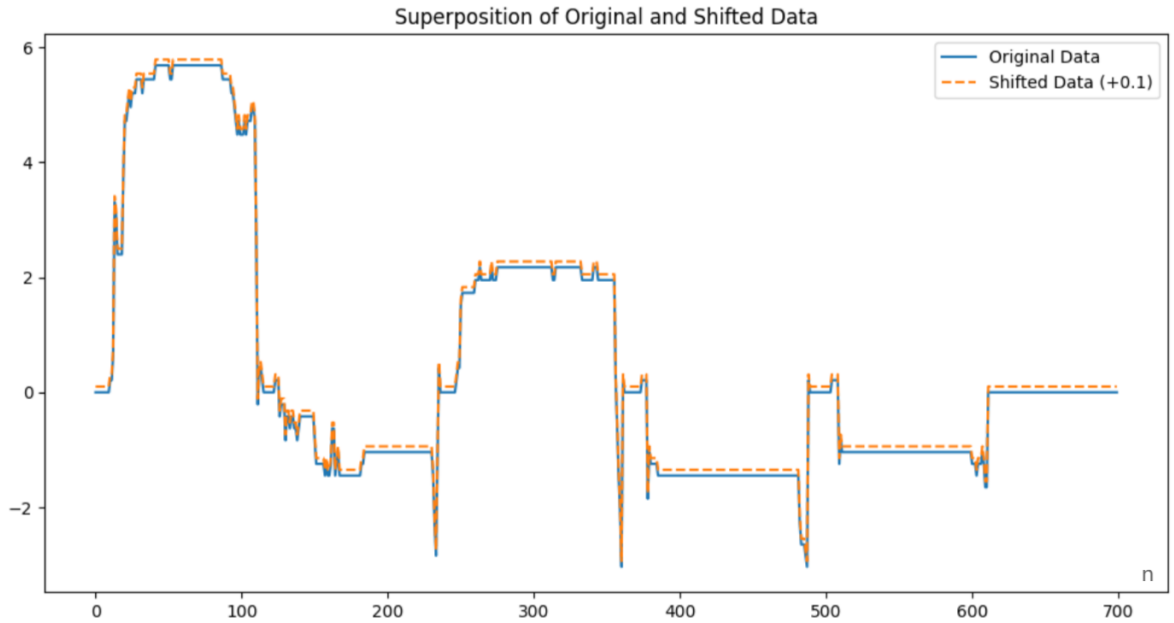

Figure 6.3: A random recording before and after shifting (shifting value=0.1).

After augmentation, we obtain six augmented datasets: three for fasting subjects and three for sportspeople. Each population has a dataset augmented with additional Gaussian noise, random shift, and random scaling. The size of each augmented dataset is double the original dataset size, as it includes both the original samples and the augmented samples.
The augmented Ramadan datasets contain 1400 samples each (700 original samples plus 700 augmented samples), while the augmented sportspeople datasets contain 240 samples each (120 original samples plus 120 augmented samples).
These augmentation techniques are applied to the datasets with the final setup chosen in the previous chapter.

6.2.2 Classification performance with data augmentation

We apply classifiers to this newly augmented data to evaluate its performance.

Tables 6.1 and 6.2 present the results for the new augmented data. (1) represents the original Ramadan dataset with no augmentation, (2) represents the dataset augmented with Gaussian noise, (3) represents the dataset augmented with a random scaling factor, and (4) represents the dataset augmented with random shift values.

	SVM		D_T		R_F n=100		KNN		L-R 1		max	
Number of classes	5	2	5	2	5	2	5	2	5	2		
(1)	0.42	0.65	0.48	0.74	0.64	0.76	0.36	0.62	0.72	0.87	**0.72**	**0.87**
(2)	0.61	0.77	0.78	0.91	0.87	0.95	0.67	0.79	0.95	0.97	**0.95**	**0.97**
(3)	0.53	0.75	0.73	0.86	0.95	0.97	0.69	0.86	0.95	0.97	**0.95**	**0.97**
(4)	0.58	0.76	0.81	0.88	0.91	0.93	0.69	0.83	0.92	0.95	**0.92**	**0.95**

Table 6.1: Results of data augmentation techniques on the Ramadan dataset.

	SVM	D_T	R_F n=100	KNN	L-R 1	max
(1)	0.83	0.83	0.87	0.91	0.92	**0.92**
(2)	0.85	0.91	0.95	0.93	0.95	**0.95**
(3)	0.83	0.95	0.95	0.93	1	**1**
(4)	0.85	0.91	1	0.91	0.95	**1**

Table 6.2: Results of data augmentation techniques on the sportspeople dataset.

We observe an improvement in classifier performance across both datasets following data augmentation. This enhancement underscores the value of data augmentation in expanding datasets, thereby aiding in better generalization. Moreover, each type of data augmentation reflects specific qualities inherent in the datasets.

- Gaussian noise augmentation enhances resilience to noise, indicating rich and discernible patterns within the data.
- Shifting augmentation demonstrates the diversity and well-distributed features, facilitating effective generalization across various spatial arrangements.

- Scaling augmentation highlights consistent magnitude characteristics, enabling seamless adaptation to varying scales.

Overall, these results demonstrate the effectiveness of data augmentation in enhancing dataset quality and improving classifier performance. They indicate the robustness and adaptability of the involved datasets, making them well-suited for real-world applications.

Remark

Achieving 100% accuracy is not always a reliable indicator of a model's performance; it can often signal overfitting, where the model memorizes the data but fails to generalize well to unseen real-world data. This problem is evident in the sportspeople dataset since the original dataset comprises only 120 samples. Even after augmentation, increasing the dataset to 240 samples, the number remains relatively small. To mitigate this issue, it is essential to gather more real-world data to expand the dataset and train the model on a more diverse set of examples, ensuring its suitability for real-world applications.

6.3 Neural Network models

6.3.1 Ramadan dataset

For each augmented dataset, we trained neural networks intending to achieve high classification accuracy while minimizing noise and avoiding overfitting. To accomplish this, we explore several neural network architectures and iteratively tuned parameters and hyperparameters to optimize performance. Table 6.4 outlines the architecture of each neural network.

Table 6.3 provides the final classification accuracy and loss values for the training, validation, and test sets across the three augmented datasets.

Set	**Train**		**Validation**		**Test**	
	Accuracy %	**loss**	**Accuracy %**	**loss**	**Accuracy %**	**loss**
(1)	90.48	1.12	92.86	1.09	92.14	1.07
(2)	91.87	0.49	94.05	0.51	95.71	0.45
(3)	93.95	0.45	92.06	0.53	94.28	0.5

Table 6.3: Final classification accuracy and loss values across augmented datasets.

(1) dataset augmented with Gaussian noise, (2) dataset augmented with a random scaling factor, and (3) dataset augmented with random shift values.

Figures 6.4, 6.5, and 6.6 depict the variation in train and validation accuracy and loss throughout the training process for datasets augmented with Gaussian noise, random scaling, and random shifting, respectively.

Discussion

- From the three datasets, the one augmented with Gaussian noise required a more complex model to achieve good results. This is logical since shifting or scaling are simple modifications that do not significantly alter the main features in the dataset compared to Gaussian noise.
- Similarly, regarding the number of epochs, the dataset augmented with Gaussian noise required up to 1150 epochs to achieve approximately the same results as the other two datasets, which only required 300 epochs. This discrepancy reflects the complexity introduced by the Gaussian noise augmentation.
- While the neural network models presented show no evidence of overfitting and demonstrate the ability to generalize to the test set, it is worth noting that the validation and training accuracy and

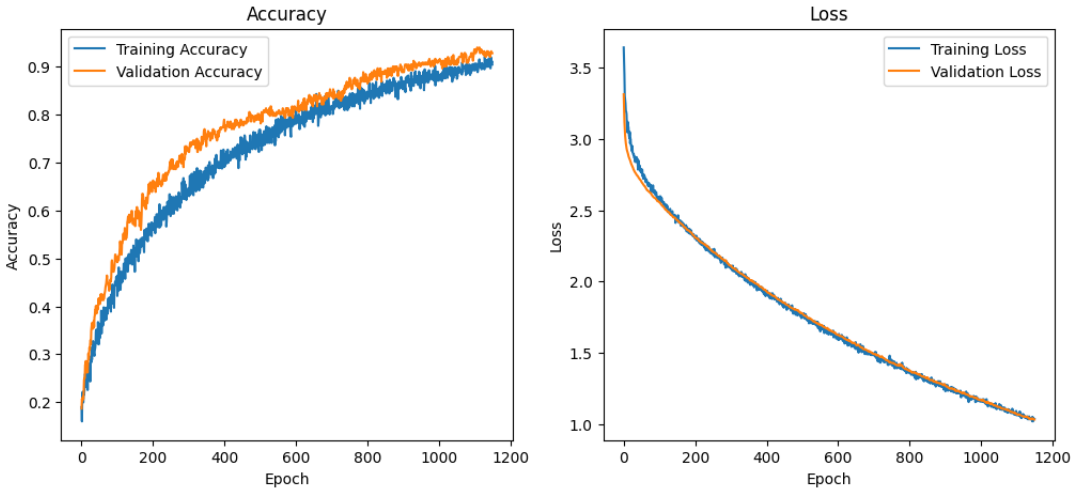

Figure 6.4: Train and validation accuracy and loss for dataset augmented with Gaussian noise.

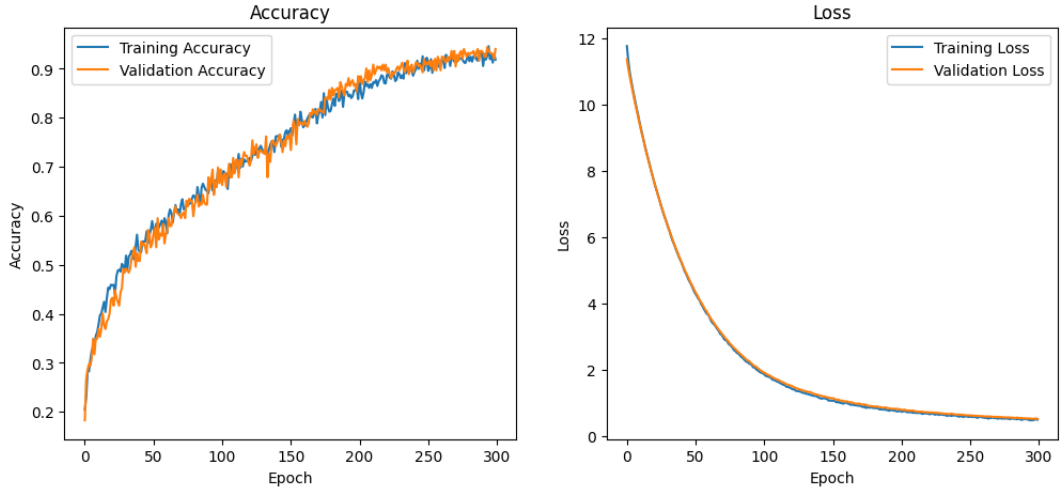

Figure 6.5: Train and validation accuracy and loss for dataset augmented with random scaling.

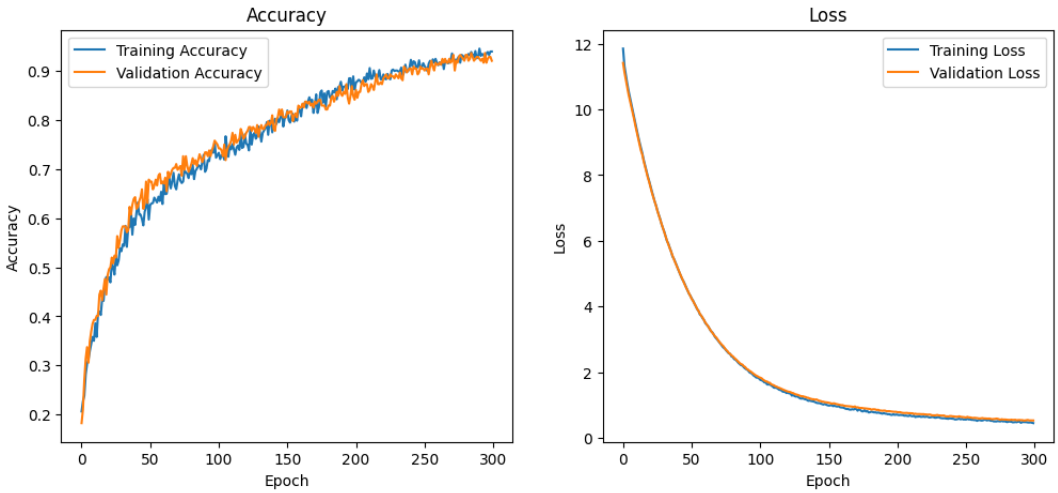

Figure 6.6: Train and validation accuracy and loss for dataset augmented with random shifting.

loss values are closely aligned in the graphs. This suggests that there remains a risk of overfitting, given the proximity of these metrics.

- The fluctuations in the accuracy plots are attributed to the dataset size, where even small changes

can have a noticeable impact on the model's performance. With larger datasets, these fluctuations tend to be smoothed out due to the increased volume and diversity of data, resulting in a more stable and reliable performance assessment.

- The loss values are relatively low compared to those achieved previously with the linear LR model (L=1.6), and indeed, the classification accuracies are higher.
- The loss values for models trained on data augmented with Gaussian noise are higher than the loss values for models trained on data augmented with shifts and scaling. This difference is attributable to the type of augmentation applied. Gaussian noise, contrary to shifting and scaling, introduces random variations to the data, which can make the learning process more challenging for the model, resulting in higher loss values.
- From Table 6.3, we observe that for data augmented with Gaussian noise, the loss for training is higher compared to validation and test sets. This discrepancy is a positive sign of avoiding overfitting, although it remains close to risking overfitting. On the other hand, for the dataset augmented with shifts and scaling, the loss for training is lower, which is a clear indicator of overfitting.

Remark

The presented models do not exhibit clear signs of overfitting, but there remains a potential risk. Avoiding overfitting proved challenging across those datasets, requiring extensive testing and hyper-parameter tuning due to the dataset's size and nature. This underscores the suitability of classic classifiers (SVM, KNN, DT, RF, LR), which have yielded accurate results in previous analyses.

6.3.2 Sportspeople dataset

Due to the limited amount of data in the sportspeople dataset, applying neural networks was not feasible. Indeed, when using classifiers, the accuracy reached 100%, indicating overfitting. Therefore, even with simple neural network models consisting of 1 or 2 hidden layers with a maximum of 8 neurons, the model exhibits overfitting within the first 5 epochs. This suggests that the dataset is insufficient to train neural networks effectively. For this dataset, using classifiers is more appropriate and sufficient.

6.4 Conclusion

This chapter highlights the pivotal role of data augmentation in showcasing the robustness of our dataset against various factors, including Gaussian noise and random shifts, underscoring the potential of our proposed technique to excel in real-world scenarios characterized by imperfect data. Our analysis leads us to the conclusion that classifiers such as SVM, LR, DT, RF, and KNN are better suited to our dataset than neural networks due to the dataset's size and the type of its features. To explore neural networks further, augmenting the dataset by gathering additional data is recommended. This expansion would enrich the dataset, enabling more effective utilization of neural network architectures.

model 1	model 2	model 3
• **Optimizer:** – Adam with a learning rate of 0.00001 • **Regularization:** – L2 regularization (0.02) on the second dense layer • **Number of Layers and Neurons:** – Input Layer: Implicit, based on the input shape of the data – First Dense Layer: 100 neurons, ReLU activation – Dropout Layer: 0.2 dropout rate – Second Dense Layer: 50 neurons, ReLU activation, L2 regularization – Dropout Layer: 0.2 dropout rate – Output Layer: 5 neurons, Softmax activation • **Callbacks:** – Reduce LR: Monitors the validation loss, reduces the learning rate by a factor of 0.02 if the validation loss does not improve for 10 epochs, with a minimum learning rate of 0.00001 • **Training Parameters:** – Number of Epochs: 1150 – Batch Size: 100 • **Number of parameters**: 333905 • **Memory space required for the model:** 1.27 MB • **Response time:** 0.21667 s	• **Optimizer:** – Adam with a learning rate of 0.0001 • **Regularization:** – L2 regularization (0.3) on the second dense layer • **Number of Layers and Neurons:** – Input Layer: Implicit, based on the input shape of the data – First Dense Layer: 50 neurons, ReLU activation – Dropout Layer: 0.2 dropout rate – Second Dense Layer: 25 neurons, ReLU activation, L2 regularization – Dropout Layer: 0.2 dropout rate – Output Layer: 5 neurons, Softmax activation • **Callbacks:** – Reduce LR: Monitors the validation loss and reduces the learning rate by a factor of 0.02 if the validation loss does not improve for ten epochs, with a minimum learning rate of 0.000001 • **Training Parameters:** – Number of Epochs: 300 – Batch Size: 50 • **Number of parameters**: 165705 • **Memory space required for the model:** 0.63 MB • **Response time:** 0.15990 s	• **Optimizer:** – Adam with a learning rate of 0.0001 • **Regularization:** – L2 regularization (0.3) on the second dense layer • **Number of Layers and Neurons:** – Input Layer: Implicit, based on the input shape of the data – First Dense Layer: 50 neurons, ReLU activation – Dropout Layer: 0.2 dropout rate – Second Dense Layer: 25 neurons, ReLU activation, L2 regularization – Dropout Layer: 0.2 dropout rate – Output Layer: 5 neurons, Softmax activation • **Callbacks:** – Reduce LR: Monitors the validation loss and reduces the learning rate by a factor of 0.02 if the validation loss does not improve for ten epochs, with a minimum learning rate of 0.000001 • **Training Parameters:** – Number of Epochs: 300 – Batch Size: 50 • **Number of parameters**: 165705 • **Memory space required for the model:** 0.63 MB • **Response time:** 0.15990 s
Type: Sequential Feedforward neural network, **Loss Function:** sparse_categorical_crossentropy, **Validation Split:** 0.2. **Test split:** 0.1		

Table 6.4: Characteristics of neural network models trained on augmented data.

Model 1 trained on data augmented with Gaussian noise, Model 2 trained on data augmented with random scaling, and Model 3 trained on data augmented with random shifting

Chapter 7

General Conclusion

In conclusion, capacitive sensing has demonstrated strong potential in differentiating between hydrated and dehydrated subjects. As hypothesized in Chapter 3, The dielectric properties of the body, which vary with hydration levels, were effectively characterized by the capacitance sensor. This suggests promising prospects for applying capacitive sensing in hydration monitoring and assessment.

The utilization of complete hand recordings of capacitance, along with additional features such as weight and gender, has played a crucial role in enhancing performance by reducing inter-finger variability.

Regarding the choice of classification models, we find that traditional classifiers such as SVM, DT, RF, KNN, and LR outperform neural networks, given the dataset size and the nature of the data.

Ultimately, our study demonstrates that Linear Logistic Regression yields the best performance metrics, achieving an accuracy of 72% for the 5-class classification 87% for binary classification for fasting subjects, and 92% binary classification for sportspeople.

It is important to note that we have identified clear differences in hydration patterns between fasting subjects and sportspeople. A model trained on one type of dehydration does not effectively generalize to the other.

It is essential to address the sweat effect for future work and perspectives, as it can potentially confound the readings. The increased capacitance observed may not necessarily indicate good hydration but may be attributed to sweat, thus leading to inaccurate assessments. Efforts to mitigate this effect and refine the methodology are crucial for developing more reliable hydration monitoring tools.

In summary, our exploration underscores the potential of capacitive sensing for hydration monitoring. By discerning nuanced hydration patterns and leveraging appropriate data preprocessing techniques and classification models, we pave the way for advancing the field of non-invasive hydration monitoring.

Bibliography

[1] Davis FA. *Taber's Medical Dictionary.* Unbound Medicine. Published, 2021.

[2] Aden Breland, ed. *Handbook of pediatric surgery.* en. USA: American Medical, Sept. 2023.

[3] E Jéquier and F Constant. "Water as an essential nutrient: the physiological basis of hydration". en. In: *Eur. J. Clin. Nutr.* 64.2 (Feb. 2010), pp. 115–123.

[4] Simon N Thornton. "Increased hydration can be associated with weight loss". en. In: *Front. Nutr.* 3 (June 2016), p. 18.

[5] Richard F Keep, Ya Hua, and Guohua Xi. "Brain water content. A misunderstood measurement?" en. In: *Transl. Stroke Res.* 3.2 (June 2012), pp. 263–265.

[6] Geoffrey Cooper. *The cell: A molecular approach.* 2nd ed. Sunderland, MA: Sinauer Associates, Aug. 2000.

[7] Swagatika Sahoo et al. "Membrane transporters in a human genome-scale metabolic knowledgebase and their implications for disease". en. In: *Front. Physiol.* 5 (Mar. 2014), p. 91.

[8] Dongyeop Lee et al. "Effects of nutritional components on aging". en. In: *Aging Cell* 14.1 (Feb. 2015), pp. 8–16.

[9] Stephen J Genuis et al. "Clinical detoxification: elimination of persistent toxicants from the human body". en. In: *ScientificWorldJournal* 2013 (June 2013), p. 238347.

[10] Stephen J Genuis et al. "Blood, urine, and sweat (BUS) study: monitoring and elimination of bioaccumulated toxic elements". en. In: *Arch. Environ. Contam. Toxicol.* 61.2 (Aug. 2011), pp. 344–357.

[11] D R Thomas et al. "Morley and Dehydration Council, "Understanding clinical dehydration and its treatment". In: *Journal of the American Medical Directors Association* 9.5 (2008), pp. 292–301.

[12] A M El-Sharkawy et al. "Dehydration and clinical outcome in hospitalised older adults: A cohort study". In: *Eur. Geriatr. Med.* 8.1 (Feb. 2017), pp. 22–29.

[13] Heather M Logan-Sprenger et al. "The effect of dehydration on muscle metabolism and time trial performance during prolonged cycling in males". en. In: *Physiol. Rep.* 3.8 (Aug. 2015), e12483.

[14] Eleonora Dupouy and Mirjana Gurinovic. "Sustainable food systems for healthy diets in Europe and Central Asia: Introduction to the special issue". en. In: *Food Policy* 96.101952 (Oct. 2020), p. 101952.

[15] Kory Taylor and Elizabeth B. Jones. *Adult Dehydration.* StatPearls Publishing, Treasure Island (FL), 2023. URL: `http://europepmc.org/books/NBK555956`.

[16] Lindsay B Baker. "Physiology of sweat gland function: The roles of sweating and sweat composition in human health". In: *Temperature* 6.3 (2019), pp. 211–259.

[17] Kurt J Sollanek et al. "Potential impact of a 500-mL water bolus and body mass on plasma osmolality dilution". In: *European journal of applied physiology* 111 (2011), pp. 1999–2004.

[18] Lawrence E. Armstrong et al. "Urinary Indices during Dehydration, Exercise, and Rehydration". In: *Intl. Journal of Sport Nutrition* 8.4 (Dec. 1998), pp. 345–355. ISSN: 1050–1606. DOI: `10.1123/ijsn.8.4.345`. URL: `http://dx.doi.org/10.1123/ijsn.8.4.345`.

[19] Denise L Smith et al. “Use of salivary osmolality to assess dehydration”. en. In: *Prehosp. Emerg. Care* 16.1 (Jan. 2012), pp. 128–135.

[20] D C Knottenbelt. “The urinary system”. In: *The Equine Manual*. Elsevier, 2006, pp. 659–712.

[21] Lawrence E Armstrong. “Assessing hydration status: the elusive gold standard”. In: *Journal of the American College of Nutrition* 26.sup5 (2007), 575S–584S.

[22] Samuel N Cheuvront and Robert W Kenefick. “Dehydration: physiology, assessment, and performance effects”. In: *Comprehensive Physiology* 4.1 (2011), pp. 257–285.

[23] Damir Zubac et al. “Urine specific gravity as an indicator of dehydration in Olympic combat sport athletes; considerations for research and practice”. In: *European journal of sport science* 18.7 (2018), pp. 920–929.

[24] Valentín E Fernández-Elías et al. “Validity of hydration non-invasive indices during the weight-cutting and official weigh-in for Olympic combat sports”. In: *PloS one* 9.4 (2014), e95336.

[25] SM Shirreffs. “Markers of hydration status”. In: *Journal of Sports Medicine and Physical Fitness* 40.1 (2000), pp. 80–84.

[26] Gemma Harvey et al. “The use of body mass changes as a practical measure of dehydration in team sports”. In: *Journal of Science and Medicine in Sport* 11.6 (2008), pp. 600–603. ISSN: 1440-2440. DOI: https://doi.org/10.1016/j.jsams.2007.05.012. URL: https://www.sciencedirect.com/science/article/pii/S1440244007001855.

[27] Volker Wizemann et al. “The mortality risk of overhydration in haemodialysis patients”. In: *Nephrology Dialysis Transplantation* 24.5 (2009), pp. 1574–1579.

[28] Wail A Hayajneh et al. “Comparison of clinical associations and laboratory abnormalities in children with moderate and severe dehydration”. In: *Journal of pediatric gastroenterology and nutrition* 50.3 (2010), pp. 290–294.

[29] Lee Hooper et al. “Water-loss dehydration and aging”. In: *Mechanisms of Ageing and Development* 136 (2014), pp. 50–58.

[30] Lee Hooper et al. “Clinical symptoms, signs and tests for identification of impending and current water-loss dehydration in older people”. In: *Cochrane Database of Systematic Reviews* 4 (2015).

[31] Talha Agcayazi et al. “Wearable infant hydration monitor”. In: *2016 IEEE virtual conference on applications of commercial sensors (VCACS)*. IEEE. 2016, pp. 1–10.

[32] Aggie Bak, Amalia Tsiami, and Carolynn Greene. “Methods of assessment of hydration status and their usefulness in detecting dehydration in the elderly”. In: *Current Research in Nutrition and Food Science* 5.2 (2017), pp. 43–54.

[33] Monirun Nessa Begum and C Shanthi Johnson. “A review of the literature on dehydration in the institutionalized elderly”. In: *e-SPEN, the European e-Journal of Clinical Nutrition and Metabolism* 5.1 (2010), e47–e53.

[34] Mehdi Rasouli, Asadollah Mohseni Kiasari, and Shahin Arab. “Indicators of dehydration and haemoconcentration are associated with the prevalence and severity of coronary artery disease”. In: *Clinical and experimental pharmacology and physiology* 35.8 (2008), pp. 889–894.

[35] Xinglin Yang, Haiting Wu, and Hang Li. “Dehydration-associated chronic kidney disease: A novel case of kidney failure in China”. In: *BMC nephrology* 21 (2020), pp. 1–5.

[36] Mark R Burge et al. “Differential effects of fasting and dehydration in the pathogenesis of diabetic ketoacidosis”. In: *Metabolism-Clinical and Experimental* 50.2 (2001), pp. 171–177.

[37] Natalie A Dick and Jason J Diehl. “Febrile illness in the athlete”. In: *Sports Health* 6.3 (2014), pp. 225–231.

[38] David R Thomas et al. “Understanding clinical dehydration and its treatment”. In: *Journal of the American Medical Directors Association* 9.5 (2008), pp. 292–301.

[39] Michele Lauriola et al. “Neurocognitive disorders and dehydration in older patients: clinical experience supports the hydromolecular hypothesis of dementia”. In: *Nutrients* 10.5 (2018), p. 562.

[40] Ahsan Mehmood et al. “Your smartphone could act as a pulse-oximeter and as a single-lead ECG”. In: *Scientific Reports* 13.1 (2023), p. 19277.

[41] Hugo Plácido Da Silva et al. “BITalino: A novel hardware framework for physiological computing”. In: *International Conference on Physiological Computing Systems*. Vol. 2. SciTePress. 2014, pp. 246–253.

[42] Sidrah Liaqat et al. “Non invasive skin hydration level detection using machine learning”. In: *Electronics* 9.7 (2020), p. 1086.

[43] Ali Rizwan et al. “Non-invasive hydration level estimation in human body using galvanic skin response”. In: *IEEE Sensors Journal* 20.9 (2020), pp. 4891–4900.

[44] Sidrah Liaqat et al. “Personalized wearable electrodermal sensing-based human skin hydration level detection for sports, health and wellbeing”. In: *Scientific Reports* 12.1 (2022), p. 3715.

[45] A Rizwan et al. “Skin conductance as proxy for the identification of hydration level in human body”. In: *2019 IEEE MTT-S International Microwave Biomedical Conference (IMBioC)*. Vol. 1. IEEE. 2019, pp. 1–3.

[46] Boyue Jiang et al. “Deep Learning and Short-Time Fourier Transform Based Non-Invasive Solution for Hydration Level Detection”. In: *2023 IEEE International Conference on Smart Internet of Things (SmartIoT)*. IEEE. 2023, pp. 300–304.

[47] https://www.biopac.com/product/eda-finger-transducer-bsl/.

[48] Nandan Kulkarni et al. “A non-invasive context-aware dehydration alert system”. In: *Proceedings of the 22nd International Workshop on Mobile Computing Systems and Applications*. 2021, pp. 157–159.

[49] Pranav Adith et al. “Smartphone based skin hydration level sensor and sunburn prediction”. In: *2023 14th International Conference on Computing Communication and Networking Technologies (ICCCNT)*. 2023, pp. 1–7. DOI: 10.1109/ICCCNT56998.2023.10307161.

[50] G Anitha et al. “Machine Learning based non-invasive method of determining total body water”. In: *2022 7th International Conference on Communication and Electronics Systems (ICCES)*. IEEE. 2022, pp. 1062–1065.

[51] Mayo Foundation for Medical Education and Research. *Ventricular Tachycardia image*. 2016.

[52] E. Rendon-Morales et al. “Towards the correlation between human hydration and the electrical activity of the heart using Electric Potential Sensors”. In: *2015 IEEE Sensors Applications Symposium (SAS)*. 2015, pp. 1–5. DOI: 10.1109/SAS.2015.7133644.

[53] Antonio Alvarez et al. “Machine learning methods in the classification of the athletes dehydration”. In: *2019 IEEE Fourth Ecuador Technical Chapters Meeting (ETCM)*. IEEE. 2019, pp. 1–5.

[54] Anthony Kaveh and Wayne Chung. “Classification of hydration status using electrocardiogram and machine learning”. In: *AIP Conference Proceedings*. Vol. 1559. 1. American Institute of Physics. 2013, pp. 240–249.

[55] George B Moody and Roger G Mark. “The impact of the MIT-BIH arrhythmia database”. In: *IEEE engineering in medicine and biology magazine* 20.3 (2001), pp. 45–50.

[56] Ary L Goldberger et al. “PhysioBank, PhysioToolkit, and PhysioNet: Components of a new research resource for complex physiologic signals”. In: *Circulation [Online]* 101.23 (2000), e215–e220.

[57] Erika Severeyn et al. “Heart rate variability analysis during a dehydration protocol on athletes”. In: *2016 XXI Symposium on Signal Processing, Images and Artificial Vision (STSIVA)*. IEEE. 2016, pp. 1–7.

[58] Valiollah Dabidi Roshan, Mahdi Hosseinzadeh, and Mehrdad Saravi. "The effects of dehydration and rehydration on electrocardiographic and echocardiographic parameters in Greco-Roman wrestlers". In: *European Journal of Sport Science* 12.1 (2012), pp. 49–56.

[59] Fahad Kamran et al. "Noninvasive Estimation of Hydration Status in Athletes Using Wearable Sensors and a Data-Driven Approach Based on Orthostatic Changes". In: *Sensors* 21.13 (2021), p. 4469.

[60] Gregory E Peoples et al. "Cardiac electrophysiology during progressive and controlled dehydration: inferences from ECG analysis during steady-state exercise and recovery". In: (2009).

[61] R. AlDisi, Q. Bader, and A. Bermak. "Hydration Assessment Using the Bio-Impedance Analysis Method". In: *Sensors* 22 (2022), p. 6350. DOI: 10.3390/s22176350. URL: https://doi.org/10.3390/s22176350.

[62] M. Jang et al. "Textile-Based Wearable Sensor for Skin Hydration Monitoring". In: *Sensors* 22 (2022), p. 6985. DOI: 10.3390/s22186985.

[63] Shanshan Yao et al. "A wearable hydration sensor with conformal nanowire electrodes". In: *Advanced healthcare materials* 6.6 (2017), p. 1601159.

[64] Xian Huang et al. "Epidermal differential impedance sensor for conformal skin hydration monitoring". In: *Biointerphases* 7.1 (2012).

[65] Ryotaro Matsukawa et al. "Skin impedance measurements with nanomesh electrodes for monitoring skin hydration". In: *Advanced Healthcare Materials* 9.22 (2020), p. 2001322.

[66] Keana De Guzman and Aoife Morrin. "Screen-printed Tattoo Sensor towards the Non-invasive Assessment of the Skin Barrier". In: *Electroanalysis* 29.1 (2017), pp. 188–196.

[67] Reem AlDisi. "Design and Implementation of Low-Cost Dehydration Sensor for Wearable Health Technology". PhD thesis. Hamad Bin Khalifa University (Qatar), 2022.

[68] Xian Huang et al. "Materials and designs for wireless epidermal sensors of hydration and strain". In: *Advanced Functional Materials* 24.25 (2014), pp. 3846–3854.

[69] Maxim Morin et al. "Skin hydration dynamics investigated by electrical impedance techniques in vivo and in vitro". In: *Scientific Reports* 10.1 (2020), p. 17218.

[70] Matthias Ring et al. "A Temperature-Based Bioimpedance Correction for Water Loss Estimation During Sports". In: *IEEE Journal of Biomedical and Health Informatics* 20.6 (2016), pp. 1477–1484. DOI: 10.1109/JBHI.2015.2466076.

[71] Javier Ramos et al. "A wireless sensor network for fat and hydration monitoring by bioimpedance analysis". In: *Proceedings of the 6th International Workshop on Wearable, Micro, and Nano Technologies for Personalized Health*. IEEE. 2009, pp. 49–52.

[72] Meha Qassem and Panayiotis Kyriacou. "Use of reflectance near-infrared spectroscopy to investigate the effects of daily moisturizer application on skin optical response and barrier function". In: *Journal of Biomedical Optics* 19.8 (2014), pp. 087007–087007.

[73] Denis Davydov et al. "Skin dehydration monitoring with optical spectroscopy allows assessment of water content in the organism: Thermal and physical loads, diuretic therapy". In: *Journal of Biophotonics* (2024), e202300509.

[74] Yarden Tzabari Kelman et al. "Optical tissue probing: human skin hydration detection by speckle patterns analysis". In: *Biomedical Optics Express* 10.9 (2019), pp. 4874–4883.

[75] Cobus Visser et al. "Investigation of the feasibility of non-invasive optical sensors for the quantitative assessment of dehydration". In: *Medical Engineering & Physics* 48 (2017), pp. 181–187.

[76] Priyeta Saha et al. "Dehydration scan: An artificial intelligence assisted smartphone-based system for early detection of dehydration". In: *Lecture Notes of the Institute for Computer Sciences, Social Informatics and Telecommunications Engineering*. Lecture notes of the Institute for Computer Sciences, Social Informatics and Telecommunications Engineering. Cham: Springer Nature Switzerland, 2023, pp. 289–312.

[77] Chenbin Liu et al. “Skin mechanical properties and hydration measured with mobile phone camera”. In: *IEEE Sensors Journal* 16.4 (2015), pp. 924–930.

[78] Rose Alaslani et al. “You can monitor your hydration level using your smartphone camera”. In: *arXiv preprint arXiv:2402.07467* (2024).

[79] Natasa Reljin et al. “Automatic Detection of Dehydration using Support Vector Machines”. In: *2018 14th Symposium on Neural Networks and Applications (NEUREL)*. IEEE. 2018, pp. 1–6.

[80] Elena Volkova et al. “Multispectral sensor fusion in SmartWatch for in situ continuous monitoring of human skin hydration and body sweat loss”. In: *Scientific Reports* 13.1 (2023), p. 13371.

[81] R Van Beers et al. “Accurate measurement of SpO2 and dermal skin hydration using a wearable miniaturized spectrometer”. In: *Biophotonics in Exercise Science, Sports Medicine, Health Monitoring Technologies, and Wearables III*. Vol. 11956. SPIE. 2022, p. 1195602.

[82] RHJ Kox. “Assessing the Severity of Dehydration of Children in Low-Resource Settings”. In: (2017).

[83] R Chad Webb et al. “Thermal transport characteristics of human skin measured in vivo using ultrathin conformal arrays of thermal sensors and actuators”. In: *PloS one* 10.2 (2015), e0118131.

[84] Kyeongha Kwon et al. “Wireless, soft electronics for rapid, multisensor measurements of hydration levels in healthy and diseased skin”. In: *Proceedings of the National Academy of Sciences* 118.5 (2021), e2020398118.

[85] Jaeho Shin et al. “Wireless, soft sensors of skin hydration with designs optimized for rapid, accurate diagnostics of dermatological health”. In: *Advanced healthcare materials* 12.4 (2023), p. 2202021.

[86] Rico Brendtke et al. “Feasibility study on a microwave-based sensor for measuring hydration level using human skin models”. In: *PLoS One* 11.4 (2016), e0153145.

[87] R. Schiavoni et al. “Microwave Wearable System for Sensing Skin Hydration”. In: *2021 IEEE International Instrumentation and Measurement Technology Conference (I2MTC)* (2021), pp. 1–6. DOI: 10.1109/I2MTC50364.2021.9460018.

[88] A. Cataldo et al. “Portable Microwave Reflectometry System for Skin Sensing”. In: *IEEE Transactions on Instrumentation and Measurement* 71 (2022), pp. 1–8. DOI: 10.1109/TIM.2022.3154804.

[89] M. Baghelani et al. “Non-Invasive Microwave Sensor for Real-Time Continuous Dehydration Monitoring”. In: *IEEE Sensors Journal* (2024). DOI: 10.1109/JSEN.2024.3362702.

[90] David Garrett. “Hydration Monitoring Using Microwaves: From Modelling and Estimation of Tissue Properties to Validation in Humans”. PhD thesis. Unviersity of Calgary Calgary, AB, Canada, 2018.

[91] D. C. Garrett and E. C. Fear. “Feasibility Study of Hydration Monitoring Using Microwaves–Part 1: A Model of Microwave Property Changes With Dehydration”. In: *IEEE Journal of Electromagnetics, RF and Microwaves in Medicine and Biology* 3.4 (2019), pp. 292–299. DOI: 10.1109/JERM.2019.2911849.

[92] D. C. Garrett et al. “Feasibility Study of Hydration Monitoring Using Microwaves–Part 2: Measurements of Athletes”. In: *IEEE Journal of Electromagnetics, RF and Microwaves in Medicine and Biology* 3.4 (2019), pp. 300–307. DOI: 10.1109/JERM.2019.2911909.

[93] Brendon C Besler and Elise C Fear. “Microwave hydration monitoring: System assessment using fasting volunteers”. In: *Sensors* 21.21 (2021), p. 6949.

[94] L. Peng et al. “A Fused Learning and Enhancing Method for Accurate and Noninvasive Hydration Status Monitoring With UWB Microwave Based on Phantom”. In: *IEEE Transactions on Microwave Theory and Techniques* 71.9 (Sept. 2023), pp. 4027–4036. DOI: 10.1109/TMTT.2023.3248788.

[95] J. Kilpijärvi et al. "A Non-Invasive Method for Hydration Status Measurement With a Microwave Sensor Using Skin Phantoms". In: *IEEE Sensors Journal* 20.2 (Jan. 2020), pp. 1095–1104. DOI: 10.1109/JSEN.2019.2945817.

[96] Raissa Schiavoni et al. "Feasibility of a wearable reflectometric system for sensing skin hydration". In: *Sensors* 20.10 (2020), p. 2833.

[97] Joan Melià-Seguí et al. "Low-cost RFID-based Sensor Integrated in Textile for Non-Invasive Pervasive Hydration Monitoring". In: *IEEE Sensors Journal* (2023).

[98] Sen Bing, Khengdauliu Chawang, and J-C Chiao. "A flexible tuned radio-frequency planar resonant loop for noninvasive hydration sensing". In: *IEEE Journal of Microwaves* 3.1 (2022), pp. 181–192.

[99] Hasan Mujtaba Buttar et al. "Non-Contact Monitoring of Dehydration using RF Data Collected off the Chest and the Hand". In: *IEEE Sensors journal* (2023).

[100] Junchao Wang, Zeljko Zilic, and Yutian Shu. "Evaluation of an RF wearable device for non-invasive real-time hydration monitoring". In: *2017 IEEE 14th International Conference on Wearable and Implantable Body Sensor Networks (BSN)*. IEEE. 2017, pp. 91–94.

[101] AP Sarvazyan et al. "Acoustical method of whole-body hydration status monitoring". In: *Acoustical physics* 62 (2016), pp. 514–522.

[102] Alan C Utter et al. "Evaluation of ultrasound velocity to assess the hydration status of wrestlers". In: *The Journal of Strength & Conditioning Research* 24.6 (2010), pp. 1451–1457.

[103] Yehenew Mengistu et al. "AutoHydrate: A wearable hydration monitoring system". In: *2016 IEEE/RSJ Intl. Conf. on Intelligent Robots and Systems (IROS)*. 2016, pp. 1857–1862. DOI: 10.1109/IROS.2016.7759295.

[104] Adam C Levine et al. "Ultrasound assessment of severe dehydration in children with diarrhea and vomiting". In: *Academic Emergency Medicine* 17.10 (2010), pp. 1035–1041.

[105] Doaa El Amrousy et al. "Non-invasive assessment of significant dehydration in infants using the inferior vena cava to aortic ratio: is it useful?" In: *Journal of pediatric gastroenterology and nutrition* 66.6 (2018), pp. 882–886.

[106] Esra Akyüz Özkan et al. "Evaluation of the inferior vena cava diameter in dehydrated children using bedside ultrasonography". In: *Emergency Medicine International* 2022 (2022).

[107] Helen Diederich and Heinrich Burkhardt. "Diagnostic efficacy of bedside ultrasound to detect dehydration in older patients attending an emergency care unit." In: *Zeitschrift für Gerontologie und Geriatrie* 54.2 (2021).

[108] Matthias Ring et al. "Salivary Markers for Quantitative Dehydration Estimation During Physical Exercise". In: *IEEE Journal of Biomedical and Health Informatics* 21.5 (2017), pp. 1306–1314. DOI: 10.1109/JBHI.2016.2598854.

[109] Yen-Pei Lu et al. "A portable system to monitor saliva conductivity for dehydration diagnosis and kidney healthcare". en. In: *Sci. Rep.* 9.1 (Oct. 2019), p. 14771.

[110] R Stewart et al. "Human hydration level monitoring using embedded piezoresistive microcantilever sensors". In: *Medical engineering & physics* 29.10 (2007), pp. 1084–1088.

[111] Neil P Walsh et al. "Saliva parameters as potential indices of hydration status during acute dehydration". In: *Medicine & Science in Sports & Exercise* 36.9 (2004), pp. 1535–1542.

[112] Matthias Ring et al. "On sweat analysis for quantitative estimation of dehydration during physical exercise". In: *2015 37th Annual Intl. Conf. of the IEEE Engg. in Medicine and Biology Society (EMBC)*. 2015, pp. 7011–7014. DOI: 10.1109/EMBC.2015.7320006.

[113] RM Morgan, MJ Patterson, and MA Nimmo. "Acute effects of dehydration on sweat composition in men during prolonged exercise in the heat". In: *Acta Physiologica Scandinavica* 182.1 (2004), pp. 37–43.

[114] P Manimegala et al. “Dehydration measurement using sweat sensor patch and pulse sensor”. In: *Journal of Physics: Conference Series*. Vol. 1937. 1. IOP Publishing. 2021, p. 012013.

[115] Shogo Nakata et al. “Wearable, flexible, and multifunctional healthcare device with an ISFET chemical sensor for simultaneous sweat pH and skin temperature monitoring”. In: *ACS sensors* 2.3 (2017), pp. 443–448.

[116] Yubin Zhou et al. “Real-time colorimetric hydration sensor for sport activities”. In: *Materials & Design* 90 (2016), pp. 1181–1185.

[117] Natalie P Holmes et al. “Organic electronics incorporating crown ethers as Na+ binding elements, towards a simple printable hydration sensor”. In: *Medical Devices & Sensors* 1.1 (2018), e10001.

[118] G. Marchand et al. “Development of a Dehydration Sensor Integrated on Fabric”. In: *2009 Sixth International Workshop on Wearable and Implantable Body Sensor Networks*. 2009, pp. 230–233. DOI: 10.1109/BSN.2009.29.

[119] Gengchen Liu et al. “Real-time sweat analysis via alternating current conductivity of artificial and human sweat”. en. In: *Appl. Phys. Lett.* 106.13 (Mar. 2015), p. 133702.

[120] Gengchen Liu, Kyle Smith, and Tolga Kaya. “Implementation of a microfluidic conductivity sensor — A potential sweat electrolyte sensing system for dehydration detection”. In: *2014 36th Annual International Conference of the IEEE Engineering in Medicine and Biology Society*. 2014, pp. 1678–1681. DOI: 10.1109/EMBC.2014.6943929.

[121] Innocent D. Lubangakene et al. “Effect of metabolite and temperature on artificial human sweat characteristics over a very wide frequency range (400 MHz–10.4 GHz) for wireless hydration diagnostic sensors”. In: *Results in Engineering* 19 (2023), p. 101328. ISSN: 2590-1230. DOI: https://doi.org/10.1016/j.rineng.2023.101328. URL: https://www.sciencedirect.com/science/article/pii/S2590123023004553.

[122] B Sahin, M Alomari, and T Kaya. “Hydration detection through use of artificial sweat in doped and partially-doped nanostructured CuO films”. In: *Ceram. Int.* 41.6 (July 2015), pp. 8002–8007.

[123] Andrea Ria et al. “Low-Cost Sweating-Rate Sensor for Dehydration Monitoring in Sports”. In: *2023 IEEE SENSORS*. 2023, pp. 1–4. DOI: 10.1109/SENSORS56945.2023.10325206.

[124] Nesli Ersoy, Gulgun Ersoy, and Mehmet Kutlu. “Assessment of hydration status of elite young male soccer players with different methods and new approach method of substitute urine strip”. en. In: *J. Int. Soc. Sports Nutr.* 13.1 (Sept. 2016), p. 34.

[125] Eric Blancaflor et al. “An IoT Design of a Dehydration Indicator System Based on Urine Color”. In: *2022 5th International Conference on Computing and Big Data (ICCBD)*. 2022, pp. 118–122. DOI: 10.1109/ICCBD56965.2022.10080279.

[126] Anton Yudhana et al. “Self-Health Monitoring Based on Dehydration Level and Glucose Content in Urine using Thermal Sensing”. In: *2021 International Conference on Engineering and Emerging Technologies (ICEET)*. 2021, pp. 1–4. DOI: 10.1109/ICEET53442.2021.9659731.

[127] Dmitry Solovei et al. “Chemical sensor platform for non-invasive monitoring of activity and dehydration”. In: *Sensors* 15.1 (2015), pp. 1479–1495.

[128] Samuel N Cheuvront et al. “Physiologic basis for understanding quantitative dehydration assessment”. In: *The American journal of clinical nutrition* 97.3 (2013), pp. 455–462.

[129] Hugo F Posada-Quintero et al. “Mild dehydration identification using machine learning to assess autonomic responses to cognitive stress”. In: *Nutrients* 12.1 (2019), p. 42.

[130] Nagender K Suryadevara, Subhas C Mukhopadhyay, and L Barrack. “Towards a smart non-invasive fluid loss measurement system”. In: *Journal of medical systems* 39 (2015), pp. 1–10.

[131] Dmitry Rodin et al. “An accurate wearable hydration sensor: Real-world evaluation of practical use”. In: *Plos one* 17.8 (2022), e0272646.

[132] Iman M Gidado et al. “Multi-Modal Spectroscopic Assessment of Skin Hydration”. In: *Sensors* 24.5 (2024), p. 1419.

[133] Siddharth Krishnan et al. “Multimodal epidermal devices for hydration monitoring”. In: *Microsystems & nanoengineering* 3.1 (2017), pp. 1–11.

[134] Sarah Tonello et al. “Design and in-vitro Characterization of a Wearable Multi-Sensing System for Hydration Monitoring”. In: *IEEE Transactions on Instrumentation and Measurement* (2024).

[135] Farida Sabry et al. “Towards on-device dehydration monitoring using machine learning from wearable device’s data”. In: *Sensors* 22.5 (2022), p. 1887.

[136] Marife A. Rosales et al. “Prediction of Total Body Water using Scaled Conjugate Gradient Artificial Neural Network”. In: *2020 IEEE REGION 10 CONFERENCE (TENCON)*. 2020, pp. 218–223. DOI: 10.1109/TENCON50793.2020.9293804.

[137] D. Solovei et al. “Non invasive possibility of body dehydration monitoring”. In: *SENSORS, 2011 IEEE*. 2011, pp. 1113–1116. DOI: 10.1109/ICSENS.2011.6127410.

[138] Shu Wang et al. “Predicting hydration status using machine learning models from physiological and sweat biomarkers during endurance exercise: a single case study”. In: *IEEE Journal of Biomedical and Health Informatics* 26.9 (2022), pp. 4725–4732.

[139] MN Bahouth et al. “Noninvasive cardiac output monitor to quantify hydration status in ischemic stroke patients: A feasibility study”. In: *Journal of the Neurological Sciences* 442 (2022), p. 120413.

[140] Feng Fu et al. “Use of electrical impedance tomography to monitor regional cerebral edema during clinical dehydration treatment”. In: *PloS one* 9.12 (2014), e113202.

[141] Rossella Marino et al. “B-type natriuretic peptide and non-invasive haemodynamics and hydration status assessments in the management of patients with acute heart failure in the emergency department”. In: *High Blood Pressure & Cardiovascular Prevention* 17 (2010), pp. 219–225.

[142] Hina Sattar et al. “Smart wound hydration monitoring using biosensors and fuzzy inference system”. In: *Wireless Communications and Mobile Computing* 2019 (2019), pp. 1–15.

[143] Jesus Antonio Sanchez-Perez et al. “A Wearable Multimodal Sensing System for Tracking Changes in Pulmonary Fluid Status, Lung Sounds, and Respiratory Markers”. In: *Sensors* 22.3 (2022). ISSN: 1424-8220. DOI: 10.3390/s22031130. URL: https://www.mdpi.com/1424-8220/22/3/1130.

[144] Texas Instruments. *FDC2x1x EMI-Resistant 28-Bit,12-Bit Capacitance-to-Digital Converter for Proximity and Level Sensing Applications*. Relese date: 2019. URL: https://www.ti.com/product/FDC2114.

[145] Shi Dong. “Multi class SVM algorithm with active learning for network traffic classification”. In: *Expert Systems with Applications* 176 (2021), p. 114885.

[146] Jan Bogaert, Reinhart Ceulemans, and David Salvador-Van Eysenrode. “Decision tree algorithm for detection of spatial processes in landscape transformation”. In: *Environmental management* 33 (2004), pp. 62–73.

[147] Yingchun Liu. “Random forest algorithm in big data environment”. In: *Computer modelling & new technologies* 18.12A (2014), pp. 147–151.

[148] Leif E Peterson. “K-nearest neighbor”. In: *Scholarpedia* 4.2 (2009), p. 1883.

[149] Statistics Solutions. “What is logistic regression”. In: *Statistics Solutions* (2019).

Appendix

1. **SVM:**
   A Support Vector Machine is a supervised machine learning algorithm that can be used for classification or regression tasks. It works by finding the hyperplane that best separates the classes in the feature space. The best hyperplane is the one that maximizes the margin between the classes, meaning the distance between the hyperplane and the nearest data point from either class (known as the support vectors) is maximized.[145]

2. **DT:**
   A Decision Tree is a supervised learning algorithm used for both classification and regression tasks. It splits the data into subsets based on the value of input features. This process is repeated recursively, forming a tree structure with decision nodes (where the data is split based on a feature) and leaf nodes (which represent the output or class label). The goal is to create a model that predicts the value of a target variable by learning simple decision rules inferred from the data features.[146]

3. **RF:**
   Random Forest is an ensemble learning method used for classification, regression, and other tasks. It operates by constructing multiple decision trees during training and outputting the class that is the mode of the classes (classification) or mean prediction (regression) of the individual trees. The key idea is to reduce the risk of overfitting and improve generalization by averaging multiple decision trees.[147]

4. **KNN:** K-Nearest Neighbors (KNN) is a simple, non-parametric, and lazy learning algorithm used for classification and regression tasks. In classification, the output is a class membership. An object is classified by a majority vote of its neighbors, with the object being assigned to the class most common among its k nearest neighbors. The value of k is a positive integer, typically small. In regression, the output is the average of the values of its k nearest neighbors.[148]

5. **LR:**
   Logistic Regression is a statistical model used for binary classification tasks. It models the probability that a given input belongs to a particular class using a logistic function. The output is a probability between 0 and 1, which can be thresholded to make a binary decision. Logistic regression is based on the logistic function, which maps any real-valued number into the (0, 1) interval, making it useful for predicting probabilities.[149]